T.R.

EGE UNIVERSITY

Graduate School of Applied and Natural Science

PREPARATION AND APPLICATION OF COMPOSITE ANION EXCHANGE MEMBRANES FOR SALINITY GRADIENT ENERGY PRODUCTION BY REVERSE ELECTRODIALYSIS

PhD Thesis

Mine Eti

Chemical Engineering Department

İzmir

2023

T.R.

EGE UNIVERSITY

Graduate School of Applied and Natural Science

PREPARATION AND APPLICATION OF COMPOSITE ANION EXCHANGE MEMBRANES FOR SALINITY GRADIENT ENERGY PRODUCTION BY REVERSE ELECTRODIALYSIS

Mine ETİ

Supervisors: Prof. Dr. Nalan KABAY

Assoc. Prof. Dr. Enver GÜLER

Chemical Engineering Department

Chemical Engineering Third Cycle Programme

İZMİR

2023

Mine ETİ tarafından doktora tezi olarak sunulan “Preparation and application of composite anion exchange membranes for salinity gradient energy production by reverse electrodialysis” başlıklı bu çalışma EÜ Lisansüstü Eğitim ve Öğretim Yönetmeliği ile EÜ Fen Bilimleri Enstitüsü Eğitim ve Öğretim Yönergesi’nin ilgili hükümleri uyarınca tarafımızdan değerlendirilerek savunmaya değer bulunmuş ve 14/06/2023 tarihinde yapılan tez savunma sınavında aday oybirliği/oyçokluğu ile başarılı bulunmuştur.

Jüri Üyeleri:			**İmza**
Jüri Başkanı	**:**	Prof. Dr. Nalan Kabay	
Raportör Üye	**:**	Prof. Dr. Levent Ballice	
Üye	**:**	Prof. Dr. Sacide Alsoy Altınkaya	
Üye	**:**	Prof. Dr. Müşerref Arda	
Üye	**:**	Prof. Dr. Serap Seyhan Bozkurt	

EGE ÜNİVERSİTESİ FEN BİLİMLERİ ENSTİTÜSÜ

ETİK KURALLARA UYGUNLUK BEYANI

EÜ Lisansüstü Eğitim ve Öğretim Yönetmeliğinin ilgili hükümleri uyarınca doktora tezi olarak sunduğum "Preparation and application of composite anion exchange membranes for salinity gradient energy production by reverse electrodialysis" başlıklı bu tezin kendi çalışmam olduğunu, sunduğum tüm sonuç, doküman, bilgi ve belgeleri bizzat ve bu tez çalışması kapsamında elde ettiğimi, bu tez çalışmasıyla elde edilmeyen bütün bilgi ve yorumlara atıf yaptığımı ve bunları kaynaklar listesinde usulüne uygun olarak verdiğimi, tez çalışması ve yazımı sırasında patent ve telif haklarını ihlal edici bir davranışımın olmadığını,bu tezin herhangi bir bölümünü bu üniversite veya diğer bir üniversitede başka bir tez çalışması içinde sunmadığımı, bu tezin planlanmasından yazımına kadar bütün safhalarda bilimsel etik kurallarına uygun olarak davrandığımı ve aksinin ortaya çıkması durumunda her türlü yasal sonucu kabul edeceğimi beyan ederim.

…./…./….

Mine ETİ

ÖZET

TERS ELEKTRODİYALİZ İLE TUZLULUK FARKINA DAYALI ENERJİ ÜRETİMİ İÇİN KOMPOZİT ANYON DEĞİŞTİRİCİ MEMBRANLARININ HAZIRLANMASI VE UYGULANMASI

ETİ, Mine

Doktora Tezi, Kimya Mühendisliği Anabilim Dalı
Tez Danışmanları: Prof. Dr. Nalan Kabay
Doç. Dr. Enver Güler

2023, 121 sayfa

Bu projede, polimer matris yapısı olarak doğal klorometil gruplarına sahip elastomer poli(epidoklorohidrin) kullanılarak, solvent buharlaştırma yöntemi ile çevre dostu anyon değiştirici membran sentezi yapılmıştır. Membranlar daha sonra karakterize edilmiş, en uygun özelliklere sahip membran üretim koşulları tespit edilmiştir. Gözenek dolgulu membran formları gözenekli destek malzemesi kullanmak suretiyle oluşturulmuştur. Tez çalışmasında üretilen anyon değişim membranlarına tane boyutu 100 nm olan gümüş nanopartiküller daldırmalı kaplama yöntemiyle entegre edilmiştir. Ortam pH'ının 6 olduğu koşulda membran yüzeyine entegre edilen bu partiküllerin membran yüzeyinde en iyi dağılım gösterdiği ve bu membranların *E. coli* bakterilerine karşı güçlü antibakteriyel etki gösterdiği tespit edilmiştir. Tuzluluğu az olan ortamda bu partiküllerin membran yüzeyinde daha kararlı olduğu belirlenmiştir. Yapılan kısa ve uzun dönem ters elektrodiyaliz testlerinde de üretilen membranların yüksek enerji üretme potansiyellerinin olduğu ve CMKESD ile eşleştirilmiş PECH-C membranında 0.5 W/m^2 değerlerine kadar elektriksel güç elde edilebildiği belirlenmiştir.Gümüş nanopartikül immobilize edilmiş ve edilmemiş membranlar, 0.017 M ve 0.5 M tuzlu su çözeltileri ve 0, 25, 50 ppm hümik asit çözeltileri ile 24 sa boyunca temas ettirilmiş, iyon değişim kapasitesi ve şişme derecesi değerleri ölçülmüştür. Gümüş nanopartikül immobilize edilmiş membranlarda bu değerlerin daha düşük olduğu görülmüştür. Gümüş nanopartikül immobilize edilmiş gözene dolgulu membranlar daldırma kaplama yöntemiyle elde edilmiştir. Şişme derecesi ve iyon değişim kapasitesi değerleri gözenek dolgulu membrana göre düşük gelmiştir.

Anahtar kelimeler: Anyon değiştirici membran, daldırmalı kaplama, gözenek dolgulu membran, gümüş nanotanecik, ters elektrodiyaliz

ABSTRACT

PREPARATION AND APPLICATION OF COMPOSITE ANION EXCHANGE MEMBRANES FOR SALINITY GRADIENT ENERGY PRODUCTION BY REVERSE ELECTRODIALYSIS

ETİ, Mine

PhD in Chemical Engineering.

Supervisors: Prof. Dr. Nalan Kabay
Assoc. Prof. Dr. Enver Güler

2023, 121 pages

In this project, an environmentally friendly anion exchange membrane (AEM) was synthesized by solvent evaporation method using elastomer poly(epidochlorohydrin) with natural chloromethyl groups as polymer matrix structure. Membranes were then characterized, optimum membrane propertieswere determined. Pore-filled membrane forms were prepared using porous support material. Silver nanoparticles (AgNPs) with 100 nm grain size wereimmobilized into the AEMs produced in the thesis study by dip coating method. pH 6.0 AgNPs immobilized AEMs showed the best distribution on the membrane surface and that these membranes had a strong antibacterial effect against *E. coli* bacteria. AgNPs were more stable on the membrane surface in the environment with low salinity. In the short and long term reverse electrodialysis tests, it was determined that the produced membranes have high energy generating potential and electrical power up to 0.5 W/m^2 values can be obtained with PECH-C and CMKESD membrane. The AgNPs immobilized and non-immobilized membranes were contacted with 0.017 M and 0.5 M saline solutions and 0.25, 50 ppm humic acid solutions for 24 h, and the ion exchange capacity and swelling degree values were measured. It was observed that the values were lower in the silver nanoparticle immobilized membranes. Silver nanoparticle immobilized pore filling membranes were prepared with dip-coating method. Swelling degree and ion exchange capacity values were lower than the pore-filling membrane.

Keywords: Anion exchange membrane, dip coating, pore filling membrane, silver nanoparticle, reverse electrodialysis

ÖNSÖZ

Tez çalışması Concert Japan kapsamında TÜBİTAK (Proje No: 118M804) tarafından desteklenmiştir. Tez çalışmamın planlanmasında, araştırılmasında, yürütülmesinde ve tamamlanmasında ilgi ve desteğini esirgemeyen, engin bilgi ve tecrübelerinden yararlandığım, yönlendirme ve bilgilendirmeleriyle çalışmamı bilimsel temeller ışığında şekillendiren değerli hocalarım Prof. Dr. Nalan Kabay ve Doç. Dr. Enver Güler'e sonsuz teşekkürlerimi sunarım.

İZMİR

…/…/2023

Mine ETİ

TABLE OF CONTENTS

LIST OF FIGURES

Figure Page

LIST OF TABLES

INDEX OF SYMBOLS AND ABBREVIATIONS

Symbols	Explanation
α	Permselectivity
σ	Blend ratio
ν	Excess diamine ratio

Abbreviations

EDR	Excess diamine ratio
BR	Blend ratio
SD	Swelling degree
IEC	Ion exchange capacity
RED	Reverse electrodialysis
ICP-MS	Inductively coupled plasma mass spectroscopy
XPS	X-Ray photoelectron spectroscopy
AgNP	Silver nanoparticle
AEM	Anion exchange membrane
PFAEM	Pore filling anion exchange membrane
AgNP PFAEM	Silver nanoparticle immobilized pore filling anion exchange membrane

CHAPTER 1

1. INTRODUCTION

1.1. Salinity Gradient Energy (Blue Energy)

The combustion of fossil fuels has various detrimental impacts on the surrounding environment, which encompass the emission of greenhouse gases and the depletion of finite resources. As a direct result of this, there is a greater demandfor energy sources that are both renewable and environmentally friendly. At present, sustainable energy conversion technologies such as solar power, wind energy, biomass utilization, and hydroelectricity have gained significant popularity as effective and environmentally friendly alternatives (Post et al., 2007). Salinity gradient energy has an estimated worldwide potential of 1.4-2.6 TW, making it a highly attractive and vital resource. (Pawlowski, 2015).

Salinity gradient is created when two bodies of water with different salt concentrations are deliberately mixed together. It's different from solar and wind power in that it can be used wherever a river empties into the sea. (Simoes et al., 2020).

Chemical potential (concentration difference) is employed in the salinity gradient energy to produce electricity. There are several techniques to produce blue energy such as reverse electrodialysis (RED), pressure retarded osmosis (PRO) and capacitive mixing (CapMix) (Silva et al., 2016).

PRO and RED technologies perform differently in terms of power generation because the working theories, operational factors, and membrane characteristics of the their technologies differ. In PRO, water flows across a semipermeable membrane, with osmotic pressure difference serving as the propelling force. In RED, driving force produces a Nernst potential. The movement of ions generates an electric current, I, by moving an electrode solution between the anode and cathode. The external load of resistance, R_L, then turns thiscurrent into electrical power (Yip and Elimelech, 2014). The CapMix technique utilizes a pair of activated carbon electrodes with porous structures. In order to finish the mixing process, a super capacitor is used in this technology. The CapMix technologies comprise energy extraction by “Capacitive Double Layer Expansion” (CDLE) and “Capacitive Donnan Potential” (CDP). In CDLE, external power supply is used and electrodes are presented in the electrolyte,

while in CDP, driving force is Donnan potential and on the outermost part of electrodes, ion exchange membranes are placed. This technology differs from PRO in that it is not mechanical, and from RED system in that it does not contain redox reaction (Liu, 2015).

1.2. Reverse Electrodialysis System (RED)

RED is a prospective technology for the generation of energy from salinity gradients, offering greater power density and functionality than other methods. (Tristan et al., 2020; Tian et al., 2020). Vermaas et al. (2013) demonstrated clean energy generation using capacitive electrodes in RED. Although Pattle submitted the first RED study in 1954 (Pattle, 1954), research on this technology was halted for some time due to poor membrane performance. However, in recent times, there has been a significant increase in research focusing on the development of membrane synthesis specifically for the application of reverse electrodialysis (RED) (Güler et al., 2012, 2013; Cho et al., 2017; Fan and Yip, 2019).

Similarities in structure exist between the RED system and traditional electrodialysis (ED). The fundamental distinction lies in the contrasting characteristics of the two systems that while the ED system receives a feedsolution of the same composition in each compartment, the RED system is fed with two separate solutions of differing salinities (Figure 1.1) (Tedesco et al., 2016).

The membrane stack utilized in RED consists of ion-exchange membranes (IEMs) positioned between electrodes to form cell pairs. Each cell pair is made up of a cation exchange membrane (CEM) and an anion exchange membrane (AEM). The salinity differential on either side of the membrane causes ions to migrate across it in opposing directions. Only cations, such as Na+ ions, and anions, such as Cl- ions, can flow through CEMs and AEMs, respectively. The movement of these ions causes a potential difference in the cell pair. The redox pairs in the electrode section, which are also referred to as the "electrode solution," play an extremely significant role in the transformation of the the flow of ionic current converted into the electrical current. The anode and cathode are constantly swapping places, and the solution between them is being circulated.The transfer of electrons is made possible by an external circuit that connects the

anode to the cathode. This creates an electrical current, which in turn provides electrical power (Güler et al., 2013; Güler and Nijmeijer, 2018).

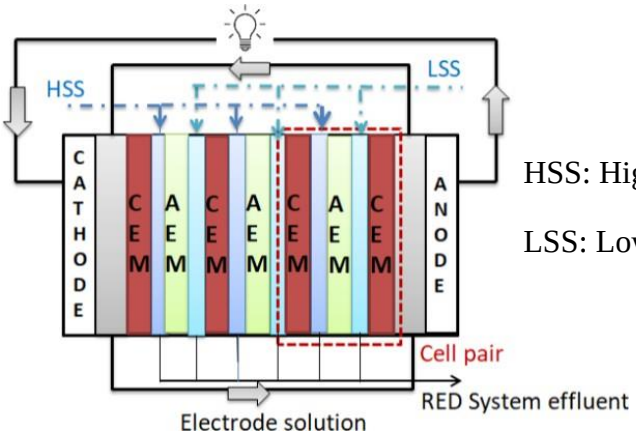

Figure 1.1. A RED system (Eti et al., 2022)

The current-voltage relations (I-V), current density and power density values are evaluated during RED tests. Open circuit voltage (OCV) is defined as the maximum potential difference when there is no current and the circuit is not closed. The potential difference across a membrane can be determined by Nernst equation as given in Equation 1.1 :

$$E_{OCV} = N\frac{2\alpha RT}{zF}\ln(\frac{a_c}{a_d}) \qquad \text{Equation 1.1}$$

where α is the average membrane permselectivity of membrane pairs (-), N is the number of membrane cells (-), R is the gas constant (8.314 J/mol.K), T is the absolute temperature (K), z is the electrochemical valence, F is the Faradayconstant (96485 coulombs/mol), a_c is the activity of the concentrated salt solution (mol/L) a_d is the activity of the diluted salt solution (mol/L). Increasing the concentration ratio $(\frac{a_c}{a_d})$ leads to higher salinity gradient, which increases the voltage resulting in higher output.

The power generated (W) as Watt is found by multiplication of the pre- determined current values (I) with corresponding potential differences (V), calculated by using Equation 1.2.

Power density is defined as the energy generated per membrane area (A), calculated by using Equation 1.3:

$$W = V \quad I \qquad \text{Equation 1.2}$$

$$P = \frac{W}{2AN} \qquad \text{Equation 1.3}$$

where P is power density (W/m^2), W is electrical power (W), A is active membrane area (m^2) and N is the number of membranes (Güler et al., 2013).

Over the course of the last decade, there has been a rise in the total number of RED-related publications (Mei and Tang, 2018). The performance of the RED system is greatly influenced by operational conditions, specifically the properties of the feed solution (Othman et al., 2022), feed flow velocity (Ortiz-Martinez et al., 2022), temperature (Mehdizadeh et al., 2019), ion exchange membranes (Abidin et al., 2022), spacers (Li et al., 2022, Mehdizadeh et al., 2019), and fouling (Vital et al., 2021). The power density plays a crucial role in determining the performance of the RED system, as it exhibits an inverse relationship with the membrane area. A high power density is necessary for the system to be economically viable because membrane area directly correlates to the cost of establishing a power plant. (Veerman, 2011).

Ciofalo et al. (2019) conducted a study on optimizing the net power density in RED by examining the effect of different flow velocities and concentrations. Similarly, Imedio et al. (2019) investigated the performance of salinity gradient-powered RED under different operating conditions such as flow rate, concentration, and temperature. They evaluated important parameters such as the open circuit voltage (OCV), internal resistance (Ri), and gross power (P). Post et al. (2007) showed that raising the concentration of the high salinity stream from 0.5 M to 5 M can enhance the power density by up to ten times. Furthermore, the temperature of the feed solution is a significant parameter in reverse electrodialysis (RED) applications as it impacts the conductivity of both the high and low concentration compartments (Mei and Tang, 2018). The study of Daniilidis et al. (2014) reported that the permselectivity value decreased to 68% at

60°C. However, power performance at 60°C was greatly enhanced in another study (Mei and Tang, 2018). Finally, the flow velocity of the system is also important as increasing it reduces electrical resistance but increases the need for pumping energy. "The ideal flow velocity is determined by various factors, including stack design, membrane thickness, spacer geometry, and operational conditions like the concentration of the feed solution (Mei and Tang, 2018).According to Tedesco et al. (2015), the flow velocity should be maintained at 1 cm/s to maximize the net power density.

1.3. Motivation

In recent years, as the effects of global warming and climate change have accelerated, there has been a worldwide increase in interest in carbon-free renewable energy technologies. Active research is being conducted on salinity gradient power generation, among other eco-friendly renewable energy technologies. Power generation from a salinity gradient has the advantage of being less susceptible to environmental factors and having less pronounced power swings than competing energy technologies like solar and wind. The membrane based salinity gradient power generation technology is RED. In RED, electricity is generated via the direct conversion of chemical energy. The IEM is one of the critical component that determine the performance of RED power generation. The main motivation in this thesis study was to support the use of renewable energy sources and contribute to efforts in the development of composite anion exchange membranes.

1.4. Thesis Overview

The main objective of this PhD thesis was to develop AEMs for salinity gradient production by RED.

The details of each chapter in thesis were described below:

i. In Chapter 2, preparation of AEMs by solution casting technique followed by solvent evaporation and their characterization were explained.
ii. In Chapter 3, preparation of silver nanoparticles (AgNPs) and immobilization of AgNPs onto AEMs by dip coating method were explained.
iii. In Chapter 4, preparation of pore filling anion exchange membranes (PFAEMs) were discussed.

iv. In Chapter 5, humic acid fouling tests for AEMs synthesized were explained. Ion exchange capacity and swelling degree of AEMs were measured.

1.4. Contributions to the Literature

The contributions to literature were listed below:

i. Chapter 2: In the literature AEMs are prepared with the blend ratios (BRs) ranging from 0.1 to 1.04 and excess diamine ratios (EDRs) ranging from 2.63 to 7.31 (Güler, 2014). In this study, EDR of 1, 1.62, 2 and 4, BR of .07, 1.23, 1.5, 2 were prepared.
ii. Immobilization of AgNPs to the PECH based AEM synthesized was performed for the first time.
iii. Chapter 3: Antibacterial activities of PECH based AEMs and AgNPs immobilized AEMs were studied for the first time in the literature.
iv. Chapter 4: PFMs with PECH based AEMs and AgNPs immobilized AEMs were prepared for the first time in literature.
v. Chapter 5: In the literature, humic acid contamination tests were performed with the RED test. In this study, adsorption studies were carried out to investigate the fouling effect by HA on ion exchange capacity and swelling of AEMs synthesized for the first time.

CHAPTER 2

PREPARATION AND CHARACTERIZATIONS OF AEMs

2.1. Introduction

The transfer of substances between two neighbouring compartments is generally facilitated or supported by a membrane, which functions as a selective barrier that interfaces with or separates them (Strathmann et al., 2006). When these barriers are functionalized with charged groups, they become known as ion exchange membranes (IEMs). The IEMs can be categorized into two types as cation exchange membrane (CEM), which contain negatively charged groups, andanion exchange membrane (AEM), which contain positively charged groups that are fixed to the polymer matrix (Mei and Tang, 2018).

Cations can freely pass through CEMs, but anions are unable to do so because of their negative charges. In AEMs, the positive fixed charges in the polymer matrix enable anion transport, while cations are blocked by this membrane. This behavior stems from the "Donnan exclusion" principle, in which only the counter ions can cross the membrane while the co-ions are retained by the fixed charges (Strathmann et al., 2006). Figure 2.1 depicts how current is transported by both ions in an electrolyte solution

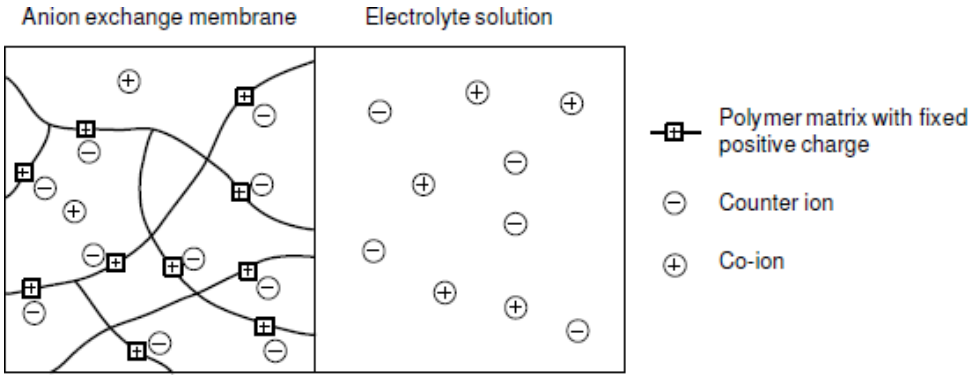

Figure 2.1. Anion exchange membrane ionic separation principle (Güler, 2014)

The IEMs can be classified as either homogeneous or heterogeneous, depending on the production method and structure of the membrane. The ion exchange component is directly incorporated into the polymer matrix of homogeneous membranes, which exhibit uniform charge distribution. Conversely,

heterogeneous membranes feature a non-uniform charge distribution (Jang et al., 2020).

Presently, commercial IEMs are primarily designed for electrodialysis (ED) applications and do not fully align with the specifications of the RED system. Ideally, IEMs utilized in the RED system should exhibit a high level of selective permeability (exceeding 95%), low electrical resistance, good mechanicalstrength, acceptable chemical stability, and low cost (Bolto and Jackson, 1984; Strathmann et al., 2006). To enhance their mechanical durability, current IEMs often contain reinforcing filler materials, rendering them relatively thick. In general, these membranes require modification to meet the specific demands of the RED system.

An alternative option for RED applications involves the production of pore-filling membranes with a relatively thin film thickness (<100 μm). These membranes are constructed by introducing polymer electrolyte structures into a finely-porous support material (Kim et al., 2015; 2016; Yang et al., 2019). Choi et al. (2020) have reported successful optimization of the RED stack design using ultra-thin (16-μm-thick) pore filling membranes with wave patterns, resulting in a maximum gross power density of 1.39 W/m^2. This implies that synthesizing a membrane with a particular thickness is feasible, depending on the thickness of the underlying porous support material.

To prepare AEMs for RED applications, a sequence of polymerization-chloromethylation-amination steps are required (Tongwen and Weihuen, 2001; Güler et al., 2012). However, because the chloromethylation reaction involves the emission of some hazardous compounds, it should be avoided during membrane formation. Using a polymer containing a chloromethyl group, such as polyepichlorohydrin polymer, is a good alternative (Güler et al., 2012). This thermoplastic material is both inexpensive and easy to synthesize and also offers high elastic properties that enhance the mechanical strength of the membrane when combined with supporting inert polymers. One option for creating a homogeneous mixture with these polymers in the same solvent is by utilizing polymers such as polyacrylonitrile. Crosslinking the polymer chains and creating a reticulated (network) structure is an additional approach that can be used in the pursuit of increasing the material's mechanical strength. Diamine crosslinkers,

such as DABCO-1,4-diazobicyclo[2.2.2]octane, can be used to both cross-link and ionize membranes in a single step, thereby providing a significant advantage in the preparation of AEMs (Güler et al., 2014). The reaction mechanism for this process is explained in Figure 2.2.

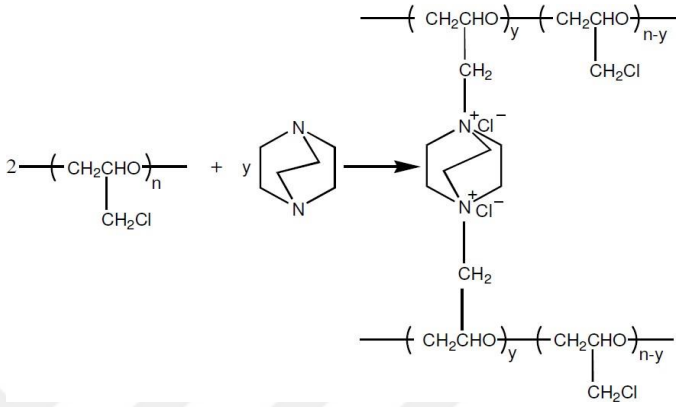

Figure 2.2. Amination and crosslinking mechanism of PECH polymer (Altmeier, 1998; Güler, 2014)

The IEMs are vital to the efficacy of RED processes (Tufa et al., 2018). The key characteristics and parameters that determine their effectiveness are the swelling degree, ion exchange capacity, fixed charge density, permselectivity, and area resistance (Jang et al., 2020). In electrochemical processes, low resistanceand high ionic conductivity are desirable membrane properties (Tufa et al., 2018). However, for optimal RED performance, the membrane's area resistance and permselectivity must also be considered (Jang et al., 2020).

To achieve optimal performance, IEMs must possess several desirable properties, including high permselectivity, low electrical resistance, good mechanical stability and high chemical stability (Nagarale et al., 2006). These properties are crucial for ensuring the prosperous operation of IEMs.

The aim of this work was to prepare AEMs suitable for RED applications with low swelling degree, high ion exchange capacity, fixed charge density, and low

fouling character. These properties are essential for achieving optimal RED performance and ensuring the long-term stability of the membranes.

2.2. Material and Methods

In this study, AEMs were fabricated from a polymer solution using the casting procedure, which was then followed by the evaporation of the solvent. Poly (epichlorohydrin), also known as PECH (37 weight percent chlorine, Osaka Soda Co., Ltd), was employed in the production of membranes as the active membrane material. Poly (acrylonitrile), also known as PAN (Mitsubishi Chemical Co.,Ltd.), was utilized as the inert polymer in this process. It was decided to employ the crosslinker 1,4-diazabicyclo[2.2.2]octane, also known as DABCO (Reagent Plus 99%, Sigma-Aldrich), because it had diamine functionality. This was done sothat the membranes would have improved mechanical stability. A solution containing dimethyl sulfoxide (DMSO) was used to dissolve the components ofthe base membrane.

In RED tests, EDR4-BR1.07, EDR2-BR0.6 as AEM, NEOSEPTA CMX and non commercial CMKESD membranes were used as CEMs. The characteristics of the membranes are provided in Tables 2.1 and 2.2.

Table 2.1. Technical properties of CMKESD membranes (Dlugolecki et al., 2010)

Composition of polymer matrix (%)	%30 Styrene, %68 PE, %2 DVB
Thickness (μm)	87±18
Ion exchange capacity (mmol/g)	1.95± 0.03
Permselectivity (%)	88± 2.3
Swelling degree (%)	38.1± 0.9
Area resistance ($\Omega.cm^2$)	0.95± 0.04

Table 2.2.Technical properties of commercial NEOSEPTA CMX membranes (Dlugolecki et al., 2010)

Ion exchange capacity (mmol/g)	1.64±0.01
Area resistance ($\Omega.cm^2$)	3.43±0.16
Permselectivity (%)	92.5 ± 0.6
Swelling degree (%)	21.5 ± 0.2
Thickness (μm)	181±2

2.2.1. Synthesis of AEMs

In the RED system, it is aimed to synthesize AEMs, which are difficult to synthesize from two types of membranes that represent the polymer electrolyte part, and whose properties (electrical resistance and selective permeability) are often not at the desired level as cation exchange membranes. These membranes will be further developed in the next stages, and they will be provided in a composite (containing antifouling particle) structure. At the same time, thesestructures are the basis for pore-filling membrane structures.

2.2.1.1. Preparation of Polymer Solutions

The membrane casting solution consists of three functional components: polyepichlorohydrin (PECH) as active polymer, polyacrylonitrile (PAN) as an inert polymer to improve the mechanical stability of the membranes and 1,4-diazobicyclo [2.2.2] octane (DABCO) used for crosslinking. The polymers were dissolved in DMSO solution. The AEMs were synthesized by pouring the polymer solution into petri dishes.

The quantity of PAN that was going to be added to the casting solution was changed in order to get various blend ratios of the membrane that was going to contain a particular quantity of active anion exchange polymer.

Blend ratio (σ) defined as the mass ratio of PECH to PAN in a mixture, as shown in Equation 2.1:

$$\sigma = \frac{m_{PECH}}{m_{PAN}} \qquad \text{Equation 2.1}$$

To facilitate the formation of the positively charged fixed groups necessary for ion exchange, DABCO was included into the casting solution for amination and crosslinking prior to interaction with the chloromethyl groups of PECH.

Excess diamine ratio (ν) represents the molar ratio between the amine compopnent in DABCO (m^d, mmol/g diamine) and chloromethyl groups in PECH solution (m^p, mmol/g-CH_2Cl) as shown in Equation 2.2:

$$\nu = \frac{m^d}{m^p} \qquad \text{Equation 2.2}$$

According to the experience gained from previous membrane studies with PECH, membranes made with values such as blend ratio 1 and diamine ratio 4 gave good results (Güler, 2014). In these studies, the blend ratio was tried to be 1 and above and the diamine ratio was up to 4, and optimum conditions were triedto be found. Accordingly, the membranes were produced with blend ratios of 1.07, 1.23 and diamine ratios of 1.62, 2 and 4. The blend ratios (BR) and excess diamine ratios (EDR) of the produced membranes are given in Table 2.3.

Table 2.3. Excess diamine ratio and blend ratio employed in experiments

Sample name	Exces Diamine ratio (EDR)	Blend ratio (BR)
EDR1-BR1.07	1	1.07
EDR1.62-BR1.07	1.62	1.07
EDR2-BR1.07	2.00	1.07
EDR4-BR1.07	4.00	1.07
EDR1.62-BR1.23	1.62	1.23
EDR1.62-BR1.5	1.62	1.5
EDR1.62-BR2	1.62	2

2.2.1.2. Synthesis of Quaternized PECH

The preparation of the active polymer solution began with the dissolution of PECH in DMSO. The preparation of the inert polymer solution involved first dissolving PAN in DMSO and then stirring the resulting liquid at 700 rpm on a

magnetic strirer for a period of 24 h while keeping the temperature at room temperature. (Figure 2.3). The amination solution was obtained by dissolving DABCO in DMSO with a stirring speed of 600 rpm on a magnetic stirrer for 3 h. Prior to synthesis, a pre-reaction step was carried out by keeping the casting solution in an oil bath at 80 ^{o}C for 30 minutes (Figure 2.4-a). This step causes a pre-reaction between PECH and DABCO without crosslinking in the PECH polymer and limits the eavporation of DABCO during amination process (Güler, 2012). The image of the casting solution after the reaction is shown in Figure 2.4-b.

Figure 2.3. Preparation of active and inert polymer solution

a **b**

Figure 2.4. Casting solution a) pre-reaction stage b) Image after reaction

After taking the casting solution from the oil bath, a certain amount of this solution was transferred to the petri dishes with diameters of 48 and 55 cm with a syringe and to keep the DABCO from evaporaing throughout the amination process, the petri dishes were covered with glass lids.

To finish the amination reaction and generate the crosslinks, the petri dishes were heated to 110ºC for 2 h in an oven under the atmosphere of nitrogen gas. After removing the covers from the petri dishes, the samples were placed in the oven at 130ºC for 30 min. while being surrounded by an atmosphere of nitrogen. The images of the polymer films formed after being removed from the oven are given in Figure 2.5-a. The polymer films were left in the 0.5 M NaCl solution in the petri dishes until they reached room temperature. After a few minutes, the film was carefully removed from the glass and immersed in a 0.5 M NaCl solution (Figure 2.5-b).

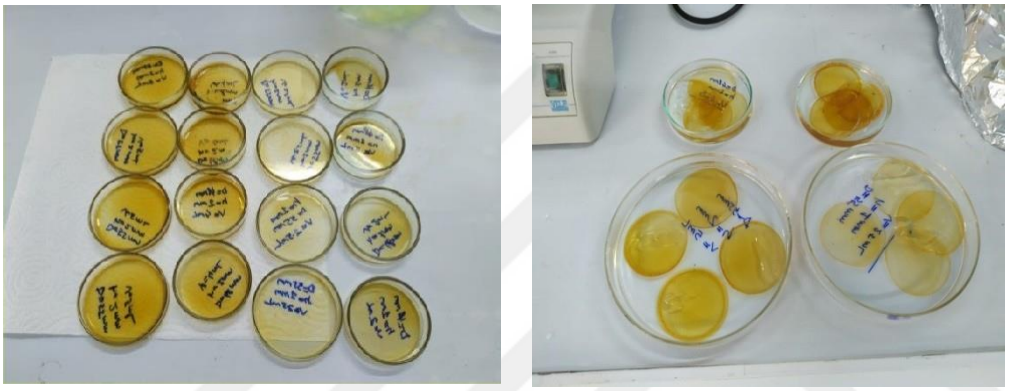

a **b**

Figure 2.5. a) Polymer films b) Membranes stored in sodium chloride solution

2.2.1.3. Large scale AEM synthesis for RED system

To evaluate the performance of the AEMs in the reverse electrodialysis (RED) system, a series of tests were conducted. Polyepichlorohydrin based membranes with the size of 15 cm×15 cm (required membrane size for the RED system were produced. While producing large-scale AEMs, the results of previous characterization tests were taken into account. Membranes with high ion exhange capacity and reasonable swelling degree have been identified.

First of all, casting glasses (20 cm×20 cm) required for the production of the membranes were provided and the edges of the glasses were set with a liquid gasket to prevent the membrane solution from leaking. The glass plate preparedfor membrane casting is shown in Figure 2.6.

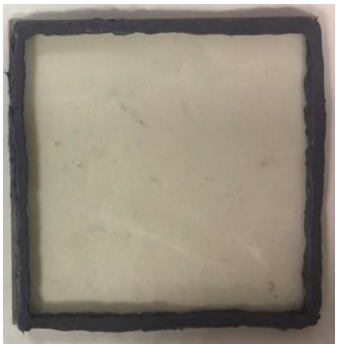

Figure 2.6. Appearance of cast glass closed with liquid gasket

In order to prevent the evaporation of DABCO in the solution, another glass cover was used as cover and the edges were covered with teflon tape to prevent leakage. The visual of the prepared glass cover is given in Figure 2.7.

Figure 2.7. The appearance of the glass cover with the edges taped with teflon tape

The prepared membrane casting solution was transferred from the center to the outside in a homogeneous manner with a 60 mL syringe (Figure 2.8). In order for the poured membrane solution to cross-link the active polymer with DABCO, the glass cover on the glass plate was opened after 2 h in the oven at 110˚C.Image of the mold before it is placed in the oven can be seen in Figure 2.9-a. The membrane solution was incubated for an additional 30 min for the solvent to evaporate. The prepared AEM was then removed from the oven and left for a while at room temperature to cool.

After pouring 0.5 M NaCl solution, the swollen membrane was taken from the casting glass, washed with deionized water and cut into the required size for the RED system and made ready for use.

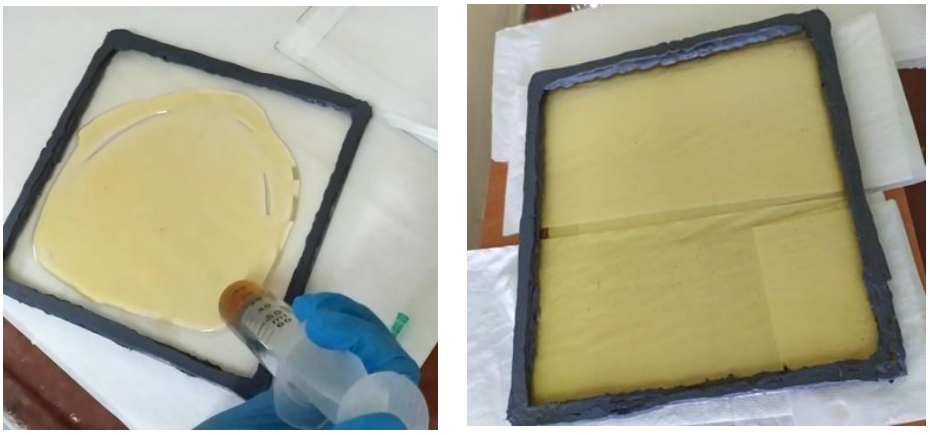

a b

Figure 2.8. Preparation of the membranes a) Transfer process of the casting solution to the mold b) Casting solution in the mold

After the mold came to room temperature, the membranes were left in 0.5M NaCl solution and the membranes were separated from the glass surface (Figure 2.9-b). Membranes (15 cm x 15 cm) were preserved in 0.5 M NaCl solution.

a b

Figure 2.9. Preparation of the membranes a) Image of the mold before it is placed in the oven b) Membrane leaving the mold

2.2.2. RED System

The RED system consists of the membrane stack, peristaltic pumps, tubing fittings, feed tanks, the electrode solution circuit and a potentiostat connected to the membrane stack. The IEMs form the membrane stack with CEM-AEM-CEM-AEM sequences (Figure 2.10). The membrane stack of the RED system consists of two end plates and electrodes (Ti-Ru alloy, 10 x 10 cm active area), CEMs and AEMs, gaskets and knitted materials called spacers.

Figure 2.10. Experimental setup of the RED system

A mixture of $K_4Fe(CN)_6$, $K_3Fe(CN)_6$, and NaCl, was used as the electrode solution and this solution was circulated between the electrode compartments. Thesystem allows to work with the desired number of membranes.

Electrochemical measurements in the RED studies were performed by a potentiostat device (Gamry Instruments Reference 3000) illustrated in Figure2.11.

Figure 2.11. Gamry potentiostat device

The EDR4-BR1.07 AEMs were tested in the available RED system after casting our AEMs in a proper size (15 cm x 15cm). In the RED tests, commercial NEOSEPTA CMX and CMKESD (interpolymer ion exchange membrane) CEMs were used together with the AEMs synthesized in this study. The technical specifications of NEOSEPTA CMX and CM-KESD (interpolymer ion exchange membrane)

The RED test were carried out with the salt ratio of 1:30 gNaCl/LH_2O in less saline solution:gNaCl/LH_2O in high saline solution. Three membrane pairs were employed with feed flow rates of 30, 75 and 120 mL/min.

2.3. Characterizations of AEMs

2.3.1. Scanning Electron Microscope (SEM)

SEM analysis was performed on produced AEMs to examine their outer layer topologies and pore design. The formation of pores in the membranes synthesized is practically undesirable as the porous membranes can leak the aqueous solutions. Therefore, it is important to observe the physical morphology of membranes by SEM. Before SEM analysis, the membrane samples were kept in a vacuum oven for one night at 30^oC. The membrane samples analyzed by SEM were prepared by freezing the membrane films in liquid nitrogen and splitting them manually. Membranes were covered with a thin layer of gold using EMITECH K550X device before the SEM image was taken. The SEM analysis of membranes were performed using the FEI QUANTA 250 FEG model SEM device at CMR of IzmirInstitute of High Technology.

2.3.2. Fourier Transform Infrared Spectroscopy (FTIR)

The FTIR analyses were performed to determine the successful completion of the amination reaction. It is aimed to see the amine groups in the synthesized membranes by the FTIR spectroscopy. Membranes were dried at 30 ^oC for 2 h in the oven before the measurements.

The chemical structures of the membranes were analyzed using Perkin Elmer Spektrum 100 Fourier Transform Infrared Spectrometer. Measurements were made using the ATR (Attenuated Total Reflection) module.

2.3.3. Ion Exchange Capacity

The ion exchange capacity (IEC) was determined using the titration method. The AEMs were transformed into their chloride ion (Cl^-) form by immersing themin a 3 M NaCl solution for a minimum of 15 h. After that, the membrane surfaces were washed with ultrapure water to eliminate the excess NaCl. A 0.1 M $AgNO_3$ solution was used to find out if the end rinse water has Cl^- ions or not. Tofacilitate the exchange of Cl^- ions in the membrane with SO_4^{2-} ions in the solution, the membranes were exposed to a 1.5 M Na_2SO_4 solution for a duration of 3 hours

following rinsing with ultrapure water. To determine the equivalence point, the sample solution was titrated with 0.1 M $AgNO_3$ solution containing Cl^- ions released.To obtain the titration end point, potassium chromate was used as an indicator and silver nitrate was added from a burette until a reddish brown color was obtained. Subsequently, the AEMs were subjected to drying in a vacuum oven at 30°C until they achieved a consistent weight.

The IEC value was calculated using Equation 2.3:

$$IEC = \frac{V_{AgNO_3}}{w_{dry}} x C_{AgNO_3} \qquad \text{Equation 2.3}$$

In this equation, V_{AgNO3} indicates the volume of $AgNO_3$ solution consumed in titration at the equivalence point, w_{dry}, dry membrane weight, and C_{AgNO_3} indicates the concentration of the $AgNO_3$ solution used.

2.3.4. Swelling Degree

When ion exchange membranes are exposed to water, the degree to which they swell provides an indication of the amount of water they contain. After removing the membranes from the salt solution, rinsing them with ultrapure water, and then allowing them to soak in ultrapure water for a period of time, the degree of swelling could then be calculated. After extracting the membranes from the ultrapure water, their wet weights were determined, and then the membranes were dried in a vacuum oven at 30 ^oC until they attained a weight that was constant.

The swelling degree, $SD(g_{H2O}/g_{dry\ membrane})$ was determined using Equation 2.4:

$$SD = \frac{m_{wet} - m_{dry}}{m_{dry}} x100\% \qquad \text{Equation 2.4}$$

In this equation, m_{wet} and m_{dry} are the wet and dry weights of the membrane, respectively.

2.3.5. Fixed Charge Density

Fixed charge density was calculated by dividing the IEC by the degree of swelling (Equation 2.5).

$$C_{fix} = \frac{IEC}{SD}$$ Equation 2.5

In Equation 2.5, (C_{fix}) is the fixed charge density (mmol/g-H_2O), IEC is the ion exchange capacity (mmol/g-dry membrane) and SD is the swelling degree (m_{wet}-m_{dry}) /m_{dry}, (g-H_2O/g-dry membrane).

2.3.6. Electrical conductivity

A potential difference is created, when two solutions of differing salinities are combined, which can then be used to generate electricity through the RED process. For this, the IEMs in the stack should have the highest electrical conductivities available. Based on the IEMs' area resistance measurements, electrical conductivity values were computed in this study.Values of the area resistances were multiplied by the thickness values of the membranes (cm) to find the electrical conductivity values of the IEMs. The thickness of the membrane was determined using a digital micrometer (Mitutoyo, Japan). Electrochemical impedance spectroscopy was used to determine the area resistance between platinum electrodes with a Zahner Zennium potentiostat. Prior to conducting the measurements, the AEMs were placed in an oven and kept at a temperature of 22°C for a duration of 18 hours. Measurements were made in University of Cantabria, Spain.

2.3.7. Measurements of area resistance

Area resistance measurements were made using a Zahner Zennium potentiostat device (Figure 2.12). Resistance measurements were measured by electrochemical impedance spectroscopy method using platinum electrodes. The membranes placed between the platinum electrodes are shown in Figure 2.13. Before measurements, samples were kept in an oven at room temperature for 18 h (Figure 2.14). Measurements were made in University of Cantabria, Spain.

Figure 2.12. Zahner Zennium Device

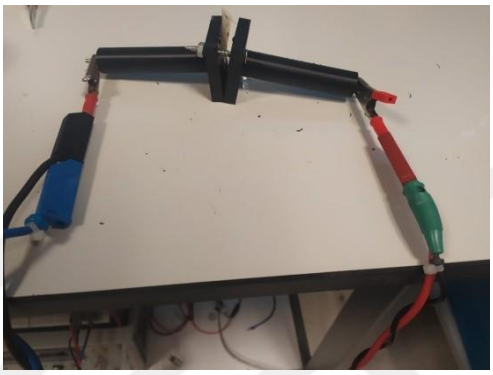

Figure 2.13. AEM placed between two electrodes

Figure 2.14. Samples kept in the oven for 18 h in NaCl solution

2.4. Results and Discussion

2.4.1. Effect of Excess Diamine Ratio and Blend Ratio on the Synthesis of Anion Exchange Membranes

The effects of diamine and blend ratio on the swelling degree and ion exchange capacity of the synthesized AEMs are shown in Figures 2.15 and 2.16, respectively. At the same diamine ratio, the ion exchange capacity and swelling ratio increased as the amount of active polymer and the blend ratio increased (Figure 2.15). This is expected and shows that the amination process in the

formed membranes is even more successful with the increasing active PECH polymer in the membrane. However, the fact that the swelling degree is above 100% has created the prediction that there may be a disadvantage in terms of mechanical strength for some membranes. This gives us information about the upper limit of the usable blend ratio. Thus, the selected blend ratio was suitablefor the study and enabled these effects to be seen.

It is anticipated that the crosslinking process, and consequently the quaternization (degree of positive loading) of the membrane, would escalate with an increase in the diamine ratio. As the number of charged functional groups in a membrane increases, so does its ability to exchange ions. Since DABCO facilitates the formation of crosslinked polymer chains, it also regulates the water retention properties of the AEMs. In this study, the effect of DABCO amount on membrane behavior was examined.

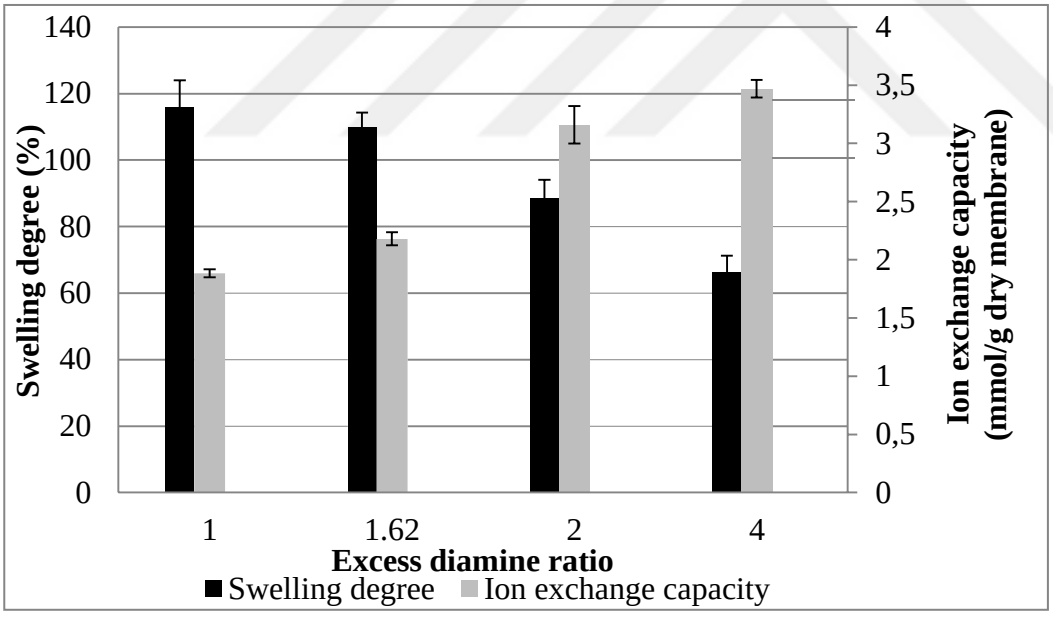

Figure 2.15. The effect of excess diamine ratio on swelling degree and ion exchange capacity of the AEMs synthesized (BR:1.07)

As can be seen in Figure 2.15, as the diamine ratio increases, the cross- linking ratio will increase and the swelling capacity of the membranes will be limited, and a decrease in the degree of swelling has been observed. On the other hand, as the quaternary ammonium groups increased with the increase of diamine ratio, the ion exchange capacity also increased.

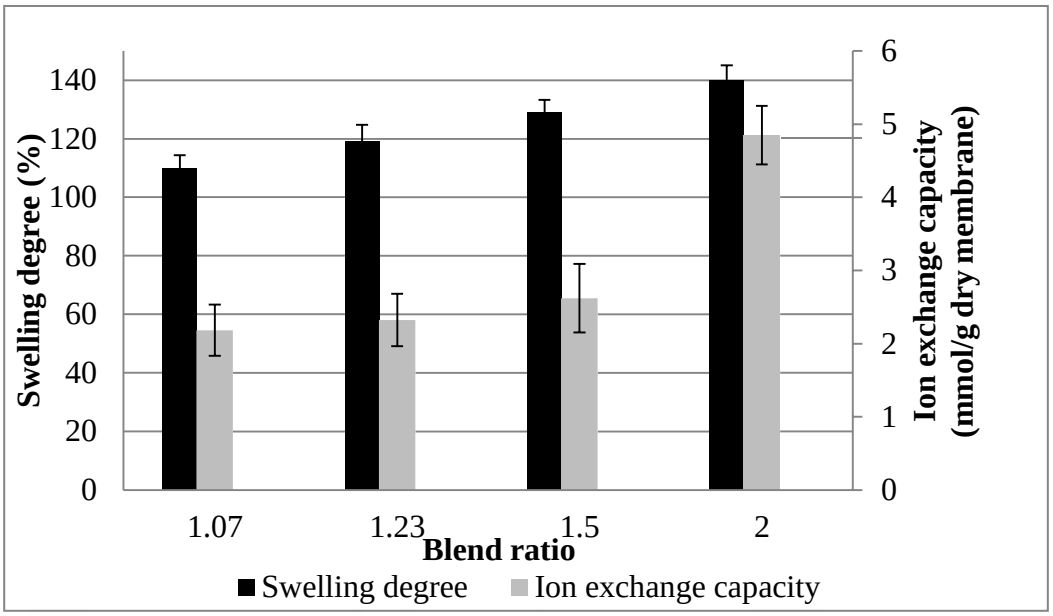

Figure 2.16. The effect of blend ratio on swelling degree and ion exchange capacity of the AEMs synthesized (EDR:1.62)

The blend ratio is defined as the mass ratio of PECH over Pan and expresses the ratio of actibe polymer per unit of inert polymer, by mass. An increase in the blend ratio means that the amount of active polymer PECH increases compared to the inert polymer. Thus, relatively more functional groups are formed in the membranes, which means that the membrane retains more water. Membrane with increased water holding capacity swells. This is undesirable at very high values, because the swelling degree reduces the mechanical strength of the membrane.

The ion exchange capacity also depends on the PECH amount of the membrane. The ion exchange capacity of the membrane with more functional groups increases if the quaternary ammonium groups are high. This is actually a sign that membrane will hold more water. The main purpose of these studies is to determine the behavior of the formed membranes in which compositions.

The swelling degree, ion exchange capacity, and fixed charge density values of the AEMs synthesized in different compositions are given in Table 2.4.

Table 2.4. Physicochemical properties of AEMs synthesized

Membrane	Swelling degree (%)	Ion exchange capacity (mmol/g dry membrane)	Fixed charge density (mmol/g H_2O)
EDR1-BR1.07	116	1.88	1.62
EDR1.62-BR.07	110	2.18	1.98
EDR2-BR1.07	88	3.16	3.57
EDR4-BR1.07	66	3.47	5.24
EDR1.62-BR1.23	119	2.32	1.95
EDR1.62-BR1.5	129	2.62	2.03
EDR1.62-BR2	140	4.85	3.46

2.4.2. SEM Analysis of AEMs Synthesized

In order to investigate the morphology of the prepared PECH AEMs, a SEM analysis approach was applied. Figure 2.17 displays SEM images of AEMs at magnifications of 2500, 5000, and 10000x that were acquired after the solvent evaporation process had been carried out. The EDR in these samples was 4, and the BR was 1.07.

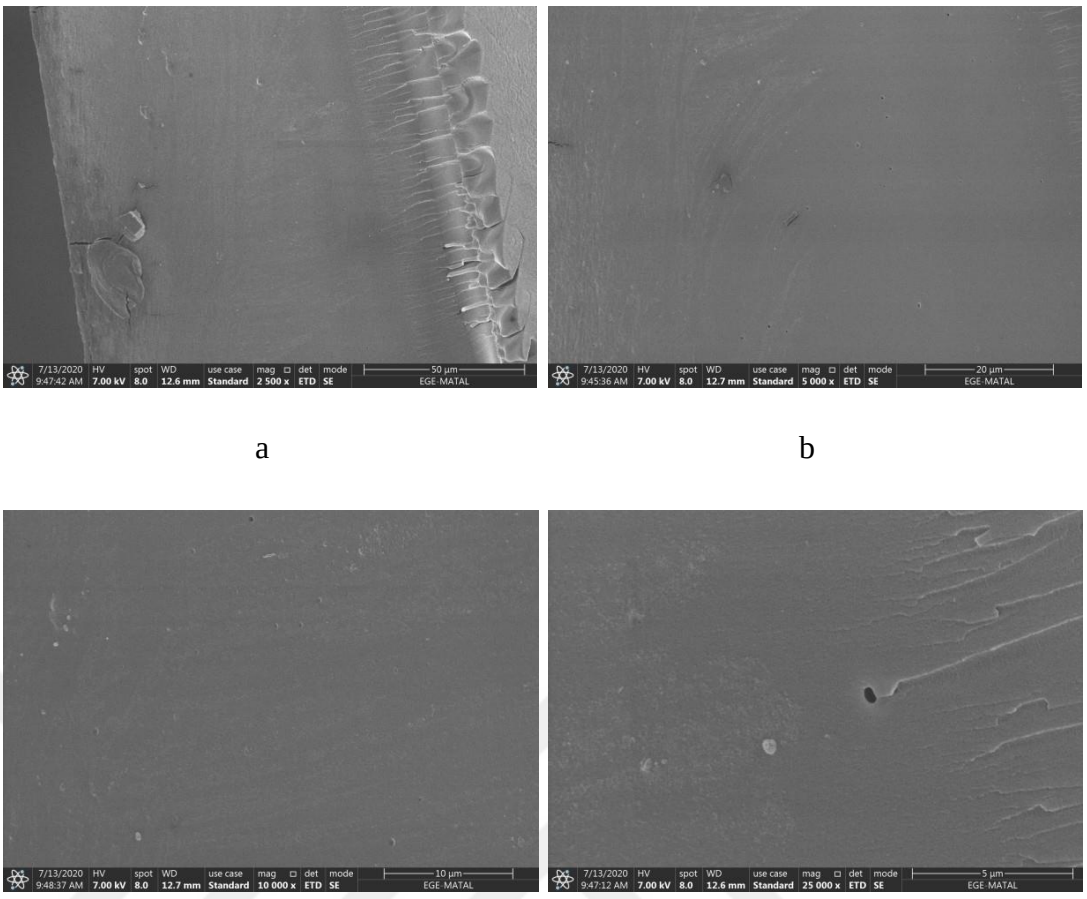

Figure 2.17. Cross section SEM images of EDR4-BR1.07 AEM a) 2500x b) 5000x c) 10000x d)25000x

In Figure 2.17 (a), near the membrane's surface, wrinkly-looking structures were observed. The evaporation of the solvent causes these uneven formations. The high-resolution pictures make it clear that the membrane structure has no actual pores. The membranes' lack of pores proves that the solvent evaporation technique succeeded. Similar recognition of the dense structure of poreless AEMs was found in the research of Güler (2014). According to Lopez et al. (2019), AEM displays a highly uniform, pore-free surface.

2.4.3. FTIR Analysis

The reactivity of PECH polymer chains with DABCO was confirmed by FTIR analysis. FTIR spectra were given in Figure 2.18. A peak, representing the nitrile group (CN) of the inert polymer PAN, was seen at a wavelength of 2240 cm^{-1} after two different polymers were combined and blended. Compared with the spectrum of the PECH polymer (Figure 3.4 (a)), two new peaks were observed at

1640 cm^{-1} representing the C-N bond and 3400 cm^{-1} representing the O-H group. Peaks at 2877 cm^{-1},1452 cm^{-1} and 1108 cm^{-1} indicate that CH_2-, CH_2 and C-O-C groups, respectively.

As seen in Figure 2.18, the peaks observed at 1640 cm^{-1} and 2240 cm^{-1} indicate that the amination was carried out and thus it is clearly seen that the integration of PAN has been successful. The prominence of the peaks observed at 3400 cm^{-1} indicates the presence of water molecules.

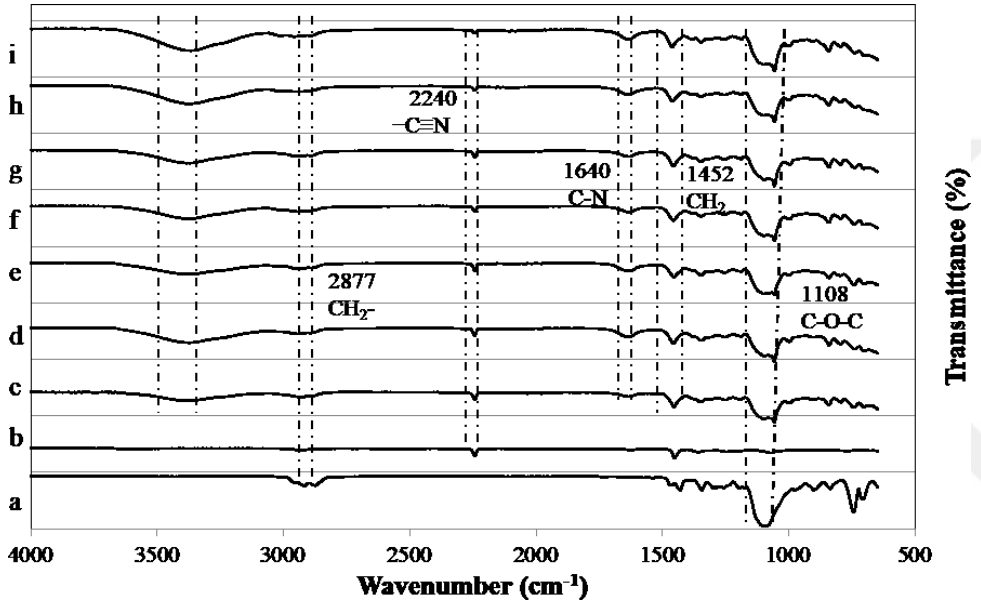

Figure 2.18. FTIR spectra of (a) PECH (b) PAN (c) EDR4-BR1.07 (d) EDR2-BR1.07 (e) EDR1.62-BR1.07 (f) EDR1-BR1.07 (g) EDR1.62-BR1.23 (h) EDR1.62-BR1.5 (i) EDR1.62-BR2 samples

2.4.4. Electrical conductivity results

Results of the electrical conductivity values of AEMs synthesized in this study are given in Table 2.5. The highest conductivity value was obtained with the membrane with EDR value of 4 and BR valu$\pm A \quad \pi r^2$e of 1.07. Commercial AEM (Nafion 212) has a conductivity of 3 mS/cm at 30 °C, as reported by Germer et al. (2015). As the temperature increased, they saw the conductivity rise to 8 mS/cm. Diaz and Kamcev (2021) determined the conductivity of AEMs with 152 μm of thickness as 7 mS/cm. Tuan et al. (2020) measured the conductivity of commerical AEM (AHA, Astom Corporation, Japan) as 4.5 mS/cm at 30 ^oC, that value reached up to 22 mS/cm in quaternized polyepichlorohydrin membranes

crosslinked with polyaryleneter ketone. Sarode (2015) examined the solvent and ion transport in AEMs under humidified conditions and obtained the membrane conductivity as 9 and 10 mS/cm at 30 ^{o}C and 95% relative humidity. Pandey et al. (2015) found the electrical conductivity value as 7 mS/cm for the electron beam grafted polyethylenetetrafluoroethylene based AEMs at 30 ^{o}C and 95% of relative humidity, while Vandiver (2015) determined the electrical conductivity values as 4.8±0.1 and 3.3 ±0.2 mS/cm in AEMs (PFMA, methyl ammonium and PFTMBA, trimethylbenzyl ammonium). In this study, electrical conductivity values of synthesized AEMs are consistent with the literature findings.

Table 2.5. Results of the electrical conductivity values of AEMs

Membrane	**Thickness (µm)**	**Electrical conductivity (mS/cm)**
EDR1.62-BR1.07	134	3.5497±0.156
EDR1.62-BR1.23	115	3.3055±0.487
EDR1.62-BR1.5	149	4.77260.102
EDR1.62-BR2.0	80	2.8050±0.248
EDR1-BR1.07	155	4.4993±0.185
EDR2-BR1.07	138	3.6031±0.735
EDR4-BR1.07	209	6.4427±0.100

2.4.5. Area resistance measurements results

Results of the area resistances measurements for AEMs are given in Table 2.6. At the same diamine ratio, as blend ratio increases, area resistance values decrease. At the same blend ratio, as the diamine ratio increase, area resistance values decrease. The diamine ratio refers to the ratio of DABCO, a tertiary amine that imparts a positive charge to the membrane and crosslinker, to the totalnumber of chloromethyl groups present. Consequently, the magnitude of these two parameters is directly correlated with the quantity of positive functionalgroups that will be incorporated into the membrane structure. Hence, the observedreduction in area resistances aligns with our anticipated outcomes. The ability to diminish area resistances is an advantageous trait, as it has the potential to enhance ion transport within membranes.

Table 2.6. Results of the area resistance measurements

Membrane	Thickness (μm)	Area resistance (Ωcm^2)
EDR1.62-BR1.07	134	3.775±0.156
EDR1.62-BR1.23	115	3.479±0.487
EDR1.62-BR1.5	149	3.122±0.102
EDR1.62-BR2.0	80	2.852±0.248
EDR1-BR1.07	155	3.445±0.185
EDR2-BR1.07	138	3.830±0.735
EDR4-BR1.07	209	3.244±0.100

* EDR: Excess diamine ratio; BR: Blend ratio

2.4.6. RED Tests with EDR4-BR1.07 Membrane

RED tests were done with EDR4-BR1.07 membrane. Technical properties of EDR4-BR1.07 membrane is given in Table 2.7. This membrane was prepared with solution casting followed by solvent evaporation technique.

Table 2.7. Technical properties of EDR4-BR1.07 membrane

Ion exchange capacity (mmol/g dry membrane)	3.47
Swelling degree (%)	66.00
Thickness (μm)	140±60
Fixed charge density (mmol/g H_2O)	5.258
Area resistance (Ωcm^2)	3.244

In this study, the ion exchange capacity and swelling degrees of large-scale and small-scale membranes were compared. Characterization of small and large scale membranes are given in Table 2.8. Thickness of large scale membrane is 250±50 μm while thickness of the small scale membrane is 140±20 μm. Swelling degree value is very high for large scale membranes because of the thickness of the membrane and there is no supporting material (porous reinforcement) so swelling increases.

Table 2.8. The characteristics of membranes at both small and large scales

Membrane	Membrane structure	Thickness (μm)	Ion Exchange Capacity (mmol/g-dry membrane)	Swelling Degree (%)
Small scale EDR4-BR1.07	Diamine ratio:4 Blend ratio:1.07	140±20	3.47	66.00
Large scale EDR4-BR1.07		250±50	3.42	90.00

In RED tests, large-scale AEMs synthesized were paired with commercial NEOSEPTA CEMs and tailor made CMKESD membranes. As a parameter, flow velocity of feed solutions were 30, 75 and 120 mL/min. Number of membrane pair was 3 and salt ratio was 1:30 (1 gNaCl/LH_2O: 30 gNaCl/LH_2O). .

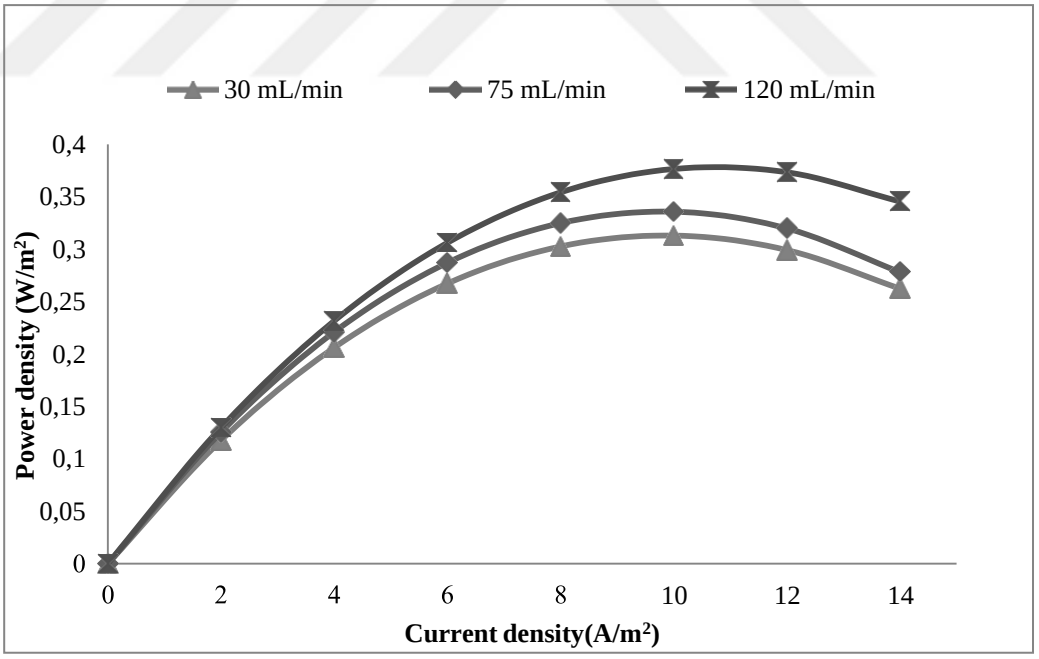

Figure 2.19. Power density vs. current density plots obtained with EDR4-BR1.07 and NEOSEPTA CMX membrane pairs at different volumetric flow rates

Power density vs. current density graph with ER4-BR1.07 and NEOSEPTA CMX CEMs membrane pairs at different feed flow rates are illustrated in Figure 2.19. The power density values demonstrated an upward trend as the flow rate

increased. The highest power density value of 0.376 W/m^2 was achieved at a flow rate of 120 mL/min.

Power density vs. current density graphs with EDR4-BR1.07 and CMKESD CEMs membrane pairs are shown in Figure 2.20. The highest power density value at 120 mL/min flow rate is achieved with EDR4-BR1.07 AEMs and CM-KESD CEMs with a value of 0.429 W/m^2.

All results of the RED tests are summarized in Table 2.8. Highest power density obtained with 3 pairs of NEOSEPTA CMX CEMs and NEOSEPTA AMX AEMs was 0.395 W/m^2 with a flow rate of 30 mL/min. A 0.190 W/m^2 of power density value was achieved with 3 pairs of CMAESD AEMs and CMKESD CEMs with a volumetric flow rate of 30 mL/min.

Although Neosepta CMX membrane has a high ion exchange capacity,higher power density was considered to be related to the differences in permselectivities and thicknesses of NEOSEPTA CEMs coupled with EDR4-BR1.07 AEMs.

In the study performed with tailor-made CM-AESD and CM-KESD membrane pairs using the volumetric flow rate of 75 mL/min, the lowest power density value was observed because of the lower ion exchange capacity and higher thickness values of CM-AESD and CMKESD membranes than ER4- BR1.07 AEM synhesized in this study. Thickness of the CM-AESD, CM-KESD and ER4-BR1.07 membranes are 300μm and 211 μm and 250 μm, respectively.

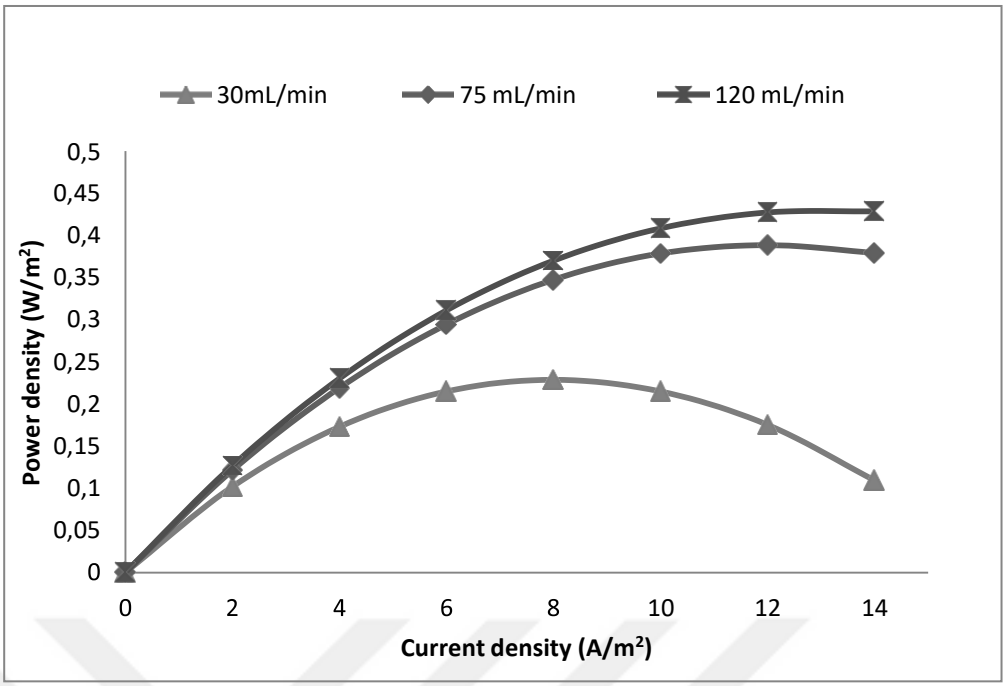

Figure 2.20. Power density vs. current density plots with EDR4-BR1.07 and CMKESD membrane pairs at different volumetric flow rates.

Power density value with NEOSEPTA AMX and NEOSEPTA CMX couple is better than CM-AESD and CM-KESD membrane pair. Also power density value with EDR4-BR1.07 and NEOSEPTA CMX couple is better than EDR4- BR1.07 and CMKESD pair because of the lower swelling degree value (Table 2.9).

Table 2.9. Results of the RED tests

Membranes	**Salt ratio (gNaCl/LH2O in low saline solution:gNaCl/ LH2O in high saline solution)**	**Number of membrane pair**	**Volumetric flow rate (mL/min)**	**Maximum power density (W/m^2)**	**Open circuit voltage (V)**
CM-AESD-CM-KESD	1:30	3	30	0.190	0.425
NEOSEPTA AMX and NEOSEPTA CMX			75	0.395	0.435
			120	0.304	0.435
EDR4-BR1.07 and NEOSEPTA CMX			30	0.313	0.395
			75	0.336	0.422
			120	0.376	0.431
EDR4-BR1.07 and CMKESD			30	0.229	0.349
			75	0.388	0.398
			120	0.429	0.414

2.4.7. Short and Long Terms RED Tests

The power density-current density plots obtained in short and long term RED studies are given in Figures 2.21 and .22. The power density for short duration runs increased with increasing feed flow rate (Figure 2.21).

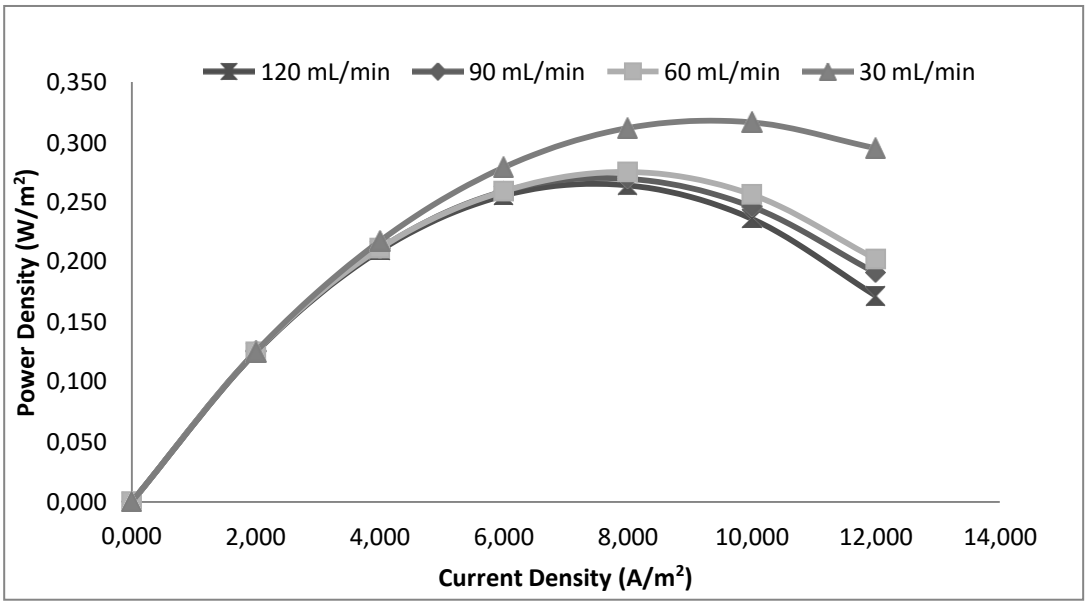

Figure 2.21. Current density vs. power density plots of short-term operation of PECH-C AEMs paired with NEOSEPTA CMX CEMs

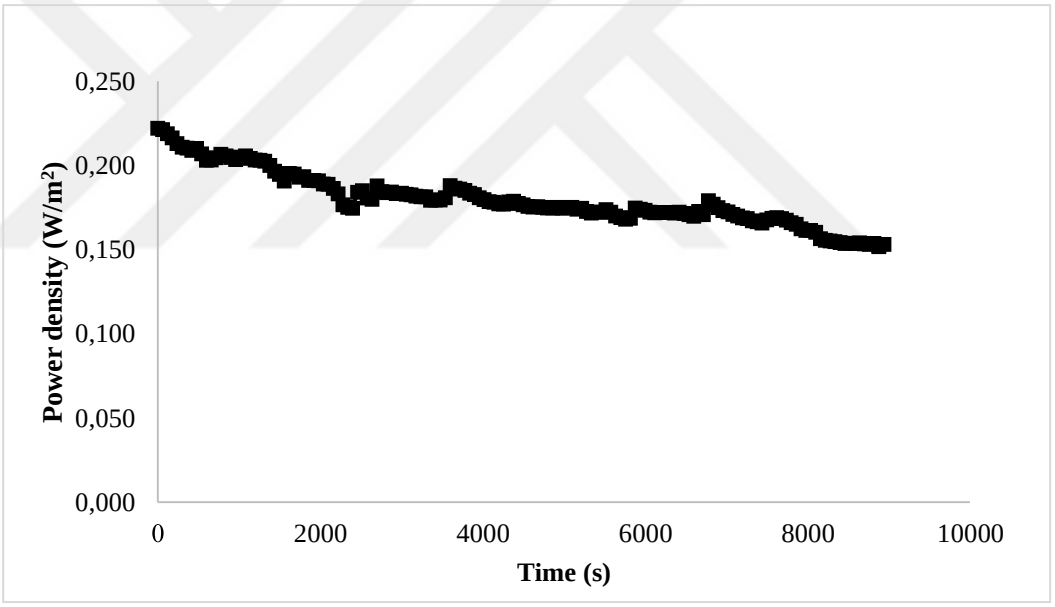

Figure 2.22. Power density versus time plots for long-term operation of PECH-C AEMs paired with NEOSEPTA CMX CEMs

2.5. Conclusion

In this study, eco-friendly AEMs were manufactured employing poly (epidochlorohydrin) (PECH) polymer, avoiding the toxic chloromethylation step. Membrane properties, such as area resistance, electrical conductivity, SD, and IEC of these PECH membranes were investigated for the excess diamine ratios of 1, 1.62, 2, and 4 units and blend ratios of 1.07, 1.23, 1.5 and 2. The optimum properties of AEMs were obtained with EDR4-BR1.07 membrane with the highest IEC (3.470 mmol/g dry membrane), the highest FCD (5.250 mmol/g H_2O), the lowest SD (66%), and the highest electrical conductivity (6.443 mS/cm). Testing the synthesized membranes for saline gradient energy recoveryin a RED stack, the performance of EDR4-BR1.07 AEM cupled with CMKESD CEMs exhibited the highest power density (0.429 W/m^2) at the feed flow rate of 120 mL/min.

CHAPTER 3

PREPARATION OF AgNPs AND IMMOBILIZATION OF AgNPs ONTO AEMS

3.1. Introduction

3.1.1. Modification of ion exchange membranes with nanoparticles

In the literature, dipping or dip coating method is widely used for the immobilization of nanoparticles on membranes. Dipcoating method emerges as a viable and suitable method, as it prevents the adhesion of microorganisms such as bacteria (or retards their adhesion) on the surface of nonporous membranes. Since microorganisms such as bacteria cannot penetrate the inner surface of dense and non-porous membranes, only a modification on the surface of the membranes will be sufficient and effective.The dipcoating method makes such a modification possible only on the membrane surface. In addition, it is simpler and more effective than other methods such as chemical or radiation inoculation, surface polymerization, physical mixing.

When the nanoparticles were added to the surface of membrane by dipcoating method, membrane reach the desired properties (fouling resistant, high ion exchange capacity and reasonable swelling levels). Thus, the final membranes will gain a composite structure and be prepared as a high-strength thin film. Surface modification is suitable for the purpose of the study, as micro-pollutants such as bacteria only act on the membrane surface.

Different surface modification methods have been used to control membrane hydrophilicity in terms of both permselectivity and antifouling properties (Kotoka et al., 2020). Nanoparticles are added to IEMs using solution blending, in situ polymerization, melt mixing, and sol-gel techniques. Solution blending is the most prevalent method employed in the creation of polymeric nanocomposites. In this process, the polymer is dissolved in a solvent prior to the addition of nanoparticles. With sonication or mixing, homogeneous distribution of nanoparticles throughout the polymer is accomplished. The solvent is subsequently eliminated (through phase inversion), and the nanoparticles are rearranged and encapsulated within the polymer to form mixed matrix membranes

(Alabi et al., 2018). It is an easy-to-reproduce method, which makes it suited for large-scale production.

Similar to the solution blending approach, in-situ polymerization utilizes monomers as opposed to polymers. Typically, polymerization is performed by diffusing an appropriate initiator or by using heat or ultraviolet light, resulting in additional effort and expense. The process of melt mixing requires no solvent. Nevertheless, it cannot be used with thermosetting polymers, which is a disadvantage. The in-situ sol-gel method involves the combination of a polymer with a nanoparticle precursor, such as tetraethoxysilane (TEOS) for silica or titanium dioxide, through hydrolysis and polycondensation of the precursor. The sol-gel process is generally more costly and time-consuming compared to solution blending due to the additional hydrolysis and polycondensation steps (Alabi et al., 2018).

Nanocomposite membranes are divided into two categories: mixed matrix and thin film. Nanocomposite membranes are fabricated by combining nanoparticles with polymer casting, dip coating, or pressure deposition (Jhaveri & Murthy, 2016). Nanoparticles were combined with a casting solution in order for Vatanpour et al. (2012) to produce a TiO_2-entrapped mixed matrix membrane, which was then used in an investigation of the fouling resistance of membranes. In another study, polyethersulfone (PES) / poly (vinyl alcohol) (PVA) / titanium dioxide (TiO2) composite nanofiltration membranes were produced by dippingthe membrane into solutions comprised of TiO_2 nanoparticles (Pourjafar et al., 2012). These membranes were then used to filter water. Using the nanoparticle solution dipping technique, Madaeni and Ghaemi (2007) investigated the characterization of anti-fouling self-cleaning reverse osmosis membranes coated with TiO_2 particles. Damodar et al. (2009) studied the fouling resistance of polyvinylidene fluoride membranes that were formed by integrating varied amounts of TiO_2 particles into the casting solution. The number of TiO_2 particles used ranged from 0% to 4% of the total weight of the casting solution. Overall, these studies demonstrate that different methods can be used to prepare nanocomposite membranes with various properties, depending on the specific materials and applications.

Silver is the most efficient nanoparticle against viruses, bacteria, and other eukaryotic organisms compared to zinc, titanium, copper, alginate, and gold (Sprick, 2017). In addition to its antibacterial capabilitiesThe application of AgNPs coating on AEMs resulted in improved selective permeability, ionic permeability, ionic flux, ionic conductivity, thermal stability, and membrane potential values in comparison to untreated membranes (Alabi et al., 2018).

The addition of nanoparticles to casting mixtures for membrane formation can significantly improve separation properties without sacrificing rejection, especially for less porous membranes (Sprick, 2017).

Polyvinylidene fluoride (PVDF) membranes grafted with silver nanoparticles were made in three simple processes by Li et al. (2013). Membrane fouling resistance was investigated after silver ions were bonded from silver nitrate using a PAA brush and subsequently reduced to nanoparticles using sodium borohydride. The fouling resistance of thin film polyamide composite membranes with silver nanoparticles placed on them using a polymer blending process was also studied (Lee et al., 2007). Another study looked into the effect of incorporating AgNPs into thin film composite membranes through blending witha polymer casting solution in an effort to reduce the likelihood of biological contamination (Yin et al., 2013). Antibacterial polyacrylonitrile membranes trapped with AgCl-TiO_2 xerogels were developed by Uz et al. (2020). Phase inversion is used to prepare the membrane in which nanoparticles are included viamixing with the polymer casting solution and fouling resistance is evaluated.

3.1.2.Composite ion exchange membranes for RED system

Composite ion exchange membranes made by incorporating inorganic materials into an organic polymer matrix are viable candidates for RED because they permit the transport of additional ion exchangeable functional groups by modifying membrane structure. In addition, organic-inorganic composites combine the distinctive properties of inorganic substances with those of organic substances and have garnered increasing interest for more than a decade due to their extraordinary synergistic properties (Hong and Chen, 2014). The use of nanocomposite IEMs in reverse electrodialysis (RED) applications was first explored in a study on CEMs by Hong and Chen in 2014. They compared this

nanocomposite membrane with a custom-made membrane and a commercial membrane in terms of electrochemical properties and power generation performance. Their findings suggest that nanocomposite CEMs have potential in RED power generation systems. In a later study, Tong et al. (2017) explored nanocomposite CEMs made of oxidized multi-walled carbon nanotubes (o-MWCNT) blended with sulfonated poly(2,6-dimethyl-1,4-phenylene oxide). They found that these membranes had significantly improved properties compared to those without o-MWCNTs.

Overall, these studies demonstrated the potential of nanocomposite IEMs in RED applications, particularly in the context of improving electrochemical properties and power generation performance.

No nanocomposite AEMs have been reported despite the fact that only a few types of nanomaterials and polymeric components have been used to manufacture IEMs for RED applications. Commercial AEMs have instead been widely used in RED research. These membranes were surface-coated with a polyelectrolyte solution to prepare an antifouling membrane for ED and RED systems. This coating reduced the ionic resistance of the membranes and increased their selective permeability (Vaselbehagh et al., 2014; Vaselbehagh et al., 2017; Gao et al., 2018However, nanocomposite membranes tailored for RED applications are still in their infancy. More study is needed to build nanocomposite membranes with optimal characteristics that might allow enhancedstorage of energy, as pointed out by Hong et al. (2019). As such, there is significant potential for further progress and innovation in this field.

3.1.3.Membrane fouling

Colloidal fouling, organic fouling, inorganic scaling, and biofouling are the most common forms of membrane fouling. When fouling builds up, the process becomes less efficient and more expensive to run. The presence of oil, carbohydrates, proteins, aromatic compounds, humic acid, and anti-foaming chemicals in the treated solution is said to constitute organic fouling. It has been reported that aliphatic AEMs have superior anti-organic-fouling characteristics to aromatic AEMs. As water's salts precipitate out and build up on a membrane's surface, a process known as inorganic scaling occurs. Calcium, magnesium,

barium, sulfate, and bicarbonate are the most common scaling ions (Mikhaylin and Bazinet, 2016).

Membrane performance during the RED process to generate electricity from the salinity gradient is significantly hampered by biofouling, which is caused by living microorganisms such as bacteria sticking to membrane surfaces and forming a cohesive biofilm. This is a further challenge that has prevented the commercialization and widespread implementation of the RED technology, in addition to its low power density and expensive cost. Reduced RED efficiency is a direct result of fouling's effect on ion IEMs. For example, in RED systems, AEMs with positively charged fixed groups are more susceptible to organic fouling and biofouling, whereas CEMs with negatively charged fixed groups are more prone to inorganic fouling (scaling) (Vaselbehagh et al., 2017).

In practical applications of reverse electrodialysis (RED) using seawater as high salinity water, biofouling of anion exchange membranes (AEMs) is a significant concern. Biofouling, according to some research, can be much more destructive than organic fouling in RED systems (Güler et al., 2014, Post et al., 2007). Post et al. (2009) discovered that biofilm formation may have a major unfavorable effect on power density. Ratjke et al. (1986) found that power densitydropped by 67% when utilizing natural saltwater and artificial river water owing to biofouling. As a result, biofouling is widely regarded as one of the greatest obstacles to actualizing the RED process.

Another major risk posed by biofouling in RED systems is the obstruction of flow channels and spacers, which increases pumping costs and wastes energy. Redesigned stacks, pre-treatment, additional operational precautions, and cleaning processes are just some of the methods that can be used to reduce the possibility of biofouling. For example, periodic reversal of salt and fresh water, changing the flow direction, and adding chlorine have been effective in preventing biofouling. These measures can help to mitigate the impact of biofouling on RED systemsand ensure efficient operation (Post et al., 2009).

Fouling can be classified according to the kind of membrane, with organic and biofouling being the most common types of issues that arise with AEMs (Lee et al., 2009, Vaselbehagh et al., 2014). Diatoms and clay minerals tend to accumulate on AEMs, leading to biofouling. Inorganic salt precipitation leading to

scaling was only observed on CEMs (Mikhaylin and Bazinet, 2016, Vermaas et al., 2013).

In order to avoid and manage fouling in RED systems, periodic washing has been included (Di Salvo et al., 2018). To address membrane fouling, various solutions are available, including pretreatment, optimization of operation, and chemical cleaning. However, these solutions can pose some challenges, as listed below (Lee and Nunes, 2016):

- Ineffective pretreatment may result in high rates of membrane fouling
- There is a lack of in-depth understanding of the nucleation kinetics and scale formation
- Fouling can potentially cause structural damage to the membrane.

Continuous forces on the membrane surface influence the fouling type and rate (Mei and Tang, 2018). Fouling of AEMs reduces open circuit voltage and RED performance (Rijnaarts et al., 2019).

According to Vermaas et al. (2013), fouling is a significant obstacle that must be overcome before possible deployment of RED. This is because fouling canhave a considerable impact on the performance of the system. Fouling of the membranes and spacers in a RED stack caused by using water from natural sources can raise the pressure drop and reduce the net power density. In point of fact, fouling can cause a reduction in power density of up to sixty percent as it enhances resistance and reduces permselectivity. It is worth noting that spacersare particularly susceptible to biofouling, which is a common cause of membrane fouling (Mei and Tang, 2018).

Highly selective AEMs that don't compromise membrane electro-resistance are a viable solution. This can be accomplished by the use of surface modification methods as graft polymerization, dip coating/immersion, electrodeposition, layer-by-layer deposition, plasma treatments, and solution casting (Kotoka et al., 2020).

Immersion (dipping or dip-coating) is a common approach in the literature (Habib et al., 2020, Vatanpour et al., 2012, Pourjafar et al., 2012, Rana and Matsuura, 2010) for immobilizing nanoparticles on membranes. Dip-coating has emerged as a promising method due to its ability to impede or slow down the adhesion of microorganisms, such as bacteria, on the surfaces of non-porous membranes. As germs are incapable of penetrating tight, impermeable membranes, only a modification of the membranes' exterior will be sufficient and

effective. The bacterial killing processes of antibacterial membranes are classified as release killing and contact killing. Continuous antibacterial agent discharge makes the release killing approach environmentally hazardous. Recent research has therefore focused on the creation of membranes with antibacterial activity through contact-killing properties (Cihanoğlu and Altınkaya, 2020).

Silver acts as the most effective nanoparticle against viruses, bacteria, and other eukaryotic organisms (Qin et al, 2010). In addition to its antibacterial capabilities, coating AEMs with AgNPs enhanced their selective permeability, ionic permeability, ionic flux, ionic conductivity, thermal stability, and membrane potential relative to unmodified membranes.

There is currently no particular nanocomposite AEM manufacturing for RED applications. To date, there have only been a limited number of nanomaterials and polymeric substances used in the construction of RED-specific IEMs. In the majority of RED research, commercial AEMs were utilized. Their surfaces were covered with a polyelectrolyte solution to create an antifouling membrane for ED and RED systems, therefore decreasing their ionic resistance and increasing their selective permeability (Vaselbehagh et al., 2014, Gao et al., 2018). The development of nanocomposite membranes tailored for RED applications is still in its early stages. It is anticipated that substantial research will be conducted in this area to create nanocomposite membranes with desirable properties, facilitating improved energy storage capabilities (Güler, 2014).

3.2. Material and Methods

For the synthesis of silver nanoparticles (AgNPs), silver nitrate ($AgNO_3$), ascorbic acid ($C_6H_8O_6$), trisodium citrate ($Na_3C_6H_5O_7$), citric acid ($H_3C_6H_5O_7$), sodium hydroxide ($C_6H_8O_6$), procured from Sigma-Aldrich Co. St. Louis, IL, U.S.A. and used in experiments as received.

3.2.1. Synthesis of nanoparticles

Silver nanoparticles were synthesized in a water bath at a constant temperature of 30°C using ascorbic acid as a reductant and trisodium citrate as a stabilizer with solution pH of 6.0 and 9.0. The pH of an aqueous solution containing ascorbic acid at a concentration of 6.0×10^{-4} M and trisodium citrate at a concentration of 3.0×10^{-3} M was changed from 6.0 to 9.0 by adding either 0.2 mol/L citrate acid or 0.1 mol/L NaOH solution. In a water bath set to 30°C, 0.08 mL of an aqueous

solution containing 0.1 M of $AgNO_3$ was added while the stirring speed was 900 rpm. It was noticed that the reaction solutions turned out to be blue and cloudy. After fifteen minutes, there was no longer any variation in color, which indicated that the reactions were finished (Qin et al., 2010).

Using a spectrophotometer called a Thermoscientific Genesys 20 UV–vis, we were able to get UV–vis absorption spectra. The results of the UV-vis spectra are presented in the section labeled "Results and Discussion".

3.2.2. Synthesis of AgNPs immobilized AEMs

Studies have been carried out for the synthesis of antifouling AEMs. For this purpose, AgNPs synthesized (Figure 3.1) were added to the membrane structure.

Since the diamine ratio is proportional to the amount of DABCO, which is the crosslinker and aminifying agent added to the membrane casting solution, an increase in the diamine ratio increases the ion exchange capacity and reduces the degree of swelling. For this reason, the synthesis of AEM containing AgNPs was carried out using membranes with a diamine ratio of 4 and a blend ratio of 1.07.

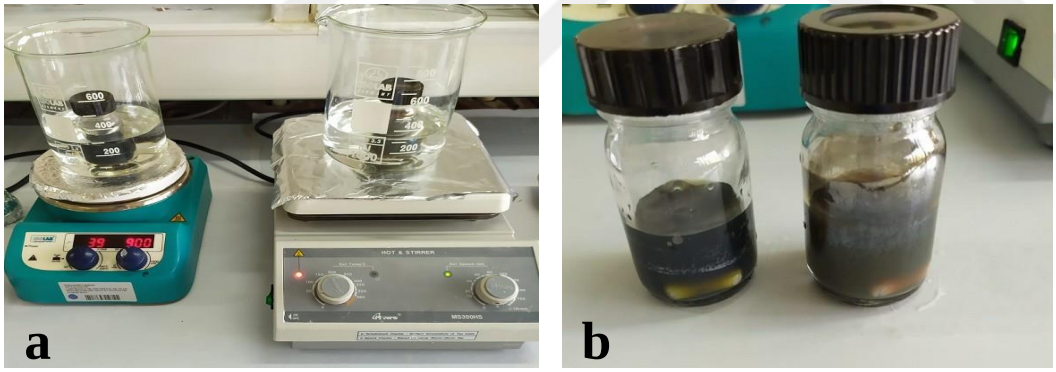

Figure 3.1. Synthesis of silver nanoparticles

The immobilization of synthesized AgNPs to the membranes in acidic medium was carried out by immersion method since it was predicted that negativelycharged AgNPs would be better immobilized to the membranes by electrostatic interaction of the membranes with protonated amine groups in acidic medium. The immersion process of the membranes in the AgNPs solution in an acidic medium is given in Figure 3.2. Inside the glass containers in Figure 3.2, there are EDR4-BR1.07 membranes immersed in pH 6.0-1, pH 9.0-1, pH 6.0-2 and pH 9.0-2 solutions, respectively. Description of the ambient conditions of the respective solutions is given in Table 3.1.

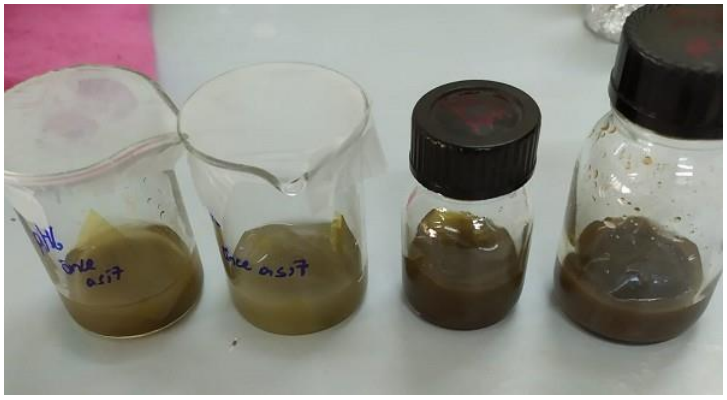

Figure 3.2. The immobilization of silver nanoparticles to the membranes in acidic medium

Table 3.1. Conditions for preparation of AgNPs

Samples	**Ambient conditions**
EDR4-BR1.07	Diamine ratio: 4 Blend ratio: 1.068
pH 6.0 pH 9.0	EDR4-BR1.07 membranes were washed with distilled water for 24 h and then immersed in nanoparticle solutions.
pH 6.0-1 pH 9.0-1	First, the pH of the nanoparticle solution was adjusted to pH 2.0 with the help of sulfuric acid, and then the washed membranes were added to the medium.
pH 6.0-2 pH 9.0-2	First, the washed membranes were immersed in the nanoparticle solution, then the pH of the medium was adjusted to pH 2.0 with the help of sulfuric acid.

The immersion of the membranes in the AgNPs solution was carried out in two ways in an acidic environment. The relevant sample names and the conditions applied are given in Table 3.1. The AEMs were interacted with AgNPs solutions for 24 h without stirring at room temperature.

Immobilization of nanoparticles to membranes in acidic environment was carried out in two different ways. In the first application pH of the silver nanoparticle solution was first adjusted to an acidic environment (pH 2.0) and then the membranes were added to this environment. In the second application, first the membranes were added to the silver nanoparticle solution and then the pH

of the nanoparticle solution in which the membranes were located was adjusted to 2.

3.2.3. Effect of washing in the synthesis of AgNPs immobilized AEMs

In the first stage, immobilization of AgNPs to the AEMs with high diamine ratios was studied. The reason for using the membrane with a diamine ratio of 4 and a blend ratio of 1.07 in the immobilization of AgNPs is that the diamine ratio is the highest among the prepared membranes. Since the diamine ratio is proportional to the amount of DABCO, which is the crosslinker and aminifying agent added to the membrane casting solution, an increase in the diamine ratio increases the ion exchange capacity. Ion exchange capacity is a parameter that increases electrical conductivity. Therefore, the membrane with a diamine ratio of
4 was chosen for the AgNPs immobilization in the first step. Since the ionexchange capacity is proportional to the conductivity of the membrane, it providessufficient information in terms of membrane selection. This membrane with a diamine ratio of 4 was used only for particle immobilization without washing. These membranes were immersed in the silver nanoparticle solution in the petri dish without washing with deionized water, and thus the nanoparticles were immobilized to the membranes (Figure 3.3).

Figure 3.3. Immobilization of AgNPs on unwashed membranes (EDR4-BR1.07).

It was considered that sodium chloride, which may be present in the structure of the membranes, may cause agglomeration of AgNPs if the membranesare not washed with deionized water. Therefore, the membrane with a diamine ratio of 2 and a blend ratio of 1.07 was washed with deionized water for 24 h. Then, the washed membranes were immersed in AgNPs solutions and the AgNPs were immobilized to the membranes (Figure 3.4).

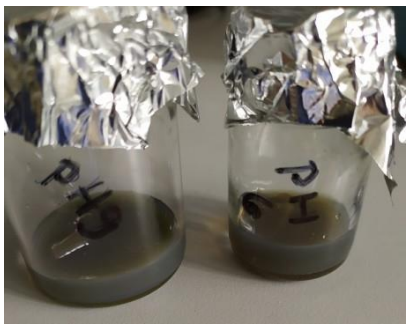

Figure 3.4. Immersion of washed membranes in silver nanoparticle solution

In the first stage, the AEMs were immersed in AgNPs solutions prepared in pH 6 and pH 9 environments. The images of the membranes after AgNPs immobilization before and after washing are given in the results and discussion section. The AgNPs distribution in the membranes was tried to be explained by SEM analysis.

3.2.4. Stability of AgNPs immobilized AEMs in acidic solution

For this purpose, sulfuric acid solution was prepared (pH 2) and membranes with diamine ratio of 2 and blend ratio of 1.07 (EDR2-BR1.07) were kept in acid solution for an h for acidic medium test (Figure 3.5). The membranes were dried in an oven at 50 °C for 2 h and then analyzed with FTIR spectroscopy. When the FTIR results of the membranes kept in acidic environment and EDR2-BR1.07 membrane were compared. Since no difference was observed in the IR spectra obtained for both membranes, it was concluded that the membranes were not degraded in acidic environment. FTIR spectroscopy results are given in the results and discussion section.

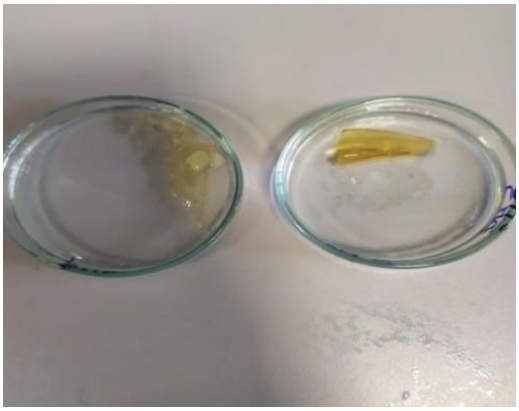

Figure 3.5. AgNPs immobilized AEMs in acidic solution

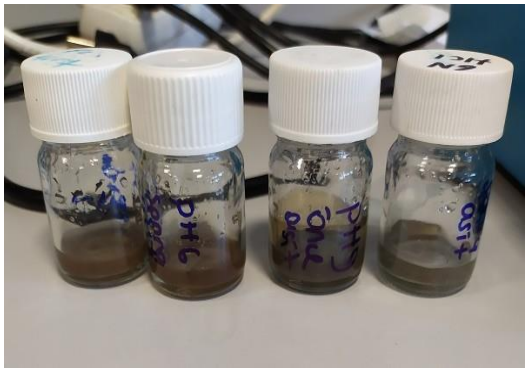

Figure 3.6. Dipping process of membranes in silver nanoparticle solution in acidic medium

3.2.5. AgNPs stability studies

AgNPs stability studies were carried out in order to observe whether agglomeration occurs in AgNPs in direct contact with NaCl solution. The stability studies were carried out to determine the amount of nanoparticle loss that passed from the membrane surface to the solution.

Stability studies of membranes containing silver nanoparticles were carried out in order to determine the loss of nanoparticles from the membrane surface in a salt solution. The EDR4-BR1.07 membranes were cut into 3 cm x 3 cm and immersed in 10 mL nanoparticle solutions for 24 h, then removed from thesolutions and dried for 24 h. The images of the AgNPs produced at pH 6.0 and theimages of the membranes immersed in the pH 6.0 AgNPs solutions are given in Figure 3.7-a and b, respectively. The image of the EDR4-BR1.07 membranes, which were removed from the pH 6.0 nanoparticle solution and left to dry, are given in Figure 3.8.

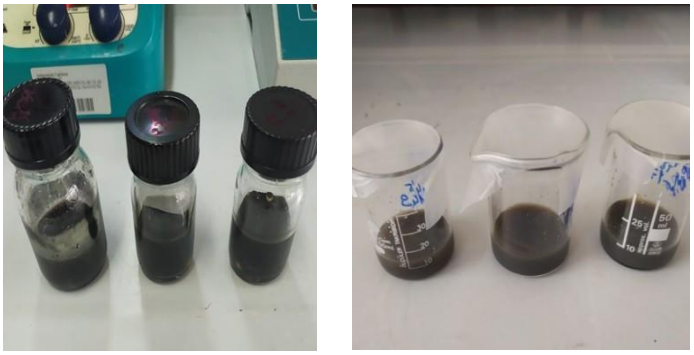

a **b**

Figure 3.7. AgNPs solutions prepared at pH 6.0 b) Membranes immersed in pH 6.0 AgNPs solutions

.

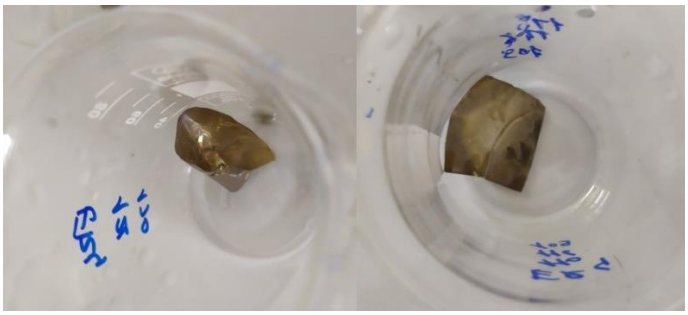

Figure 3.8. Membranes removed from pH 6.0 AgNPs solution

The membranes, which were removed from the AgNPs solutions and left to dry, then they were immersed in 0.001M NaCl solution and kept in a shaker for 3 h at 25 ^{o}C. Samples of 5 mL were taken from this mixture at different times (5, 30, 60, 90, 120 and 180 min) and absorbance values were measured. The results of the absorbance values were given in the results and discussion section.

FTIR analyses were performed to determine whether washing made a change in the membrane structure. When the SEM images of the washed and unwashed membranes after the AgNPs immobilization were examined, it was understood that the AgNPs immobilization to the washed membranes was more homogeneous. It was considered that the inhomogeneous appearance on the membranes in which AgNPs were immobilized without washing was caused by NaCl salt crystals deposited on the surface of the non-washed membranes. It is possible that NaCl in the structure of the membrane, which is not washed during the immersion process, causes agglomeration of AgNPs on membrane surface. Therefore, before immobilization, the membranes were washed with deionized water for 24 h.

Stability studies aim to determine the amount of particle loss that may occur when the AgNPs containing membranes are exposed to NaCl solution from the surface. According to the results of the SEM and EDX mapping images, the homogeneous distribution was observed in the membranes interacted with pH 6.0 AgNPs solution, and also when the images of the membranes left to dry in acidic environment, pH 6.0 and pH 9.0 medium, the color change in the membrane with pH 6.0 AgNPs immobilized was seen. For this reason, stability studies were carried out with membranes immobilized with AgNPs solution at pH 6.0. High-concentration NaCl solutions are used while performing RED tests. It is of great

importance to see whether AgNPs leaks from the antibacterial membranes to the environment. If the amount of leakage is high, the resistance of membrane against fouling will decrease. For this purpose, AgNPs immobilized membranes were left in NaCl solutions at 0.017 M and 0.5 M concentrations for different times. The reason why the NaCl solution concentrations were chosen as 0.017 M and 0.5 M is that the NaCl concentrations in the river and sea waters are at these values. In the stability tests carried out in this context, AgNPs immobilized membranes were immersed in NaCl solutions at 0.017 M and 0.5 M concentrations, and these mixtures were contacted by shaking in a water bath at 25^{o}C for 1 or 6 h. After this contact, the membranes taken from the solution were washed with deionized water, and then SEM, ICP-MS and XPS analyzes were made.

As a result of the stability tests of the AgNPs immobilized membranes, it was considered that the use of ICP-MS, SEM and XPS analyzes to determine the amount of AgNPs released from the membrane surface could yield more meaningful and accurate results, since the UV measurements were not accurate.

3.2.6. ICP-MS Analysis

5 mg sample taken from different parts of the AgNPs immobilized membrane was tried to be dissolved in 5 ml of concentrated HNO_3 after drying of the membrane immobilized with AgNPs and contacted with different concentrations of NaCl. Centrifugation was performed to remove the insoluble parts of the cross-linked membrane, then 1.0 ml sample was taken from thesupernatant and ICP-MS analysis was performed. The values obtained from the ICP-MS analysis gave the amount of silver in the membrane. The percentages of silver released from the surface in stability tests were calculated.

3.2.7. Antibacterial activity of AEMs

The antibacterial activities of the bare and AgNPs immobilized AEMs were determined using the model gram-negative bacteria (*E. coli*) suspension with the colony counting method according to the ASTM E2149 standard protocol. First, *E. coli* was inoculated in Mueller-Hinton agar. Then, the bacteria were incubated at 37 °C. After incubation, bacterial colonies were collected using a swab and mixed with 0.1% (w) peptone water to adjust the concentration to the equivalentof 0.5 McFarland (2.5×10^{7} CFU/mL) on the standard scale. Next, bacteria

suspension was diluted with nutrient broth (the dilution ratio is 1:9 bacteria suspension: nutrient broth) to adjust the concentration to 2.5×10^6 CFU/mL and this was used as a stock suspension for the antibacterial tests. Prior to conducting the antibacterial tests, membrane coupons measuring 3 cm x 3 cm (effective size) were sterilized by exposing each side to UV light for 15 minutes, totaling a 30-minute UV light treatment (Figure 3.9). Then, 100 μL of the stock bacteria suspension was added into the 250 mL of erlenmeyer flask containing 50 mL of phosphate buffered saline (PBS) solution (Figure 3.10).

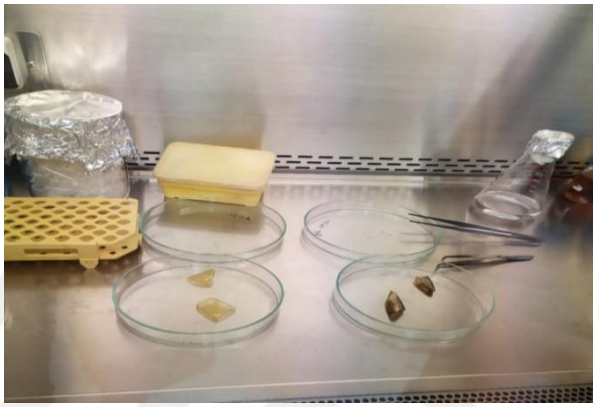

Figure 3.9. Sterilization of the membranes

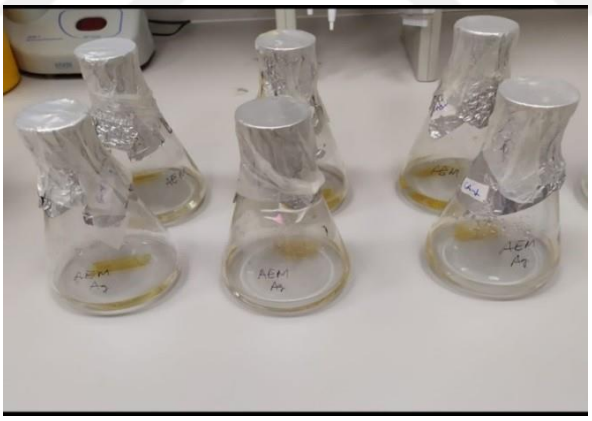

Figure 3.10. Exposure of the membranes to the bacterial solution (time t=0).

Next, the membrane coupons were immersed in the bacteria suspension in erlenmeyer and shaken at 200 rpm for 24 h at 37 ^oC. Finally, bacteria suspension was spread on the LB (Luria-Bertani) broth plates with 10^{-2} and 10^{-4} dilution rates, incubated for 24 h at 37 ^oC (Figure 3.11-a), and the colonies were counted. In antibacterial activity calculation, inoculum solution (without containing any membrane) was used as control. The antibacterial activity test was repeated three times (n=3)

a b

Figure 3.11. a) Shaking of the bacteria suspension solutions b) Incubation of suspension solution

The bactericidal rate was calculated using Equation 3.1:

$$\text{Antibacterial rate, \% (CFU/mL)} = ((N_P - N_M)/N_P)*100 \quad \text{Equation 3.1}$$

where N_P and N_M are the number of visual bacteria colonies on the agar plate after contacting with the bare and AgNPs immobilized membranes, respectively.

3.2.8. Preparation of large-scale AgNps immobilized AEMs for RED applications

Optimum membrane was synthesized with excess diamine ratio of 2 and blend ratio of 0.6 by Karakoç and Güler (2022). Large scale membranes for RED tests were synthesized with these blend and excess diamine ratios. Size of the AEMs were 15 cm x 15 cm. AgNPs were immobilized to these membranes with dip coating method and membranes were immersed to AgNPs solution during 24h (Figure 3.12-a). AgNPs immobilized AEMs were washed with deionized water after removing from AgNPs solution. The image of the membranes after washing is given in Figure 3.12-b.

a **b**

Figure3.12. Immobilization of AgNPs onto AEMs a) dip coating b) AgNPs immobilized AEMs after washing with deionized water

3.2.9. Synthesis of AgNPs with small particle size

As distinct from production of large scale nanoparticles, $NaBH_4$ was used. Two different methods were used in the synthesis of AgNPs.

In the method A applied, AgNPs were produced using trisodium citrate (TSC). For this, 0.002 g of $NaBH_4$ and 0.035 g of TSC were dissolved in 25 mL of deionized water. The mixture was stirred mechanically at 170 rpm. 10 mM $AgNO_3$ solution was prepared with the flow rate of 3.3 mL/min. $AgNO_3$ solution was added dropwise to $NaBH_4$ and TSC solution using a pump. Method A experimental setup and the produced nanoparticle solution are shown in Figures 3.13 and 3.14, respectively.

Figure 3.13. Method A experimental setup for synthesis of AgNPs with small particle size

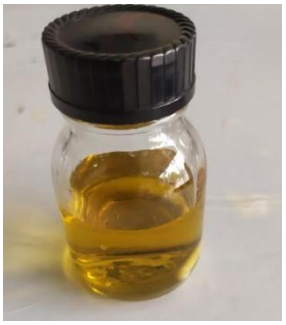

Figure 3.14. AgNPs solution produced by the method A

In the method B, mixing was carried out without using trisodium citrate. A 10 mL volume of 1.0 mM $AgNO_3$ was added dropwise to 30 mL of 2.0 mM $NaBH_4$ solution placed in an ice bath (Figure 3.15). The reaction mixture was vigorously stirred at 900 rpm on a magnetic stirrer. Meanwhile, the color of the solution turned yellow (Figure 3.16). Stirring was stopped after all the silver nitrate solution was added.

Figure 3.15. Method B experimental setup for synthesis of AgNPs with small particle size

Figure 3.16. AgNPs solution produced by the method B

In the method A, flow rates of 3.3 mL/min and 5 mL/min and stirring rates of 170 rpm and 450 rpm were used. In the method B, the pump speed (flow rate) was adjusted as 1.5, 2.5, 3.3 and 5.5 mL/min in order to examine the velocity effect.

3.3. Results and Discussion

3.3.1. Synthesis of AgNPs

Silver nanoparticles were synthesized in a water bath at a constant temperature of 30°C using ascorbic acid as a reductant and trisodium citrate as a stabilizer with solution pH of 6.0 and 9.0. Samples were taken from AgNPs solutions (pH: 6.0 and 9.0). Measurements were made in UV-Vis absorption spectrophotometer and Malvern Zeta Sizer device**.** Before measuring the particle size of AgNPs, the solutions were sonicated for 5 min. The size distributions of the AgNPs obtained from the synthesis at pH 6.0 and pH 9.0 are given in Figures 3.17 and 3.18. The average size of AgNPs obtained from the synthesis at pH 6.0 was 107.4 nm, while the average size of AgNPs synthesized at pH 9.0 was 96.92 nm.

Qin et al. (2010) determined the AgNPs sizes produced at pH 6.0 and pH 9.0 as 89 nm and 62 nm, respectively, while Steinigeweg and Schlücker (2012) determined the sizes of hemispherical AgNPs produced with citrate and ascorbic acid as 83.9 nm±26.2%. The sizes of the synthesized AgNPs are consistent with the results given in the literature.

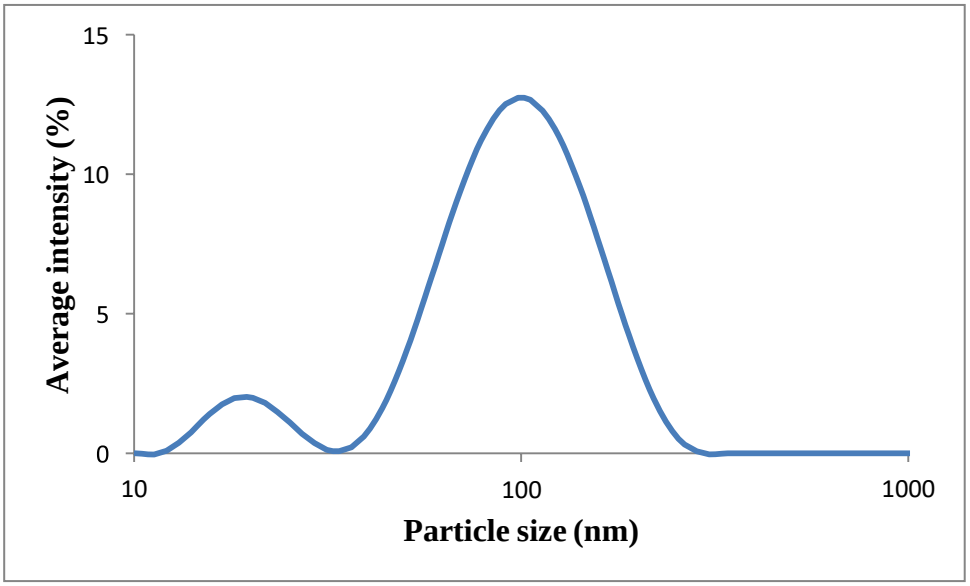

Figure 3.17. Size distribution of AgNPs prepared at pH 6.0

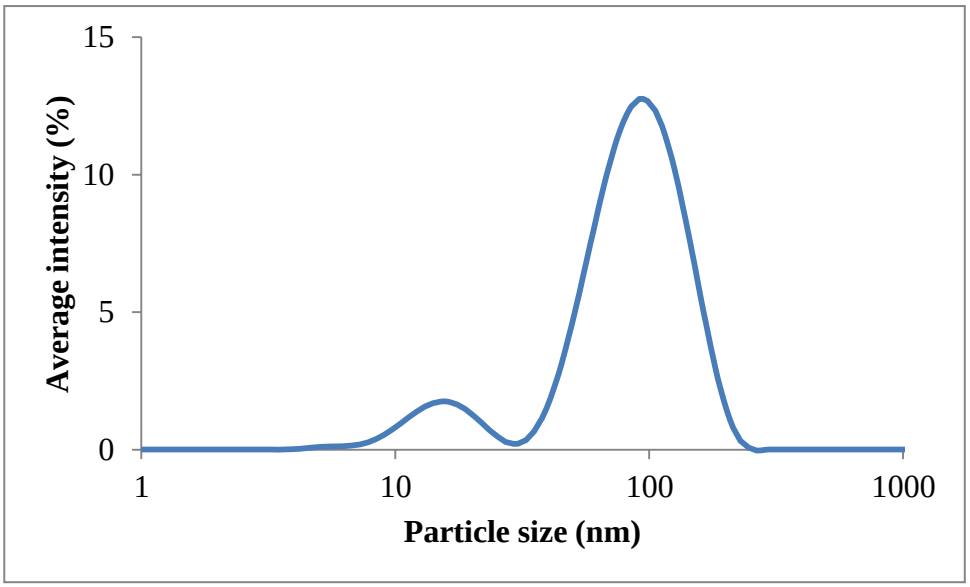

Figure 3.18. Size distribution of silver nanoparticles prepared at pH 9.0

UV-Vis absorption spectra of AgNPs produced at pH 6.0 and pH 9.0 are given in Figure 3.19. The wavelengths related to the maximum absorbance were measured as 432 nm for nanoparticles produced at pH 9.0 and as 442 nm for nanoparticles produced at pH 6.0. Qin et al. (2010) found the wavelengths of AgNPs produced at pH 6.0 and pH 9.0 as 480 nm and 433 nm, respectively. Agnihotri et al. (2014) produced AgNPs from 5 nm to 100 nm and measured the wavelength of the nanoparticle they produced at 100 nm as 462 nm. Mikac et al. (2014), in their studies using ascorbic acid as a reducing agent, found the maximum absorbance wavelength of the AgNPs they produced as 402 nm. Kamali et al. (2012) determined the maximum absorbance as 425 nm. Rashid et al. (2013) determined the wavelength at which the maximum absorbance of AgNPs produced using ascorbic acid was observed as 402 nm. It is seen that the maximum absorbance of the AgNPs synthesized in this study are agreed well withthe literature.

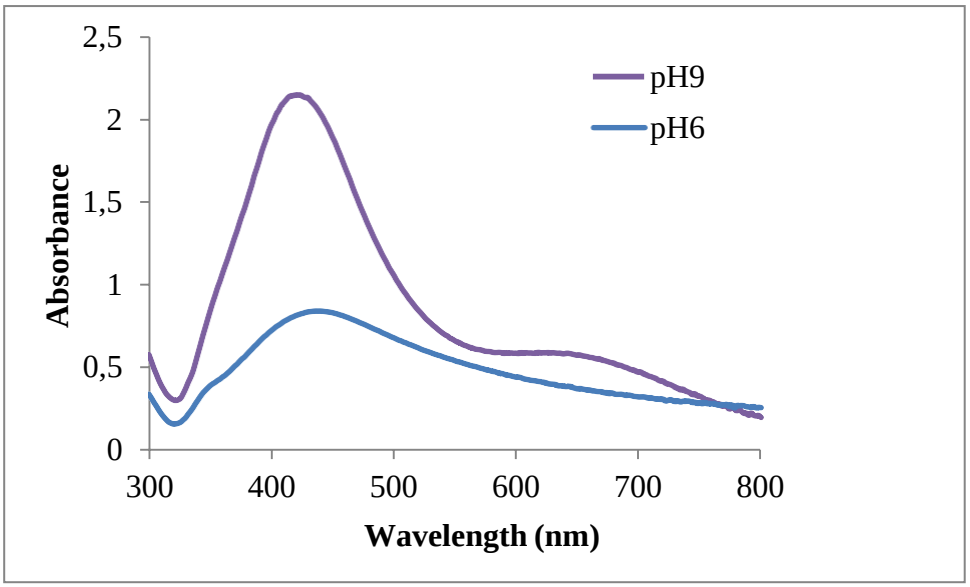

Figure 3.19. UV-Vis absorption spectra of AgNPs produced at pH 6.0 and pH 9.0

In this study, no problems were encountered during the synthesis of AgNPs. However, the grain sizes of the AgNPs were found to be slightly larger than the values given in the literature.

3.3.2. Immobilization of AgNPs onto AEMs

AgNPs were immobilized onto AEMs with dip coating method by using EDR4-BR1.07 AEM. The images of the AEMs immobilized with AgNPs at pH 6.0 and pH 9.0 in acidic medium are given in Figure 3.20.

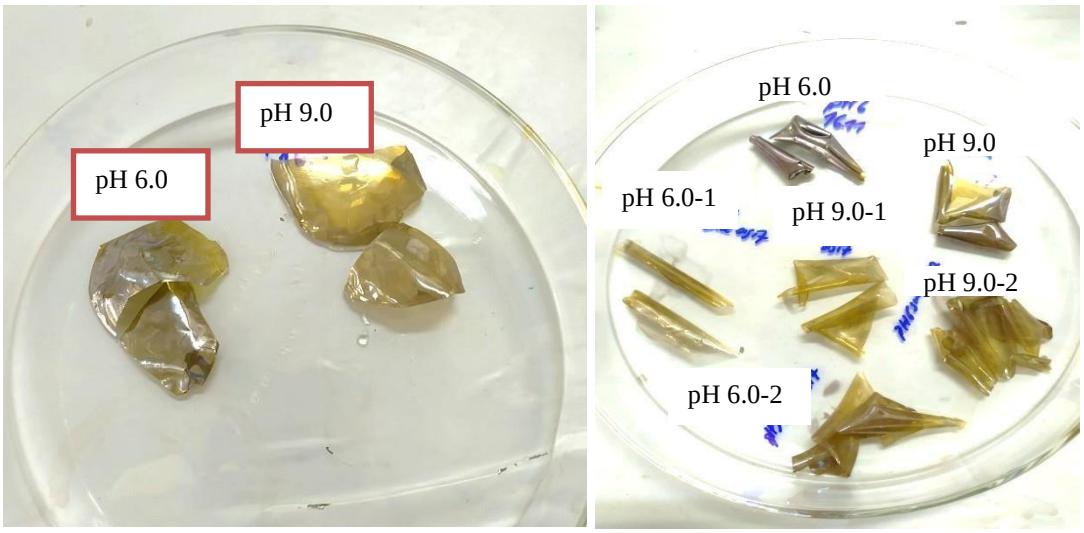

Figure 3.20. Images of the membranes after immobilization of AgNPs

The color change is clearly observed after the immobilization of the AgNPs produced at pH 6.0 to the AEM without interacting with the acidic environment. This was comparable with the SEM images.

The SEM images after AgNPs immobilization to the membranes are given in Figures 3.21 and 3.22. It is observed that there is agglomeration in membranes having AgNPs produced at pH 9.0. At high pH values, the rate of chemical reduction is high and this causes the AgNPs to aggregate. It is observed that the particle size distribution is homogeneous after the immobilization of the AgNPs produced at pH 6.0 to the membrane without interacting with the acidic medium (Figures 3.21-b and 3.22-b). Agglomerations were formed at the pH 9.0 medium (Figures 3.21-c, and 3.22-c). When ascorbic acid is used as a reducing agent, the reduction reaction occurs slowly at high pH and causes AgNPs to agglomerate and grow on the membrane surface. Intense agglomeration was observed when AgNPs interacted with membranes in an acidic environment (Figures 3.21- d, e, f, g). When switching to larger magnifications, agglomeration is clearly observed (Figures 3.22-d, e, f, g).

It was observed that the best homogeneous dispersion of AgNPs in membranes was observed with AgNPs prepared at pH 6.0 (Figure 3.22). In addition, agglomerations were observed at pH 9.0 from EDX mapping results (Figure 3.23).

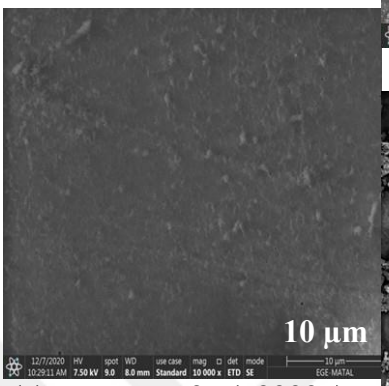

(a) ER4-BR1.07 (10000x)

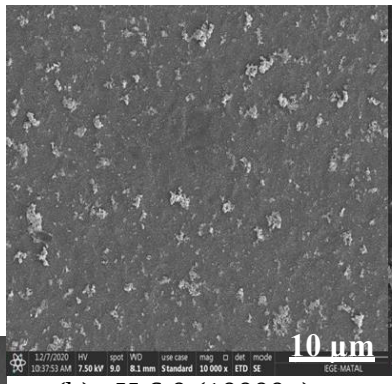

(b) pH 6.0 (10000x)

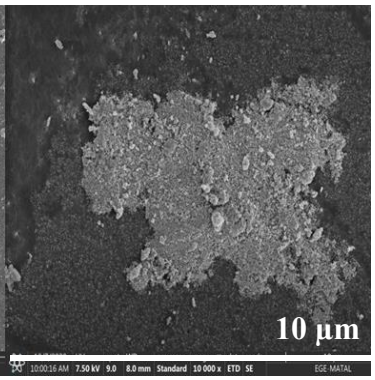

(c) pH 9.0 (10000x)

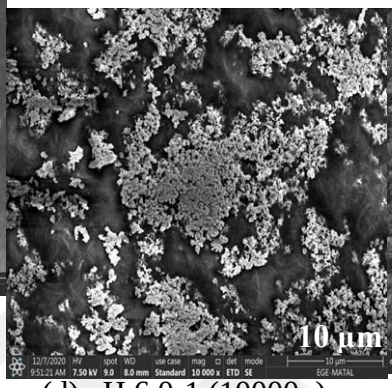

(d) pH 6.0-1 (10000x)

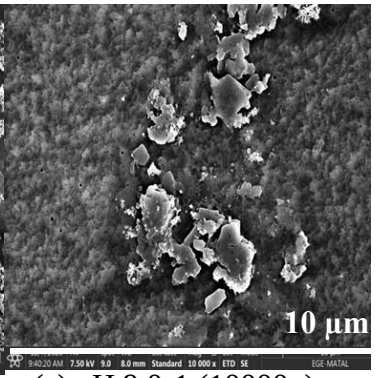

(e) pH 9.0-1 (10000x)

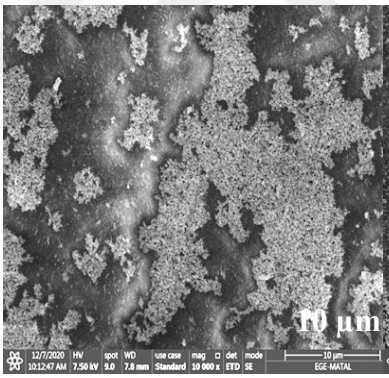

(f) pH 6.0-2 (10000x)

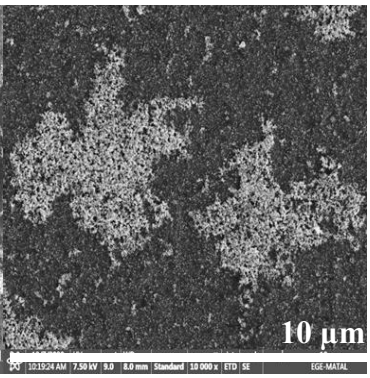

(g) pH 9.0-2 (10000x)

Figure 3.21. SEM images after AgNPs (prepared at pH 6.0 and pH 9.0) immobilization to AEMs (10000x)

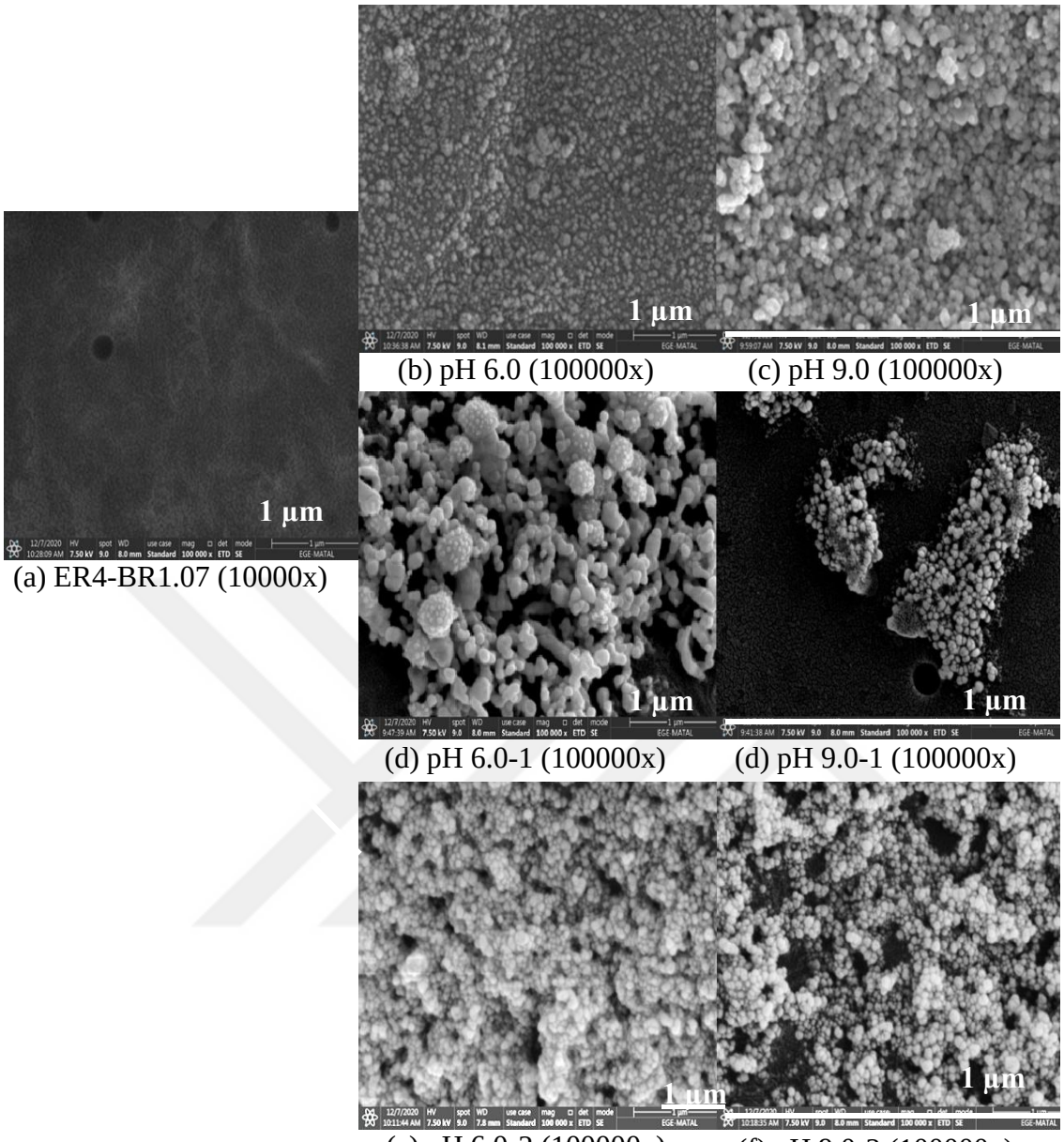

(a) ER4-BR1.07 (10000x)

(b) pH 6.0 (100000x)

(c) pH 9.0 (100000x)

(d) pH 6.0-1 (100000x)

(d) pH 9.0-1 (100000x)

(e) pH 6.0-2 (100000x)

(f) pH 9.0-2 (100000x)

Figure 3.22. SEM images after AgNPs (prepared at pH 6.0 and pH 9.0) immobilization to AEMs (100000x)

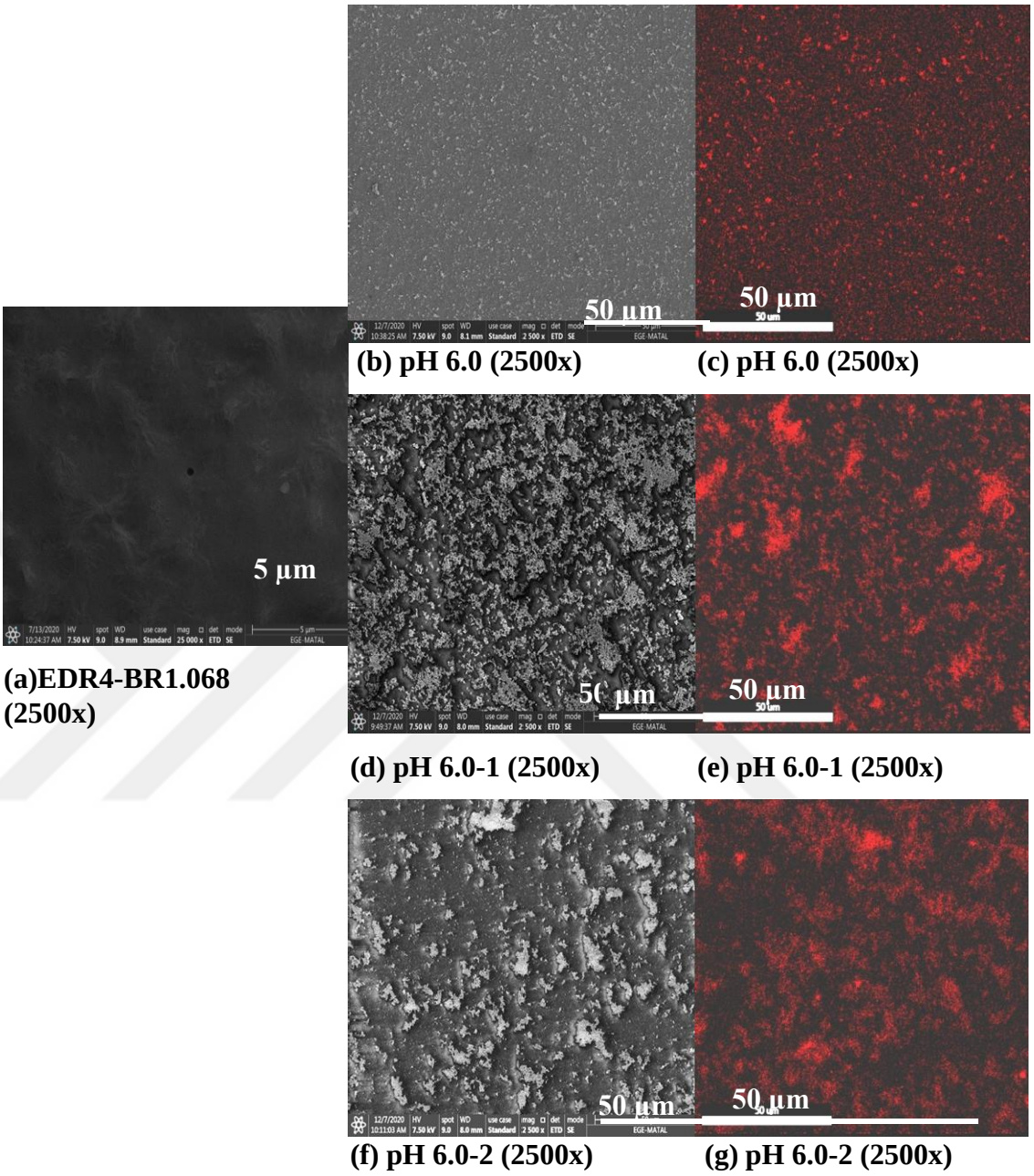

(a)EDR4-BR1.068 (2500x)

(b) pH 6.0 (2500x) **(c) pH 6.0 (2500x)**

(d) pH 6.0-1 (2500x) **(e) pH 6.0-1 (2500x)**

(f) pH 6.0-2 (2500x) **(g) pH 6.0-2 (2500x)**

Figure 3.23. SEM (b-d-f) and EDX mapping (c-e-g) images after AgNPs (prepared at pH 6.0) immobilization to the membranes (Red dots indicate silver- containing structures in the membrane.)

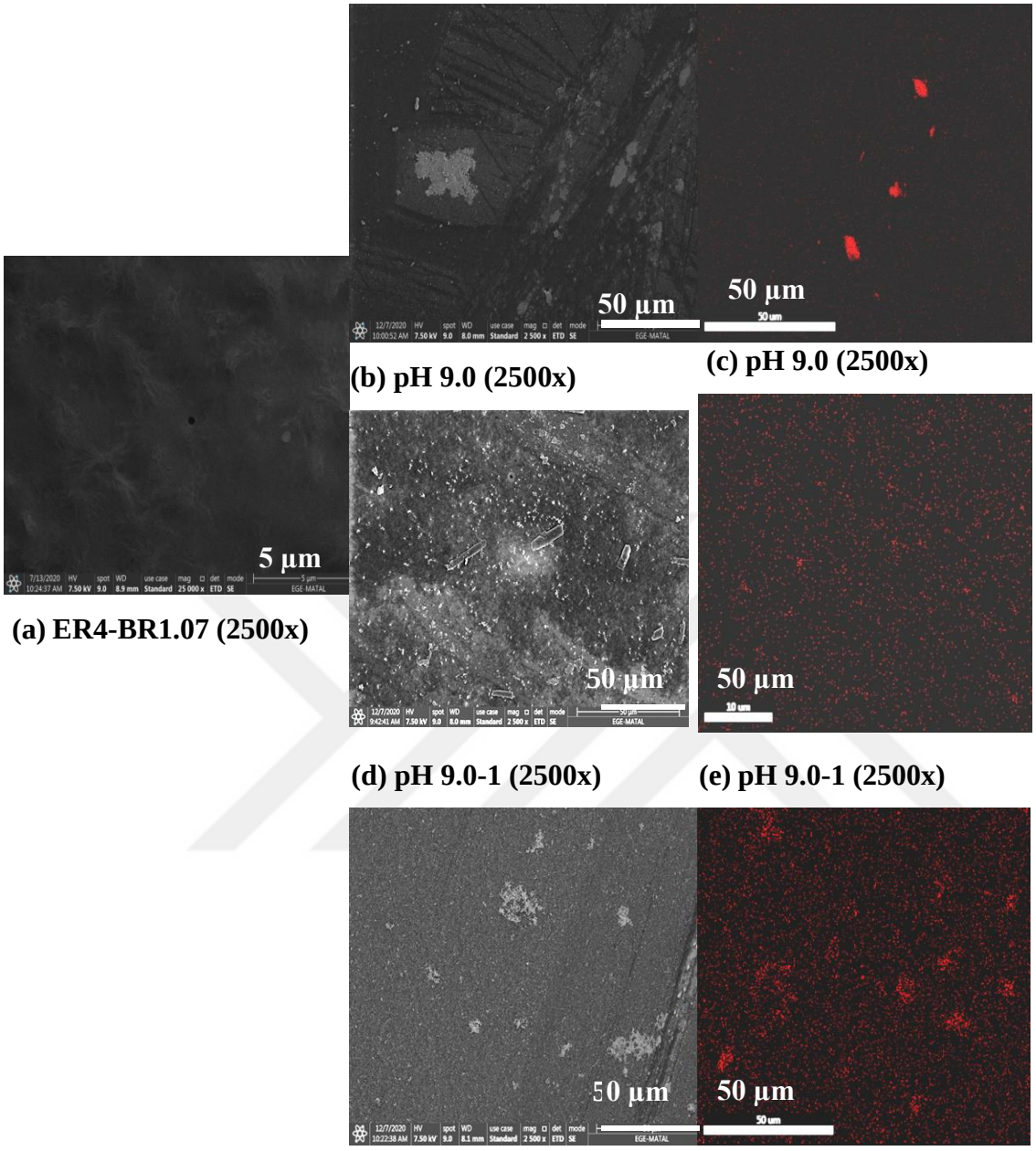

(a) ER4-BR1.07 (2500x)

(b) pH 9.0 (2500x)

(c) pH 9.0 (2500x)

(d) pH 9.0-1 (2500x)

(e) pH 9.0-1 (2500x)

(f) pH 9.0-2 (2500x)

(g) pH 9.0-2 (2500x)

Figure 3.24. SEM (b-d-f) and EDX mapping (c-e-g) images after AgNPs (prepared at pH 9.0) nanoparticle immobilization to the AEMs (Red dots indicate silver-containing structures in the membrane).

3.3.3. XPS Analyses

The XPS spectrum of the membranes (EDR4-BR1.07) immobilized with AgNPs is given in Figure 3.25. Looking at the XPS spectrum, it is seen that all the elements expected (O, Ag, N, C and Cl) are on the membrane surface. O, C, N and Cl come from the structure of the polyepichlorhydrin based AEM, and Ag comes from the AgNPs immobilized on the membrane surface.

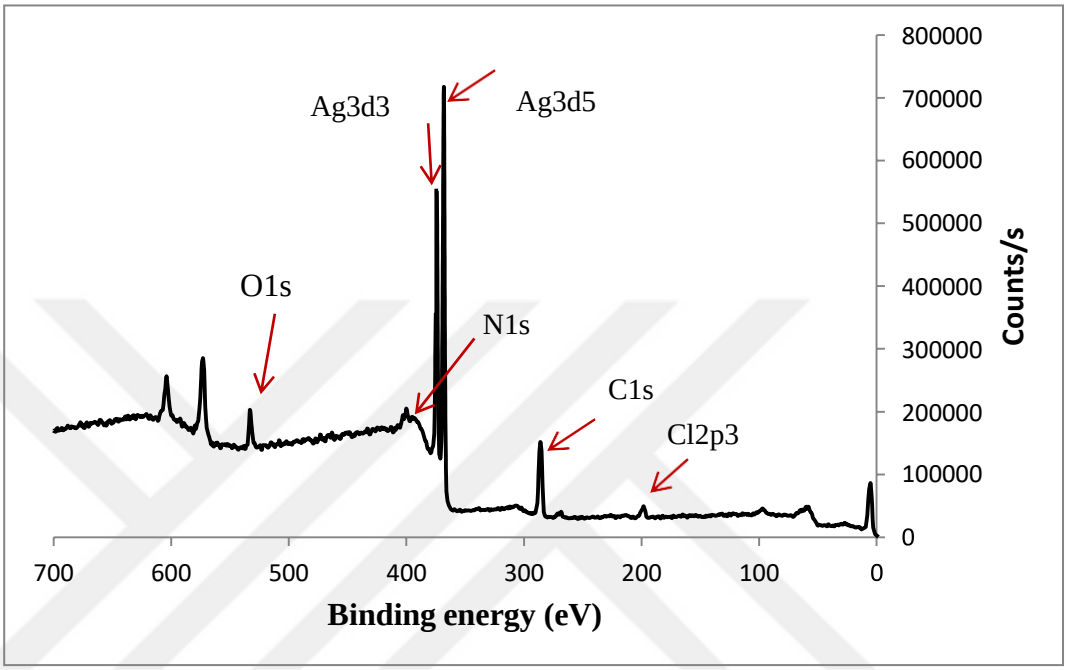

Figure 3.25. XPS spectrum of membranes immobilized with AgNPs

When the Ag3d core level XPS spectrum given in Figure 3.25 is examined, specific Ag3d bands belonging to metallic silver are seen at 368.4 eV and 374.4 eV. In addition, the absence of a specific 369.4 eV band belonging to Ag nanoclusters indicates that AgNPs are homogeneously immobilized on the membrane surface. When the O1s core level XPS spectrum given in Figure 3.26-bis examined, the specific O1s band belonging to the oxygen attached to the carbonchain is seen at 533.8 eV. This shows that the oxygen element in the XPSspectrum comes from the oxygen in the structure of the membrane. When the C1s core level XPS spectrum given in Figure 3.26-c is examined, the specific C1sband of the C-C bond is seen at 274.8 eV. This shows that the carbon element in the XPS spectrum comes from the carbon chain in the structure of the polymeric membrane. The N1s band at 400 eV seen in the N1s core level XPS spectrum given in In addition, the existence of groups of amine may be seen in the basic framework of the membrane, as depicted in figure 3.26-d.

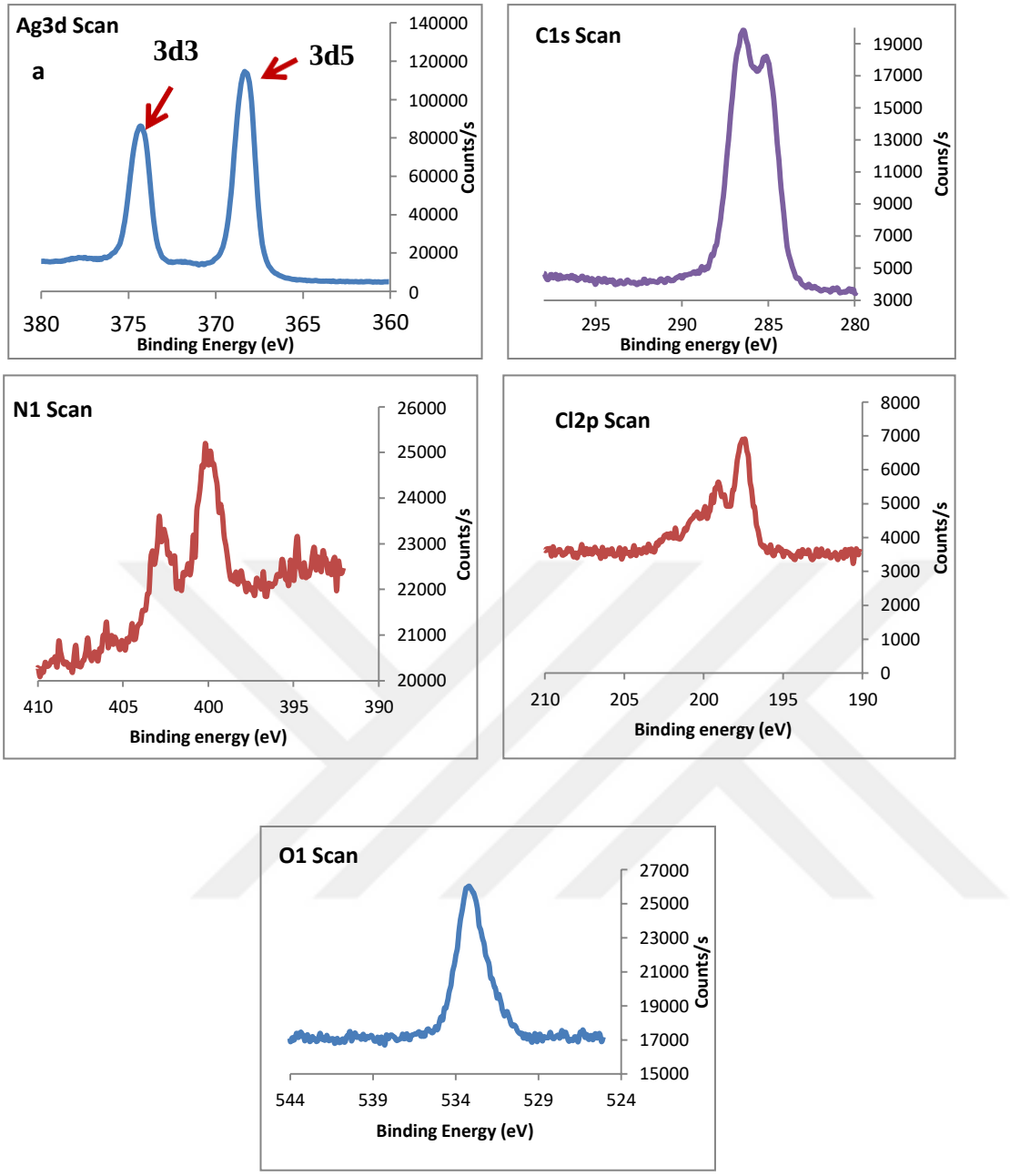

Figure 3.26. XPS spectra of a) O1s, b) N1s c) Ag3d d) C1s, e) Cl2p.

The percentage amounts of elements on the membrane surface with AgNPs immobilized as a result of XPS analysis are given in Table 3.2.

Table 3.2. Percent distribution of elements present in the AgNPs immobilized membrane

Element	Atomic (%)
Cl	4.73
C	58.37
Ag	18.93
N	7.86
O	10.11

3.3.4. Stability Studies

The purpose of these research was to ascertain the amount of AgNPs that were lost from the outer layer of the membrane when the membranes that contained AgNPs were subjected to a solution that contained sodium chloride. For this purpose, first of all, AgNPs were dispersed in 0.001 M NaCl solution and 0.5 M NaCl solution having (1 mL AgNPs in 9 mL deionized water or 9 mL NaCl solution) by applying ultrasonication for 5 min and the dispersion obtained was left for 5 min, and then UV-Vis spectrum of the supernatant was taken. The UV-Vis spectra of the AgNPs dispersions are shown in Figure 3.27. As can be seen from the UV-Vis spectra of AgNPs dispersions in deionized water and in 0.001 MNaCl, AgNPs gave a characteristic peak in the wavelength range of 405-438 nm. However, no peak was observed in the wavelength range of 405-438 nm in the UV-Vis spectrum obtained after the AgNPs immobilized AEMs were kept in 0.5 M NaCl solution for 5 min. This shows that in the medium containing 0.5 M NaCl, the AgNPs completely agglomerate and precipitate and there is no AgNPs in dispersed form at the top of the solution. A separate study was carried out using 0.001 M NaCl solution to monitor the leakage of AgNPs from the AgNPs immobilized membranes to the solution by time.

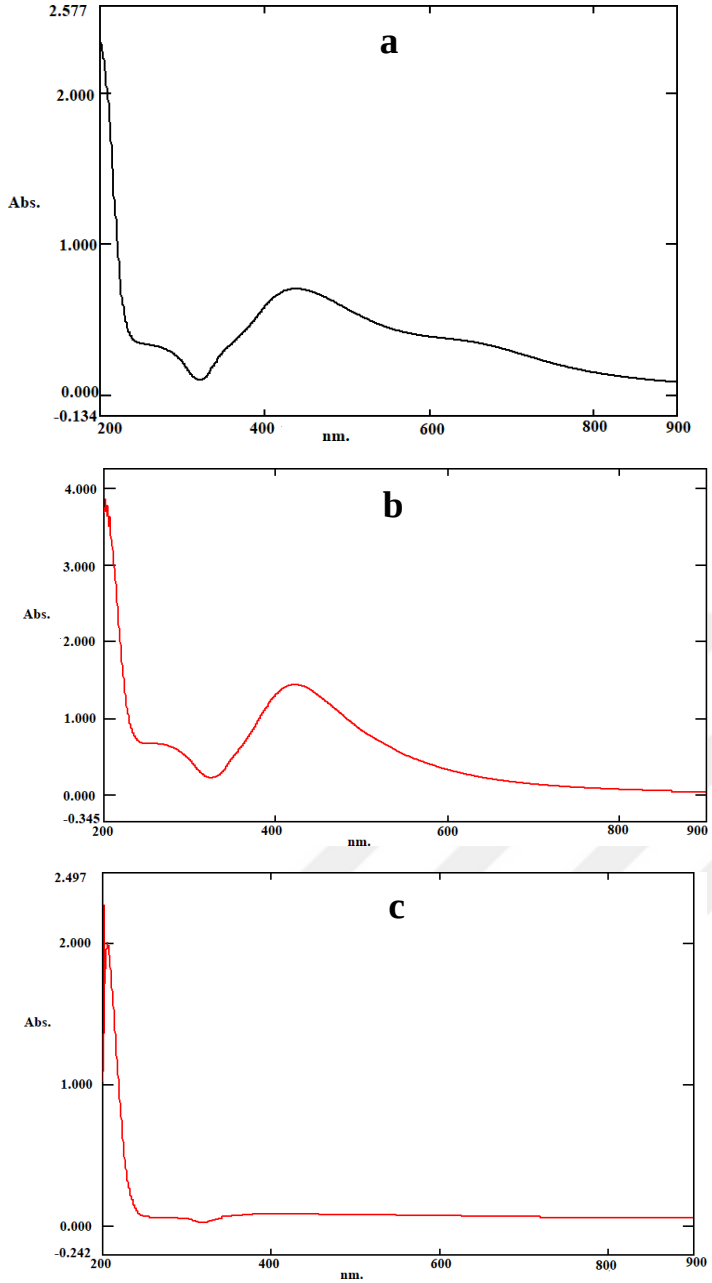

Figure 3.27. UV-vis spectra of AgNPs in salt-free and containing deionized water environments with pH 6.0. a) Deionized water, b) 0.001 M NaCl, c) 0.5 M NaCl.

During the interaction of AgNPs immobilized AEMs with 0.001M NaCl solution (pH 6.0), the UV-vis spectra of the liquid samples taken from the solution at different time intervals are illustrated in Figure 3.28. The absorbances obtained at 423 nm wavelength in these spectra are given in Table 3.3.

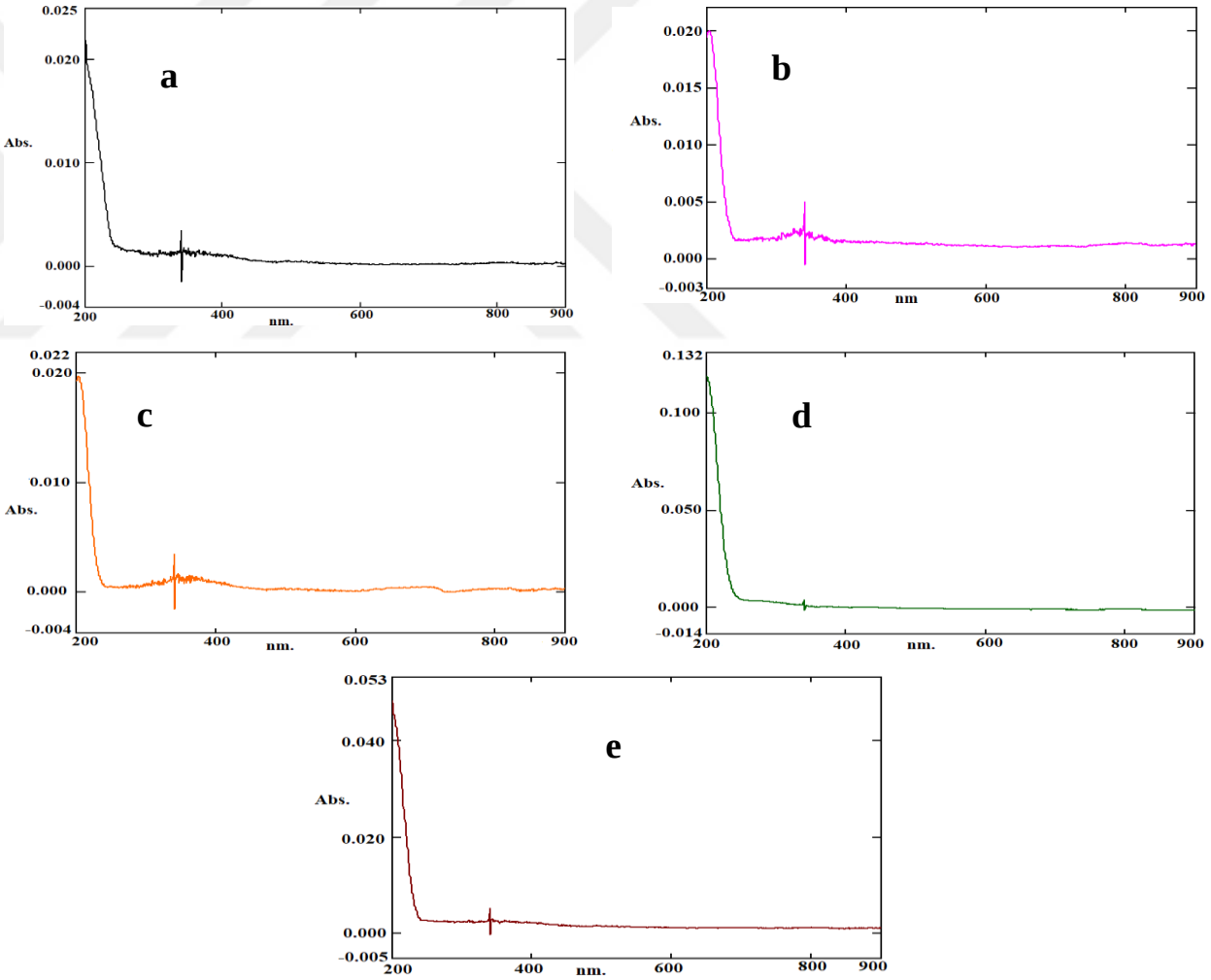

Figure 3.28. UV-vis spectra of the samples taken from the solution at different time intervals during the interaction of the AgNPs immobilized AEM with 0.001 M NaCl solution (pH 6.0) a) 5 min, b) 30 min, c) 60 min, d) 120 min, e) 180 min.

When all tables and figures were examined for stability studies, when the highest concentration of 0.5M NaCl solution was considered, it was observed that there was no particle leakage from the membrane to the NaCl solution during 180 min of contact time. The absence of particle leakage is of great importance for future RED tests.

Table 3.3. Maximum wavelength and absorbance values of supernatants taken from 0.001M NaCl solution with AgNPs immobilized membranes.

Sampling time (min)	**Maximum wavelength (nm)**	**Maximum absorbance**
5	423	0.010
30	423	0.002
60	423	0.001
120	423	0.000
180	423	0.000

Stability tests were carried out to see and determine release of AgNPs from the AgNPs immobilized AEMs when the AgNPs immobilized AEMs are in contact with NaCl solutions at different concentrations in RED studies. If the amount of AgNPs release is high, the resistance of AEMs to biofouling will decrease. It is aimed to keep the AgNPs release from AEMs as low as possible.

The XPS analyses were carried out to see the atomic percentages of the AgNPs immobilized AEMs before and after exposure to NaCl solutions.

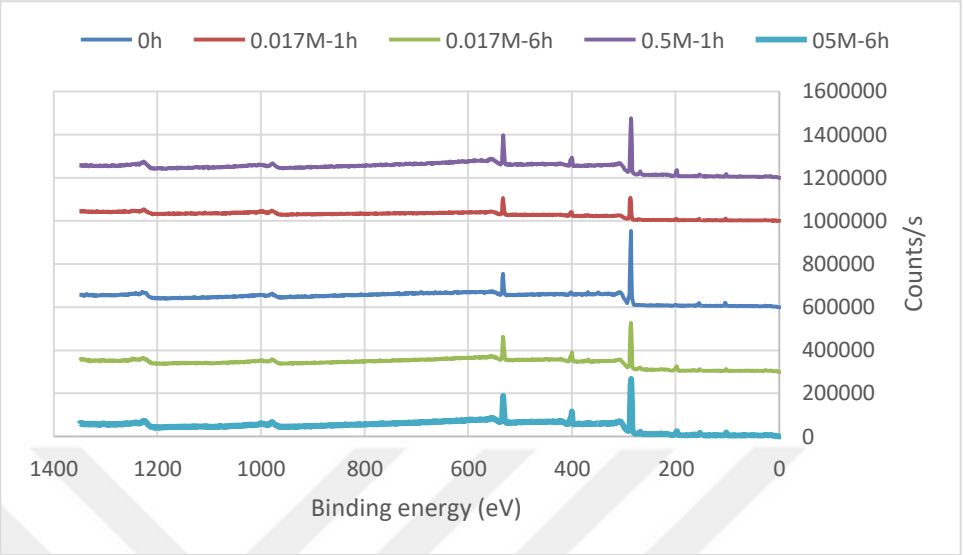

Figure 3.29. XPS results before and after stability tests

As seen in Figure 3.29, specific Ag3d bands belonging to metallic silver are seen at 368.4 eV and 374.4 eV. In addition, the absence of a specific 369.4 eV band belonging to Ag nanoclusters indicates that AgNPs are homogeneouslyimmobilized on the membrane surface.

The percentages of elements on the membrane surface with AgNPs immobilized before and after stability tests as a result of XPS analysis are given in Table 3.4. The amount of AgNPs decreased after contact with 0.5 M NaCl concentration. However, approximately the same atomic percentage values were obtained after 1 and 6 h of contact with 0.017M NaCl solution. Release of AgNPs from the AgNPs immobilized AEMs was observed when AgNPs immobilized AEMs were contacted with 0.5 M NaCl solution. But, it was considered that there was no release of AgNPs from AEMs when membrane was contacted with 0.017 M NaCl solution.

Table 3.4. Atomic results of the general XPS spectrum

Condition	S (%)	C (%)	Cl (%)	Ag (%)	N (%)	O (%)
No contact with NaCl	0.32	82.62	0.91	0.15	4.18	11.82
0.017 M NaCl-1 h	0.18	67.83	1.92	0.17	9.14	20.76
0.017 M NaCl-6 h	0.77	72.68	2.91	0.18	8.83	14.63
0.5 M NaCl-1 h	0.23	74.20	2.82	0.06	7.83	14.86
0.5 M NaCl-6 h	0.85	74.60	2.16	0.05	8.98	13.37

In addition, the ICP-MS measurements were carried out to observe the particle leakage from AgNPs immobilized AEM after contact with NaCl solution and to determine the amount of AgNPs immobilized on AEMs before and after contact with NaCl solutions. The amount of Ag on the AEMs can be seen in Table 3.5. It was understood that the amounts of silver release from the AgNPs immobilized membranes increased with increasing NaCl concentration in the salt solution. In essence, there was a reduction in the quantity of AgNPs present on the surface of the membrane. The membrane that underwent a 1-hour interaction with 0.5 M NaCl solution exhibited the lowest measured silver content of 11.2±0.8 μg/L, as determined by ICP-MS analysis. The value found for the membrane exposed to 0.5 M NaCl for 6 h is 16.8±0.8 μg/L, which is very close to the amount of silver in the membrane exposed to 0.5 M NaCl for 1 h. It was thought that the difference could possibly be an error of analysis (may be due to the resolution step performed before ICP-MS). On the other hand, it was considered that the AgNPs remaining on the membrane surface after contact with the NaCl solution may be still sufficient to ensure that the membrane has still antibacterial properties.

Table 3.5. Amount of AgNPs immobilized on the AEMs after treatment with NaCl solutions

Condition	**Ag (μg/L)**
No contact with NaCl	185±9
0.017 M NaCl-1 h	74±5
0.017 M NaCl-6 h	42±3
0.5 M NaCl-1 h	11.2±0.8
0.5 M NaCl-6 h	16.8±0.8

3.3.5. Antibacterial acitivities of AgNPs immobilized AEMs

The antibacterial properties of both the bare and AgNPs immobilized AEMs were evaluated by assessing their impact on a suspension of model gram-negative bacteria (E. coli) using the colony counting method. Results of the antibacterial tests are given in Figure 3.20. Figure 3.30-a shows the results of control group which is the incubated medium without membrane, Figures 3.30-b and c show the results of the AEMs and AgNPs immobilized AEMs. Viability of the bacteria appears to be reduced by means of AgNPs immobilized AEMs.

As seen in Figure 3.31, viability of E.coli decreased with AgNPs immobilized AEM. In AEMs, 1 log reduction (antibacterial rate, 90%) was observed in the viability of the bacteria and 5.5 log reduction (antibacterial rate, 99.999 %) was observed in AgNPs immobilized AEMs.

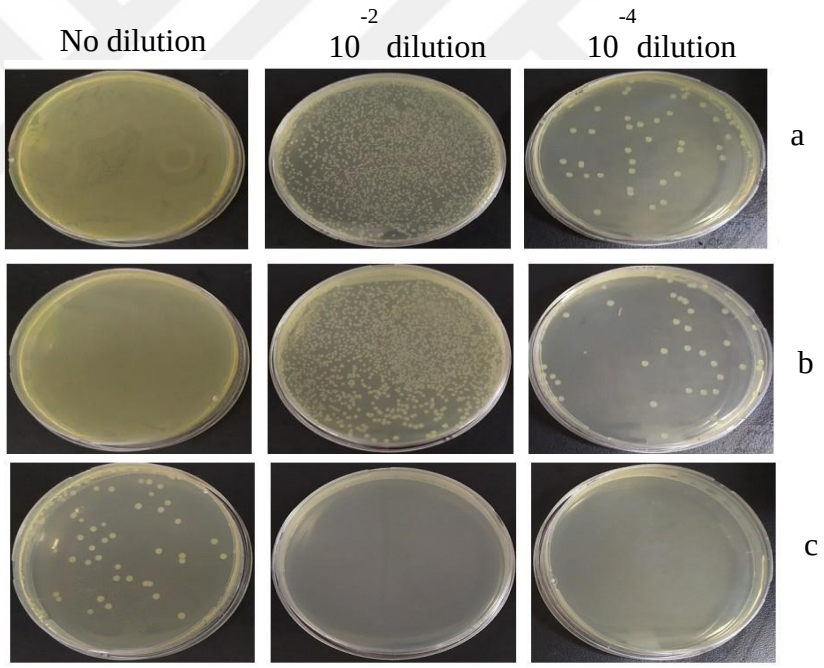

Figure 3.30. Results of the antibacterial tests a) Control (incubated medium without membrane) b) AEMs c) AEM-AgNPs

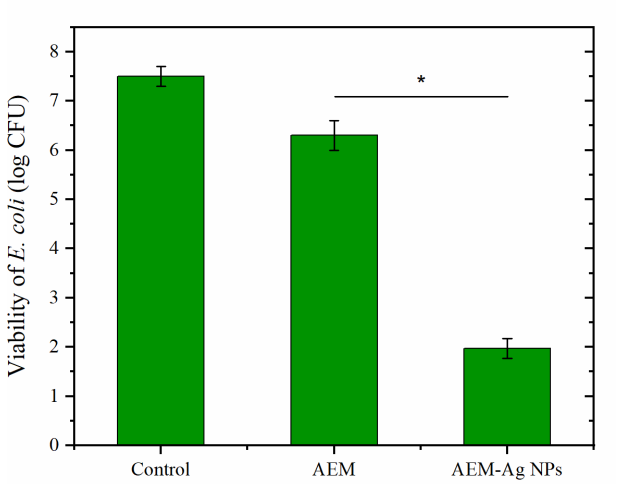

Figure 3.31. Antibacterial activity of the bare and silver coated AEM against E. coli (Control; incubated medium without membrane) (* donates a p.≤0.05 significance between membranes).

In the study of Zhu et al. (2010), silver was immobilized onto the surface of a chitosan membrane to examine the anti-biofouling performance of the membrane surface. Bare membrane had a significantly higher bacteria coverage than the silver immobilized membranes. Li et al. (2010) pointed to the possibility that nanoparticles may alter the structure of bacterial cell membranes and reduce the activity of certain membranous enzymes, ultimately leading to the death of *E. coli* bacteria. In the study of Vaselbehagh et al (2017), the results demonstrated that AEM's anti-biofouling characteristics were enhanced by a polydopamine(PDA) layer during RED operation. Yuksel et al (2014) showed that the best antibacterial effects were seen in nanocomposite membranes that incorporated surface AgNP storage. In the study of Radzig et al. (2013), it has been observed that AgNPs can inhibit the growth of Gram-negative bacteria in both planktonic cells and biofilms.

3.3.6. Preparation and characterization of large and small AgNPs

The UV-visible absorption curve of the AgNps produced at room temperature by the method A described in the experimental part is given in Figure 3.32. The maximum wavelength value was measured as 400 nm. The particle size of the AgNPs produced at 170 rpm and 3.3 mL/min flow rate is measured as 73.64 nm. A 450 rpm mixing and 3.3 mL/min of flow rate it is 78.62 nm. A 450 rpm mixing and 5 mL/min of flow rate it is 72.87 nm. The obtained results showed that the

particle size of the AgNPs produced by the method A was not significantly affected by the flow rate and mixing speed.

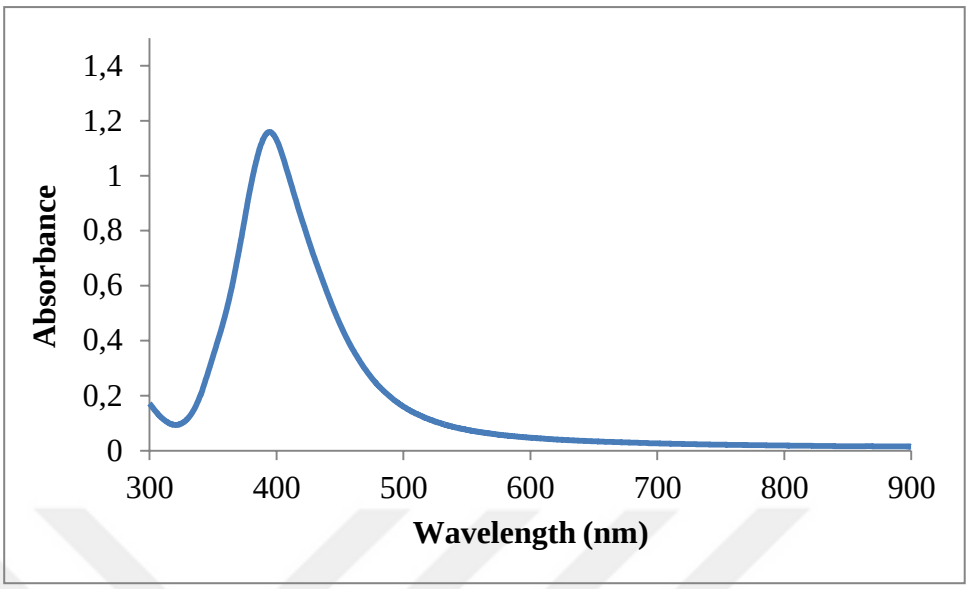

Figure 3.32. UV-vis absorption curve of AgNPs produced by the method A

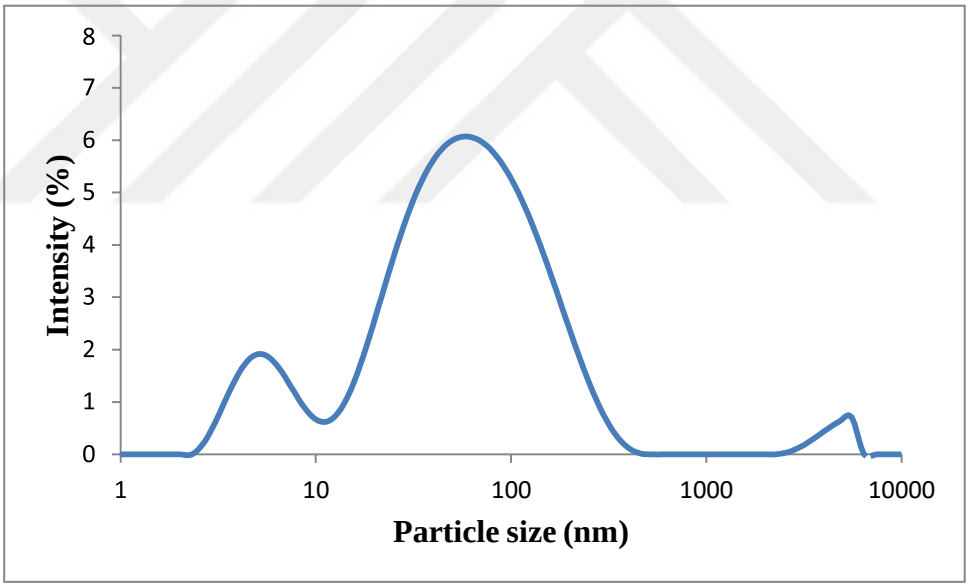

Figure 3.33. Particle size distribution of AgNPs produced with the method A at 450 rpm mixing rate and 3.3 mL/min of flow rate

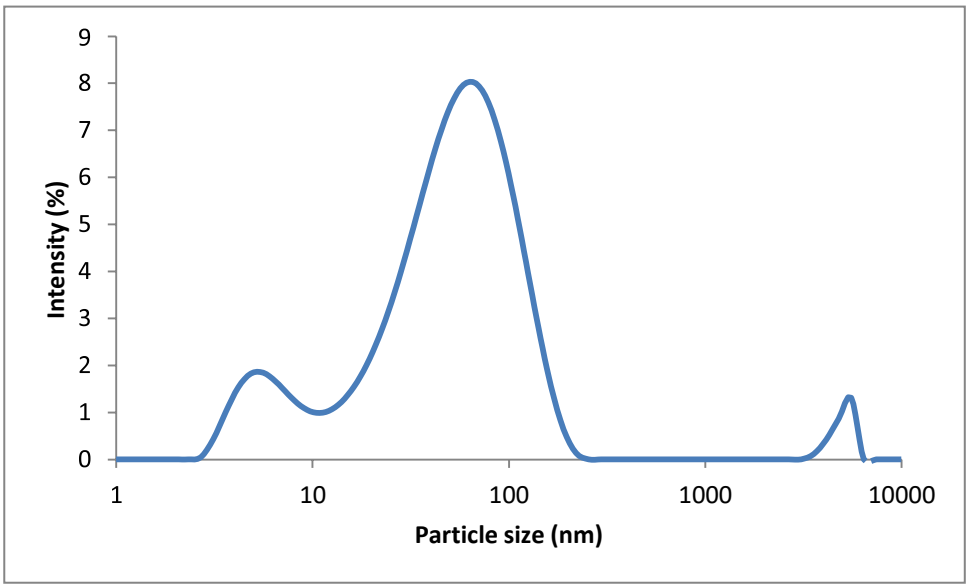

Figure 3.34. Particle size distribution of AgNPs produced with the method A at 450 rpm of mixing rate and 5 mL/min of flow rate

The UV-vis absorption curve of the AgNPs produced by the method B, the details of which are explained in the experimental part, is given in Figure 3.35. At the maximum absorbance, wavelength was measured as 400 nm.

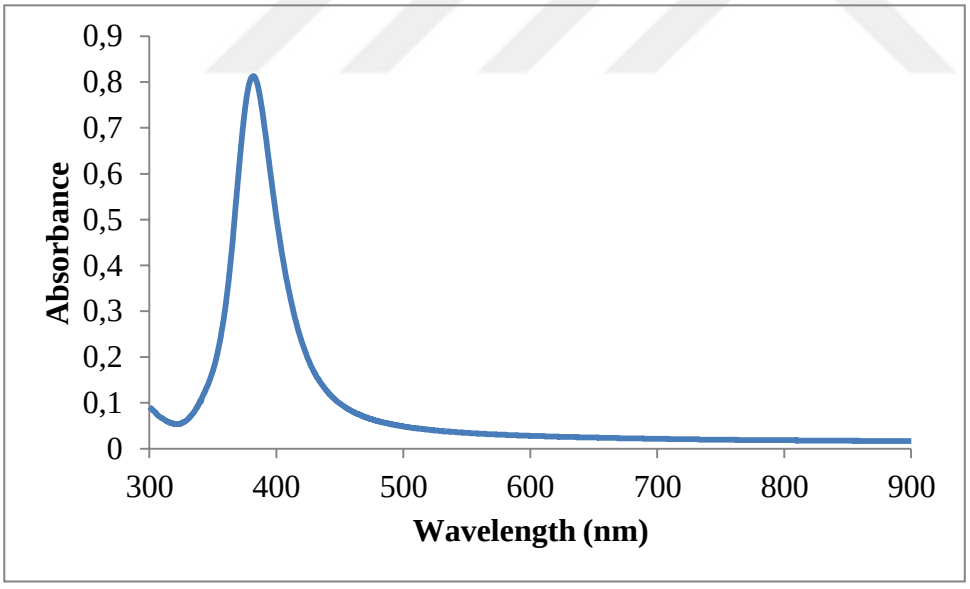

Figure 3.35. UV-vis absorption curve of AgNPs produced by the method B

Particle size distribution curves of AgNPs produced with the method B at 1.5, 2.5, 3.3 and 5.5 mL/min of flow rates are shown in Figures 3.36-3.39, respectively. Between 1.5 and 3.3 mL/min, AgNPs with a mean size of 53.3 nm were manufactured. Nanoparticles of 72 nm size were produced at a flow rate of

5.5 mL/min. The obtained results showed that AgNPs produced at the highest flow rate of larger particle size.

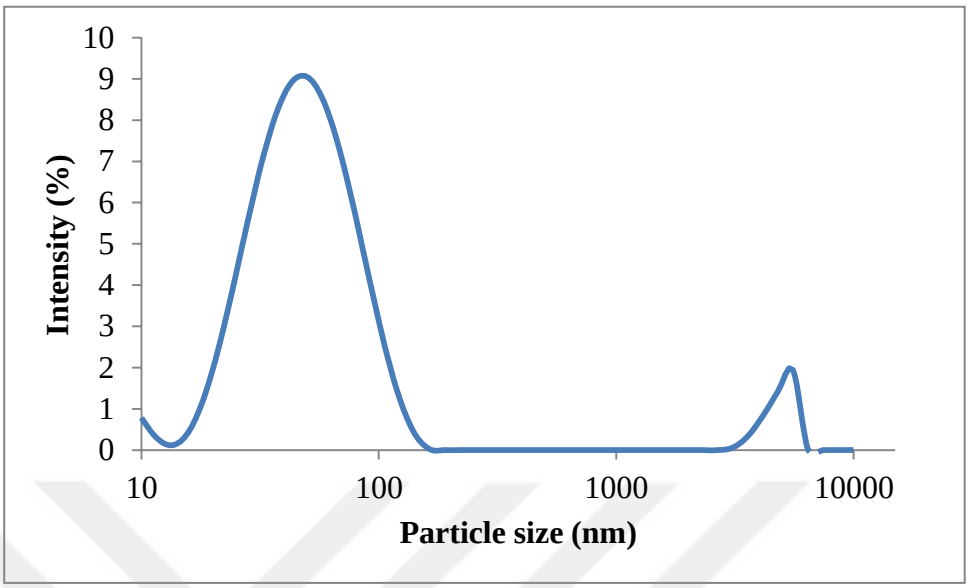

Figure 3.36. Particle size distribution curve of AgNPs produced with the method B at a flow rate of 1.5 mL/min

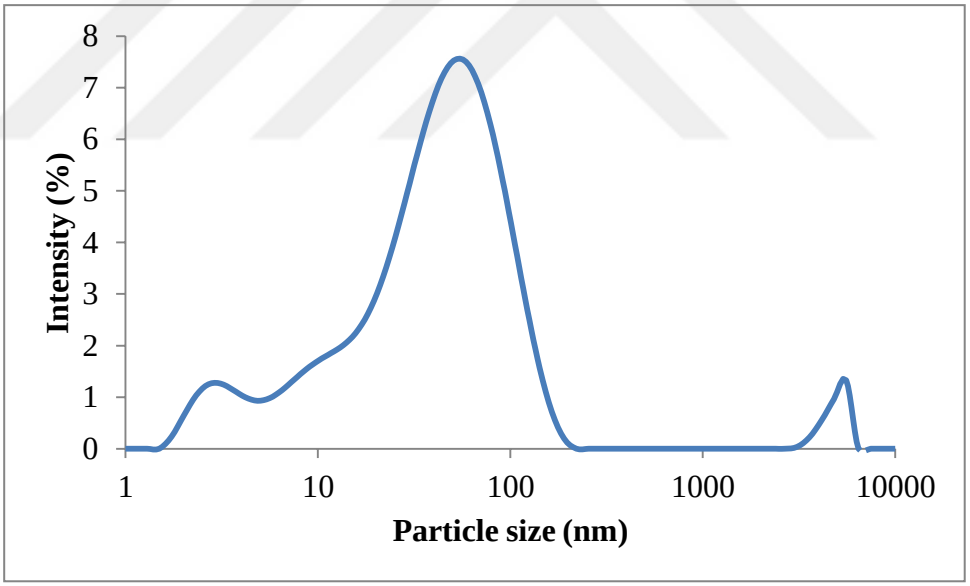

Figure 3.37. Particle size distribution curve of AgNPs produced with the method B at a flow rate of 2.5 mL/min

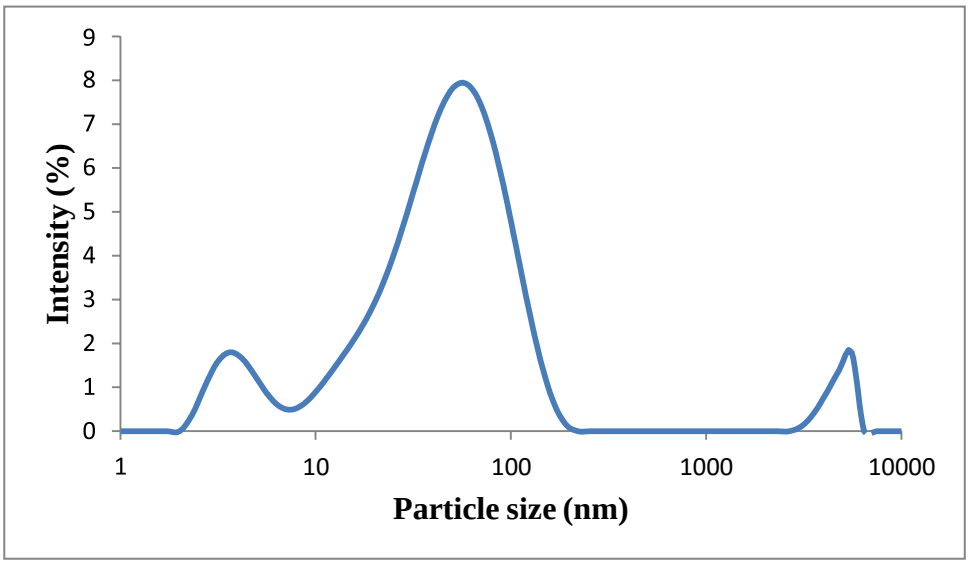

Figure 3.38. Particle size distribution curve of AgNPs produced with the method B at a flow rate of 3.3 mL/min

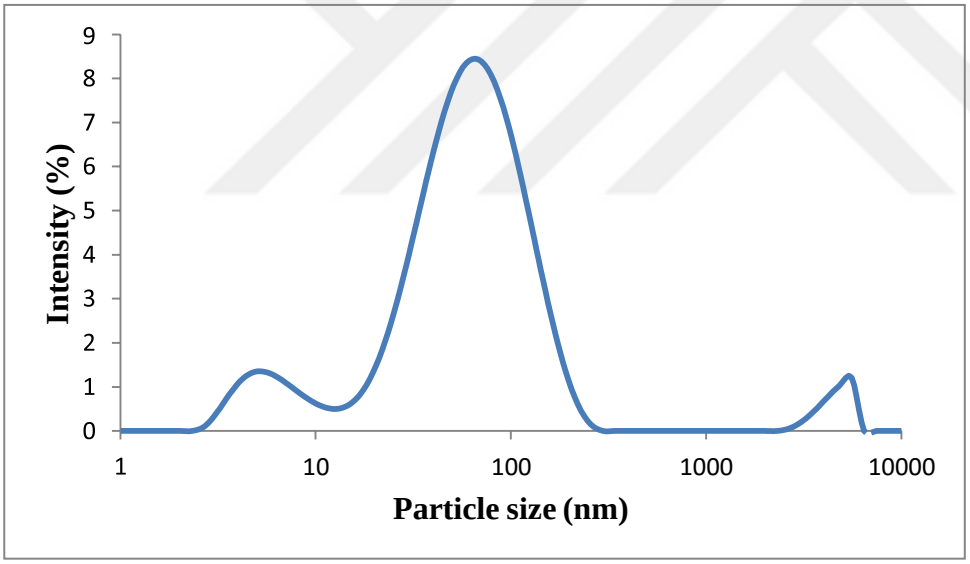

Figure 3.39. Particle size distribution curve of AgNPs produced with the method B at a flow rate of 5.5 mL/min

3.3.7. RED Tests with AgNps Immobilized AEMs

In RED tests, EDR2-BR0.6 membrane was used as AEM. Technical properties of EDR2-BR0.6 membrane is given in Table 3.6.

Table 3.6. Technical properties of EDR2-BR0.6 membrane

Ion exchange capacity (mmol/g dry membrane)	2.02
Swelling degree (%)	20.88
Thickness (μm)	154
Fixed charge density (mmol/g H_2O)	9.62

Power density vs. current density obtained with EDR2-BR0.6 and NEOSEPTA CMX and AgNP-EDR2-BR0.6 and NEOSEPTA CMX membrane pairs are shown in Figures 3.40 and 3.41, respectively. Table 3.7 summarizes these results as well. The power density values grew with the flow rate until the open circuit voltage caused them to drop. Power density values are close to each other in AgNps immobilized and non-immobilized AEMs studies. The resistance introduced by the AgNPs resulted in a marginal drop in power density value. As the open circuit voltage values increased, the power density values increased, and decreased as they decreased. In this study, maximum power density was achieved with EDR2-BR0.6 and NEOSEPTA CMX membrane couple with the value of 0.429 W/m^2. Güler et al (2013) obtained the highest power density of 1.27 W/m^2 with CMX and PECHB1 membranes. The reason for the higher power density value in that study is that the number of membrane pairs was 5 and the spacer thickness is 200 μm. In this study, number of the membrane pairs is 3 and the spacer thickness is 400 μm.

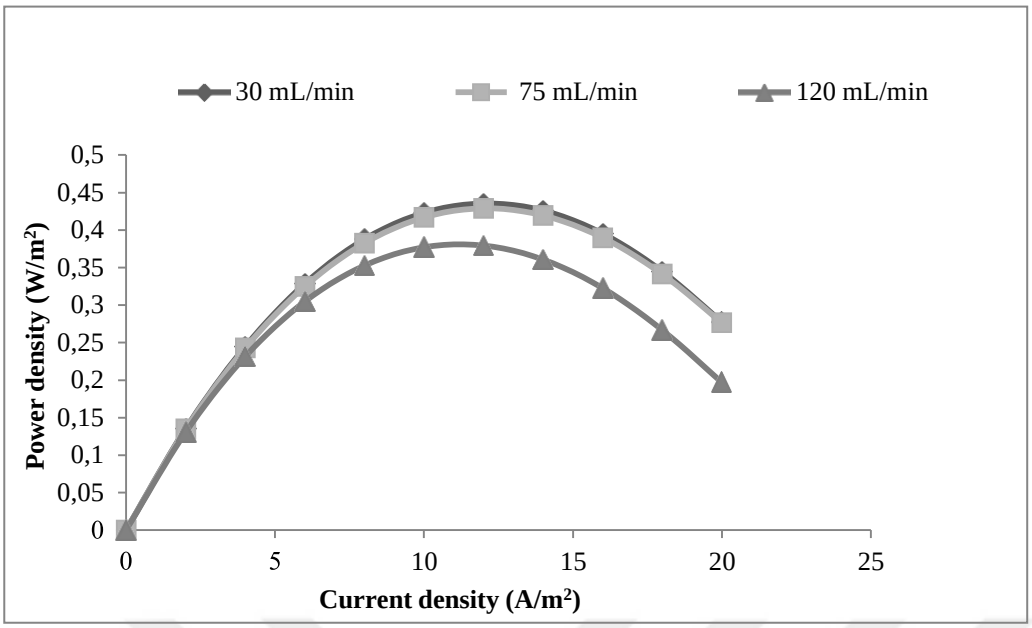

Figure 3.40. Power density vs. current density plots obtained with 3 pairs of EDR2-BR0.6 and NEOSEPTA CMX at different volumetric flow rates

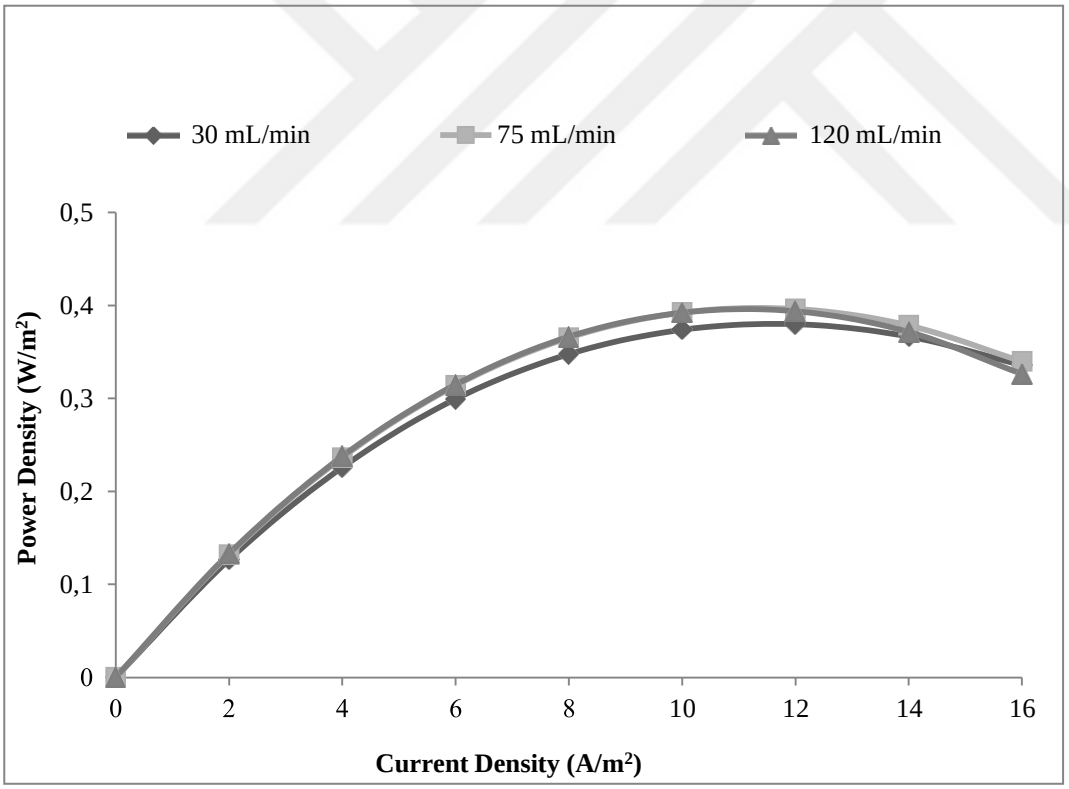

Figure 3.41. Power density vs. current density plots obtained with 3 pairs of AgNp-EDR2-BR0.6 and NEOSEPTA CMX at different volumetric flow rates

Table 3.7. Results of the RED tests with EDR2-BR0.6 AEMs and AgNPs immobilized EDR2-BR0.6 AEMs coupled with NEOSEPTA CMX

Membranes	Salinity ratio (g NaCl/L: g NaCl/L)	Number of membrane pair	Volumetric flow rate (mL/min)	Maximum power density (W/m^2)	Open circuit voltage (V)
AgNP-EDR2-BR0.6-NEOSEPTA CMX	1:30	3	30	0.374	0.415
			75	0.396	0.437
			120	0.394	0.438
EDR2-BR0.6-NEOSEPTA CMX			30	0.379	0.435
			75	0.429	0.444
			120	0.374	0.415

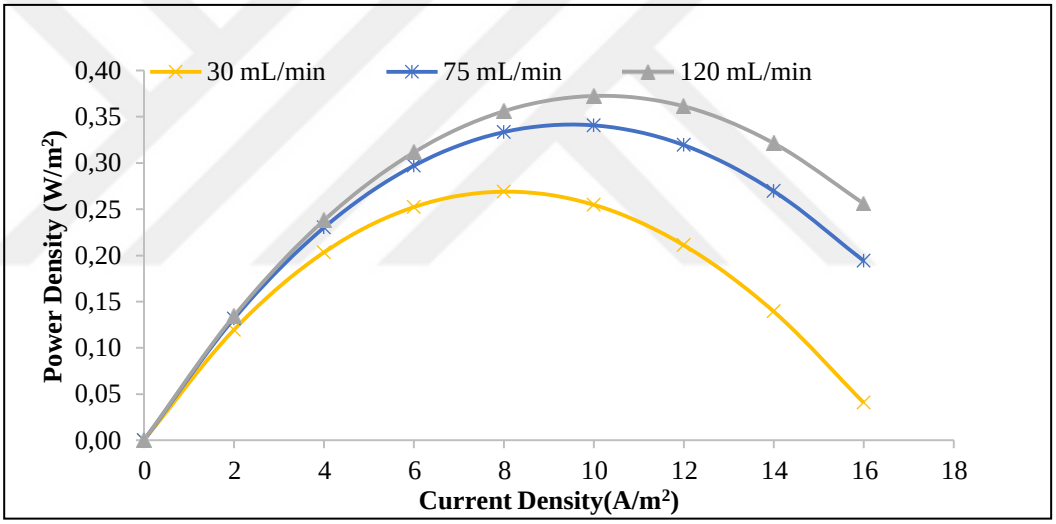

Figure 3.42. Power density vs. current density plot for short-term operation of AgNPs immobilized PECH-C AEMs paired with NEOSEPTA CMX CEMs

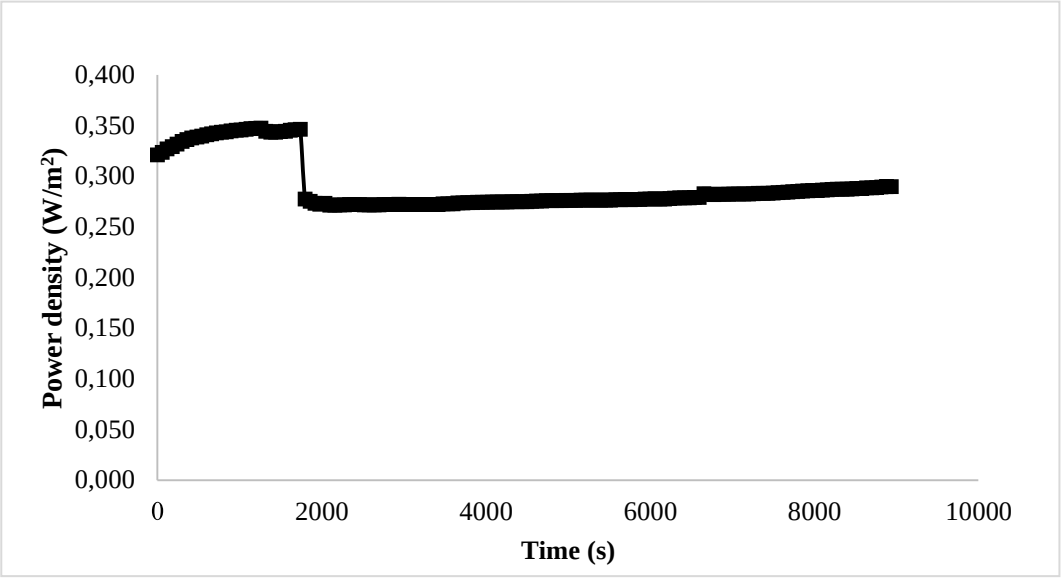

Figure 3.43. Power density versus time plot for long-term operation of AgNPs immobilized PECH-C AEMs paired with NEOSEPTA CMX CEMs

Power density versus time plots for short and long-term operation of AgNPs immobilized PECH-C AEMs paired with NEOSEPTA CMX CEMs are given in Figures 3.42 and 3.43, respectively. For PECH-C membranes paired with NEOSEPTA CMX and the AgNPs immobilized PECH-C membranes, the maximum power density values were 0.316 W/m^2 and 0.370 W/m^2, respectively (for short term RED tests). During long-term RED studies, maximum power densities of 0.222 W/m^2 and 0.346 W/m^2 were obtained for PECH-C membranes coupled with NEOSEPTA CMX and AgNPs immobilized PECH-C membranes, respectively. The maximum power density values increased due to the increase in conductivity in the AgNPs immobilized PECH-C membranes.

A decrease in power density values was observed with increasing flow rate in the short term studies of PECH-C AEMs coupled with NEOSEPTA CMX CEMs. An increase in power density values was observed with increasing flow rate in short term studies of AgNPs immobilized PECH-C AEM paired with NEOSEPTA CMX membranes. In the long term studies, power density values decreased. The reason for the decrease in power density in long-term operations isthe increase in the resistance value. 9.66% reduction was observed in AgNPs immobilized membranes. A decrease of 31.08% was observed in the bare membrane.

3.4. Conclusion

In this study, AgNPs were synthesized in a water bath at a constant temperature of 30°C using ascorbic acid as a reductant and trisodium citrate as a stabilizer with solution pH of 6.0 and 9.0. The particle size of the AgNPs was at the targeted level (107.4 nm) and absorbance value was compatible with the literature value (442 nm for pH 6.0 and 432 nm for pH 9.0). The AgNPs were immobilized onto AEMs by dip coating method. The AgNPs produced at pH 6.0 were homogeneously immobilized to the AEMs. The antibacterial activities of the bare and AgNPs immobilized AEMs were determined using the model gram- negative bacteria (*E. coli*) suspension with the colony counting method. The AgNPs immobilized AEMs showed a high antibacterial activity. Two different methods (Method A and Method B) were used in the synthesis of AgNPs. The production flow rate ranged from 1.5 to 3.3 mL/minute, which resulted in the production of AgNPs with an average size of 53.3 nm.

CHAPTER 4

PREPARATION OF PORE FILLING AEMs AND THEIR CHARACTERIZATION AND IMMOBILIZATION OF AgNPs ONTO PORE FILLING AEMs

4.1. Introduction

Porous polymer substrates can serve as the basis for pore-filling membranes (PFMs), which are created by filling the substrate's pores with ionomers. Invarious industrial applications, including RED, fuel cells, and capacitive deionization, PFMs made with the addition of ionomer or polyelectrolyte are especially valuable (Eti et al., 2021).

Yamaguchi et al. (2003) were the first to present pore-filling IEMs for use in a direct methanol fuel cell. It is essential, for both fuel cell operations and RED processes, to achieve high levels of ionic conductivity and selectivity. (Yaroslavtsev, 2020). Consequently, PFMs have been tested in RED systems to evaluate their effectiveness.

It is possible to create a viable alternative for RED applications by fabricating pore-filling membranes with a layer thickness of only about 100 μm. Filling a fine-pored support material results in these membranes (Kim and Kang, 2016, Kim et al., 2015, Yang et al., 2019), making it possible to synthesize membranes of the desired thickness depending on the thickness of the support material.

Research on fuel cells incorporating porous membranes in the electrochemical energy field has become increasingly common. Over the past decade, pore-filled IEMs for RED applications have been extensively investigated, with ongoing research currently underway. To be effective in RED systems, PFMs must meet several requirements, including low DS, high IEC, and low electrical resistance. Table 4.1 provides more detailed information on the use of PFMs in RED testing.

Lee et al. (2014) reported that anion-conducting PFMs could be produced using varying weight ratios of monomer to crosslinker in quaternized poly(styrene-co-ethylene glycol dimethacrylate). However, the commercial Neosepta AMX membranes still exhibit lower area resistance, higher IEC, and DS than the experimental membranes.

In another study by Kim et al. (2015), an AEM (KIERAEM1) and two CEMs were constructed. These membranes had low area resistances, with an open

spacer area of only 81.3%. Compared to commercial AEMs and CEMs, the low area resistances resulted in a gross power density of 2.4 W/m^2.

Table 4.1. Some characteristics of PFMs that have been discussed in the context of RED applications (Adapted from Eti et al., 2021)

Membrane	IEC (meq/g)	SD (%)	Thickness (μm)	AR (Ω. cm^2)	Permselectivity (%)	Reference
AMX	2.36	37.4	35-40	0.303	N.A.	Lee et al, 2014
KIER AEM1	N.A.	21.9	27	0.28	91.8	Kim et al., 2015
EC21-DMA1.0	1.26	21.3	25	0.764	93	Choi et al., 2018
Pore filling AEM	N.A.	N.A.	16	0.402	92.4	Kim et al., 2019
Flat AEM	N.A	N.A.	20	0.46	98.1	Choi et al., 2021

4.2. Material and Methods

In order to produce a pore-filled membrane, wet-laid non-woven polyester material (Type TH, 05TH100) supplied from Hirose Paper, Japan was used as a supporting material. The properties of the material used as the support material are given in Table 4.2

Table 4.2. Properties of the supporting material used in the preparation of pore filling anion exchange membranes (PFAEMs)

Type	**Weight (g/m^2)**	**Thickness (μm)**	**Tensile strength (N/15 mm)**	**Air permeability (cm^3/cm^2/sec)**
05-TH-100	100.4	162	Machine direction: 84 Cross machine direction: 43.5	0.50

4.2.1. Preparation of PFAEMs and AgNPs immobilized PFAEMs

Large-scale AEM casting was performed with the membrane with high ion exchange capacity and low swelling degree, EDR 4 and BR 1.07, which gave the best results. Membrane casting was carried out in the same way as the synthesis steps of large-scale AEMs for the RED system. Unlike the previous study, wet- laid non-woven polyester material was used as a support material in this case.

a **b**

Figure 4.1 a) Casting solution in the mold with support material b) PFM separated from the mold

Solution was casted to the mold onto the support material and then membrane was separated from the mold (Figure 4.1). As seen in Figure 4.2-a, AgNPs were immobilized to PFAEMs with dip coating method and membranes were immersed nanoparticle solution for 24h. AEMs were washed with distilled water after removing from AgNPs solution. The image of the membranes after washing is given in Figure 4.2-b.

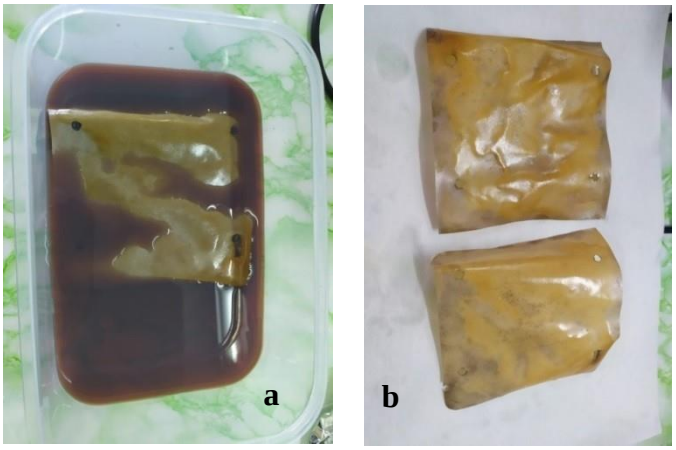

Figure 4.2. a) AEM immersed in AgNPs solution and b) AEMs removed from the solution

4.3. Results and Discussion

4.3.1. Pore filled anion exchange membranes (PFAEMs)

AgNPs immobilized PFAEMs were obtained by immersing the AEMs in to AgNPs solution for 24 h at room temperature by dip coating. The properties of pore-filled and AgNPs immobilized PFAEMs are given in Table 4.3. After the AgNPs was immobilized to the pore-filled membrane, a decrease in the ion exchange capacity and an increase in the swelling degree of the final membrane were observed. The decrease in the ion exchange capacity of the final membraneis due to the blockage of functional groups by the AgNPs on the membrane. On the other hand, the reason for the increase in the swelling degree is the hydrophiliccharacter of the AgNPs in the membrane structure.

Table 4.3. Properties of PFAEM and silver nanoparticle immobilized PFAEM

Membrane	Ion exchange capacity (mmol/g dry membrane)	Swelling degree (%)
PFAEM*	2.19±0.357	39.60±9.00
AgNp PFAEM**	1.82±0.247	51.11±5.22

4.3.2. Area resistance measurement results

Area resistance measurement values of PFAEMs and AgNPs immobilized PFAEMs are given in Tables 4.4 and 4.5. Area resistance value in AgNPs immobilized PFAEM is higher than PFAEM. Actually this was expected result.

Table 4.4. Area resistance results of PFAEMs.

Membrane	Thickness (μm)	Area resistance (Ω *cm^2)
PFM	246	8.780±0.158
AgNp-PFM	197	9.518±0.775

Table 4.5. Area resistance measurement results of PFAEMs and AgNPs immobilized AEMs.

Membrane	**Thickness (μm)**	**Area resistance ($\Omega.cm^2$)**
EDR4-BR1.07(0.5M NaCl-18h)	209	3.244±0.100
PFM*-EDR4-BR1.07 (0.5M NaCl-18h)	160	8.087±0.638
AgNp-PFM (0.017M NaCl-1h)	194	14.020±0.194
AgNp-EDR4-BR1.07 (0.017M NaCl-1h)	201	6.676±0.185
AgNp-PFM (0.5M NaCl-1h)	194	7.252±0.345
AgNp-EDR4-BR1.07 (0.5M NaCl-1h)	201	3.267±0.344

It was observed that the area resistances of the AgNPs immobilized membranes decreased as the NaCl concentration of the solution increased. The number of ions contained inside the membrane structure rose in proportion to the rise in the concentration of ions present in the solution, which increased the conductivity. According to the ICP-MS results, although the silver release from the membrane increased, the field strength decreased. Comparison of area resistances of AEMs with the literature are given in Table 4.6. In the literature, thickness values are lower than thickness values of this study and because of this reason, resistance values are higher in this research.

Table 4.6. Comparison of area resistances of AEMs with the literature

Membrane	Thickness (µm)	Area resistance (Ω *cm^2)	Reference
KIER-AEM-1	26	0.34	Kim et al., 2015
KIER AEM-2	27	0.28	
PFAEM	16	0.48	Kim et al., 2021
AEMW1-2	16	0.23	Lee et al., 2017
VBC:DMAEM 0.5:1/DVB0.10	24	1.25	Choi et al., 2018
AMX(16:1)	35-40	0.868	Lee et al., 2014
PECH-A	77	2.05	Güler et al., 2012
PECH-B1	33	0.82	
PECH-B2	77	0.94	
PECH-B3	130	1.32	
PECH-C	77	1.14	
V3A	66	0.87	Rijnaarts et al., 2019
V3B	84	1.36	

In the study of Guler et al., AEMs prepared for the RED system with a thickness of 77 µm, a swelling degree of 32%, and an ion exchange capacity value of 1.3 mmol/g-dry membrane was measured as 2.5 Ω.cm^2. Rijnaarts et al. (2019) obtained an area resistance of 1.36 Ω.cm^2 for AEMs (aliphatic Fuji V3B membrane) with a thickness of 84 µm, an ion exchange capacity of 1.7 mmol/g- dry membrane, and a swelling degree of 61%. In another study, the area resistance of AEMs (polystyrene/divinylbenzene/chloromethyl styrene AMV and APS membrane) with a thickness of 110-150 µm, a swelling degree of 17%, an ion exchange capacity of 1.78 mmol/g-dry membrane is 2.8 Ωcm^2 (Raka et al., 2021). In this study, the measured area resistances of AEMs were found to be higher thanin the literature. It was considered that the differences in the membrane thickness, swelling degree and ion exchange capacity affected the area resistance results.

4.3.3. RED Tests with PFAEMs and AgNps immobilized PFAEMs

The ion exchange capacity and swelling degrees of large-scale, small-scale and PFAEMs were compared. Characterization of small scale, large scale and PFAEMs are given in Table 4.7. Swelling degree value is very high for large scalemembranes because of the thickness of the membrane and there is no supporting material (porous reinforcement) so swelling increases. Thickness of PFAEMs waslarger.

Table 4.7. Properties of small scale, large scale and PFAEMs

Membrane	Properties	Thickness (μm)	Ion Exchange Capacity (mmol/g dry membrane)	Swelling Degree (%)
Small scale Non reinforced AEM	Excess diamine ratio:4 Blend ratio:1.07	140±20	3.47±0.100	66.0±5.00
Large scale Non-reinforced AEM		250±50	2.84±0.280	89.0±7.73
Large scale PFAEM		260±80	2.19±0.357	39.7±9.00

Power density vs. current density plots with PFAEMs and AgNPs immobilized PFAEMs are given in Figures 4.3 and 4.4. Table 4.8 summarizes the data obtained in RED tests.

Power density values decreased with increasing flow rate because of the resistance of nonvowen material. Power density value is decreasing with AgNPs immobilized PFAEMs because of the resistance of the AgNPs immobilized onto PFAEMs.

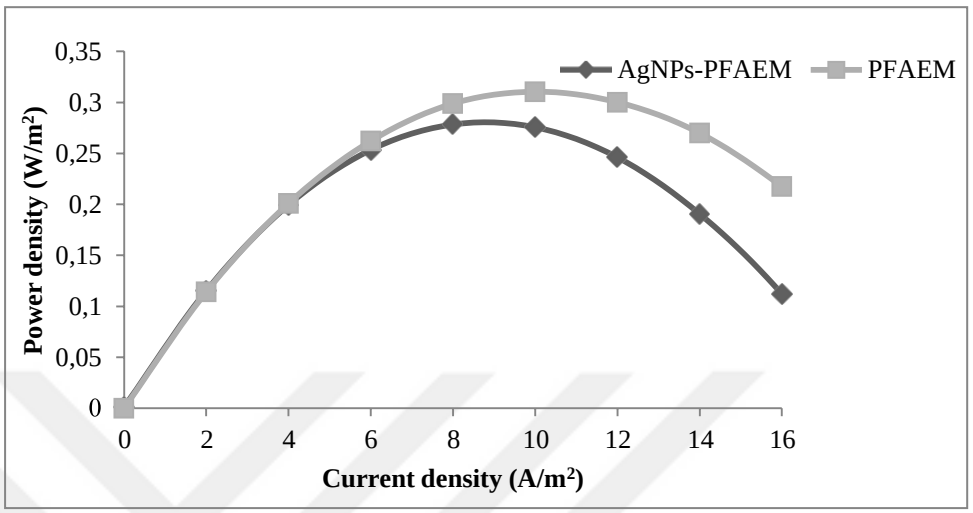

Figure 4.3. Power density vs. current density plots obtained with PFMs and AgNPs immobilized PFAEMs at 30 mL/min of feed flow rate

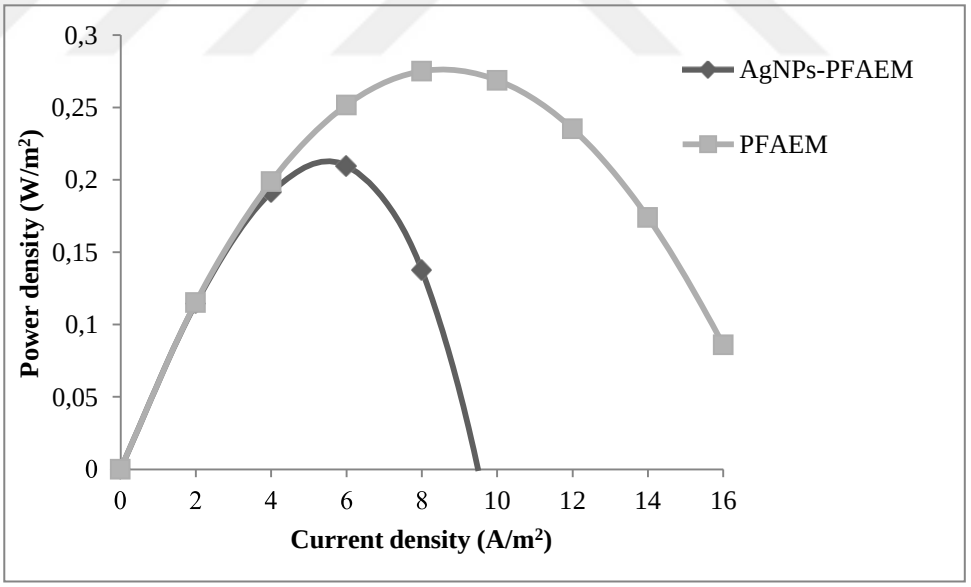

Figure 4.4. Power density vs. current density plots obtained with PFAEMs and AgNPs immobilized PFAEMs at 75 mL/min of feed flow rate

Table 4.8. Results of the RED tests with PFAEMs and AgNPs immobilized PFAEMs

Membranes	**Salt ratio (g NaCl/L-H_2O low saline solution: g NaCl/L-H_2O high saline solution)**	**Number of membrane pair**	**Volumetric flow rate (mL/min)**	**Maximum power density (W/m^2)**	**Open circuit voltage (V)**
PFAEMs	1:30	3	30	0.310	0.398
			75	0.275	0.393
AgNp-PFAEMs			30	0.278	0.381
			75	0.148	0.373

There is no any published literature on the RED performances of AgNPs immobilized PFAEMs. The data in the literature are mostly about pore filling AEMs (Lee et al., 2014, Choi et al., 2018, Kim et al., 2015). In the study of Leeet al (2014) the highest power density was achieved with the value of 0.05 W/m^2 using pore-filling membranes filled with quaternized poly(styrene co-ethylene glycol dimethacrylate. In the study of Choi et al (2018), highest power density is obtained as 1.524 W/m^2. In the study of Kim et al (2015), power density was achieved as 2 W/m^2 because of the low area resistance values of the membranes. Lower power density values were obtained in pore-filled membranes compared to AgNPs immobilized AEMs and AEMs without AgNPs immobilized, due to the resistance created by the supporting material used in the system (Table 4.9).

Table 4.9. Overall RED tests results

Membranes	**Salinity ratio (g NaCl/L: g NaCl/L)**	**Number of membrane pair**	**Volumetric flow rate (mL/min)**	**Maximum power density (W/m^2)**	**Open circuit voltage (V)**
EDR4-BR1.07 and CMKESD	1:30	3	30	0.190	0.425
			75	0.395	0.435
			120	0.304	0.435
EDR4-BR1.07 and NEOSEPTA CMX			30	0.313	0.395
			75	0.336	0.422
			120	0.376	0.431
EDR2-BR0.6-NEOSEPTA CMX			30	0.379	0.435
			75	0.429	0.444
			120	0.374	0.415
AgNPs-EDR2-BR0.6-NEOSEPTA CMX			30	0.374	0.415
			75	0.396	0.437
			120	0.394	0.438
PFM			30	0.310	0.398
			72	0.275	0.393
AgNPs immobilized PFMs			30	0.278	0.381
			75	0.148	0.373

4.4. Conclusion

In this study, PFAEMs immobilized with AgNPs were created by dipping the membranes in AgNPs solution for 24 h at room temperature. A decrease in the ion exchange capacity and an increase in the swelling degree of the final membrane were observed. RED tests were done with PFAEM and AgNPs immobilized PFAEMs. Power density value is decreasing with AgNPs immobilized PFAEMs (0.373 W/m^2).

CHAPTER 5

FOULING TESTS WITH HUMIC ACID

5.1. Introduction

Membrane fouling is caused by the many fouling elements in the feed interacting with the membrane surface in complex ways. Typically, foulants can be divided into the four categories listed below:

- Particulates: inorganic or organic particles/colloids
- Organic: humic and fulvic acids,
- Inorganic: Dissolved components
- Micro biological organisms (Guo et al., 2012)

Membrane fouling is a major drawback for RED applications, and it can significantly reduce power density by increasing membrane resistance and decreasing permselectivity (Vermaas et al., 2013). Optimizing operational conditions, developing better spacers, and modifying the membrane's surface are all necessary to reduce fouling (Vermaas et al., 2014; He et al., 2016; Vaselbehagh et al., 2017).

Humic acid (HA) is one of the principal constituents of humic substances, which are abundant in soil (humus), peat, montane streams, dystrophic lakes, and seawater (Ahmad et al., 2019). Schematic mechanism of humic acid fouling of AEMs is given in Figure 5.1. Humic acids function as big, multivalent anions that swap places with counter ions (Cl^- in this case) and fill up fixed charged groups in the AEM (Rijnaarts et al., 2019).

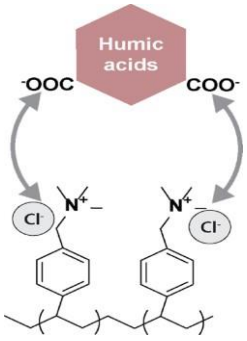

Figure 5.1 Schematic mechanism of humic acid fouling of AEMs

In RED with natural streams, several different types of fouling can arise, ranging from biofouling to scaling and organic fouling by organic molecules other than humic acids (Rijnaarts et al., 2019). In the study of Susanto et al. (2017) 0,10,30,50 mg/L HA was added to saline solutions wth two different concentrations of NaCl. A decrease in power density was observed. Santoro et al. (2021) studied addition of 5 and 8.4 mg/L HA to artificial seawater and brine solutions and after 20 days overall reduction of 23% of power density was obtained. In the study of Gao et al. (2018) 10 mg/L HA solution was added to dilute and concentrated feed solutions and the power generation was increased by up to 17% , monovalent–anion selectivity and antifouling potential were improvedby the surface modification. Pawlowski et al. (2016) studied addition of 40.4 mg/L HA solution to the synthetic aqueous solutions and after the initial period of three days, the resistances ratio increased by 11%. In the study of Vermaas et al., 2014, 19 mg/L HA+ 9 mg/L fulvic acid were added to river water. Also, 10 mg/L HA+ 3 mg/L fulvic acid were added to the sea water and The experiment begins with an apparent permselectivity of roughly 95%, but by the end of it, it has dropped to between 74% and 81%.

5.2. Material and Methods

5.2.1. Humic acid adsorption tests

HA solution containing 12% HA and fulvic acids (FA) (Ant), 2% water-soluble potassium oxide, 5% total organic matter and pH range 9-11 was used in HA adsorption studies.

In the HA adsorption studies given in the literature, the membranes were generally interacted with a HA solution with a maximum concentration of 50 mg/L. In this study, experiments were carried out with solutions containing 25 and50 mg/L of HA. Membranes were reacted with HA solutions using a shaker for 24h at room temperature.

HA solutions were prepared in 0.017 M NaCl (river water concentration). Figures 5.2 and 5.3 show the dry state of the membranes, which were treated with HA-containing solutions. As the humic acid concentration in the solution in contact with the membranes increased, a significant darkening in the color of the membranes was observed.

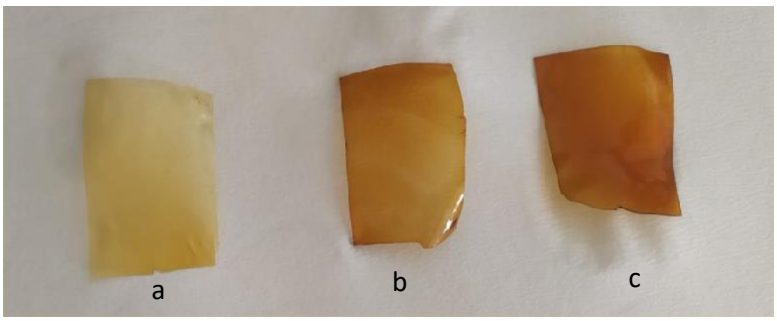

Figure 5.2. Wet membranes treated with a) 0.017 M NaCl only b) 25 mg/L HA in 0.017 M NaCl c) 50 mg/L HA in 0.017 M NaCl

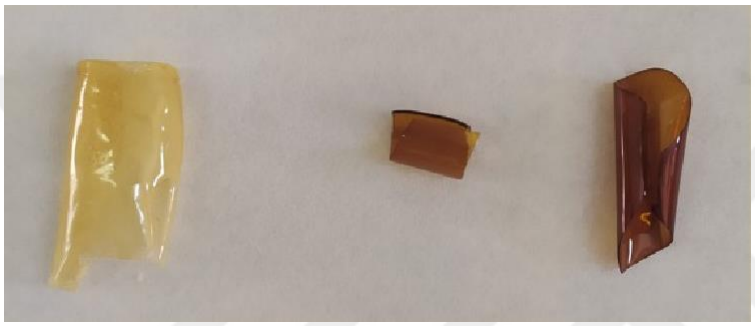

a **b** **c**

Figure 5.3. Dried membranes interacted with a) 0.017 M NaCl only b) 25 mg/L HA in 0.017 M NaCl c) 50 mg/L HA in 0.017 M NaCl

5.3. Results and Discussion

5.3.1. Humic Acid Fouling Tests with AgNPs immobilized AEMs

The FTIR results of bare and AgNPs (pH:6.0) immobilized membranes interacted with 0.017 M and 0.5 M NaCl containing HA at a concentration of 25 and 50 mg/L are given in Figures 5.4-5.6. In the FTIR spectrum, HA 3246 cm^{-1} (H-bonded OH), FA 3497 cm^{-1} H-bonded OH groups, HA 1721 cm^{-1} (C=O of COOH, ketonic C=O bond C=O extension), HA 1634 cm^{-1} (COO-, C=O carbonyl and quinone groups), FA 1648cm^{-1} (COO-, C=O carbonyl and quinone groups) and 1158 cm^{-1} (aliphatic C-H) peaks are observed.

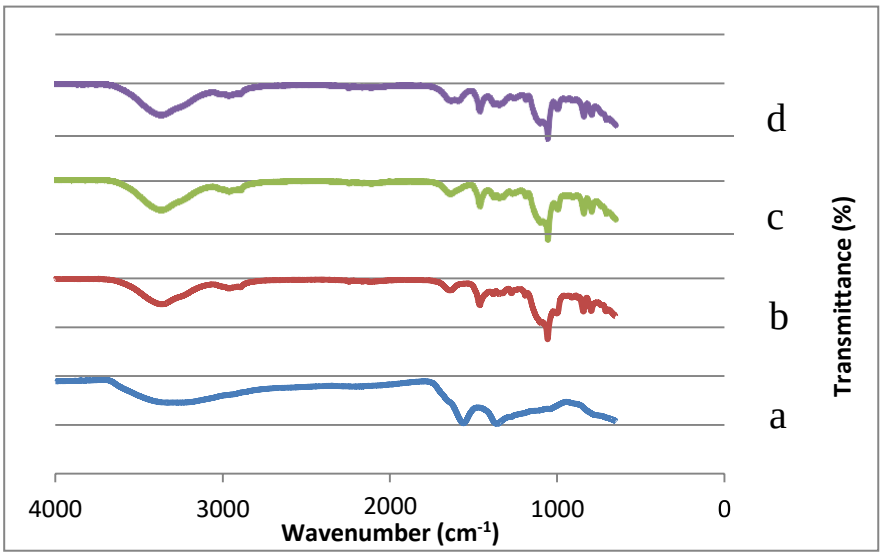

Figure 5.4. FTIR results of bare membrane a) Humic acid b) 0.017M NaCl c) 25 mg/L HA in 0.017 M NaCl d) 50 mg/L HA in 0.017 M NaCl.

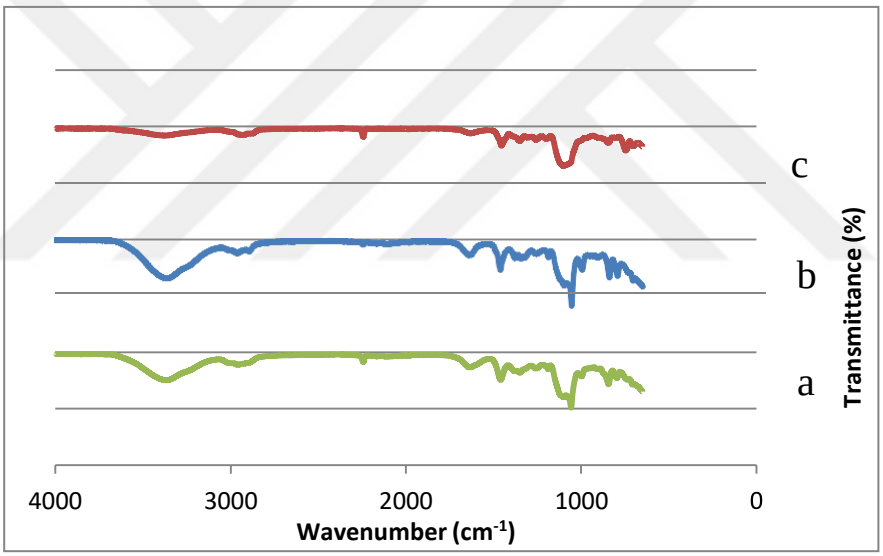

Figure 5.5. FTIR results of bare membrane a) 50 mg/L HA in 0.5M NaCl b) 25 mg/L HA in 0.5M NaCl c)0.5M NaCl

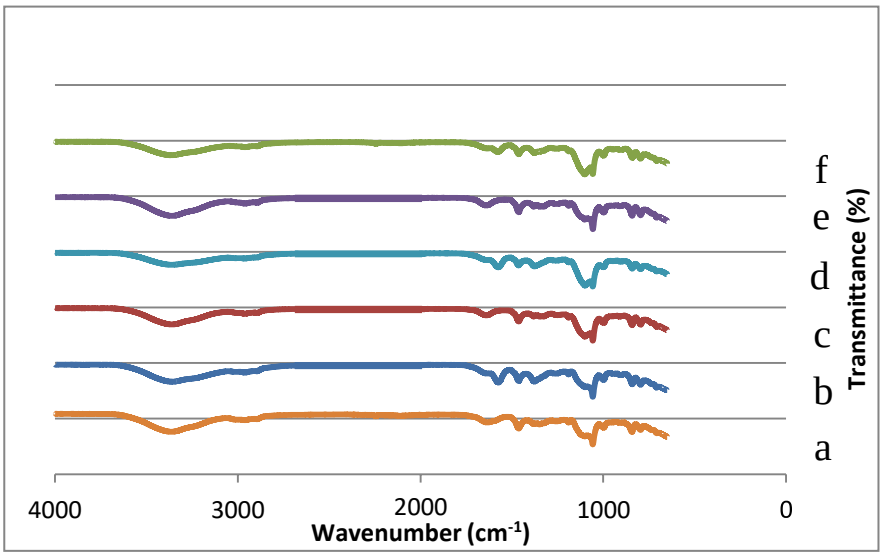

Figure 5.6. FTIR results of AgNPs immobilized membrane a) 50 mg/L HA in 0.5M NaCl b) 0.017M NaCl c) 0.5M NaCl d) 50 mg/L HA in 0.017M NaCl e) 25 mg/L HA in 0.5M NaCl f) 25 mg/L HA in 0.017M NaCl

Ion exchange capacity and swelling degree values of bare and AgNPs immobilized AEMs are given in Table 5.1. Lower ion exchange capacity and swelling degree values were obtained with AgNPs immobilized AEMs compared to bare AEMs.

Table 5.1. Ion exchange capacity and swelling degree values of bare and AgNPs immobilized AEMs.

Membrane	**Swelling degree (%)**	**Ion exchange capacity (mmol/g dry membrane)**
Bare AEMs	110±4.32	2.18±0.06
AgNPs immobilized AEMs	42±1.54	1.99±0.05

Ion exchange capacity and swelling degree values of AEMs interacted with HA solutions prepared in 0.017 M and 0.5 M NaCl are given in Tables 5.2 and 5.3, respectively. Ion exchange capacity and swelling degree values of AgNPs immobilized membranes interacted with HA solutions prepared in 0.017 M and 0.5 M NaCl are given in Tables 5.4 and 5.5. Ion exchange capacity and swelling degree values decreased as the HA concentration increased. Ion exchange capacity

and swelling degree values were lower in case of AgNPs immobilized AEMs compared to bare membranes.

Table 5.2. Ion exchange capacity and swelling degree values of the membranes interacted with HA solutions in 0.017 M NaCl.

Humic acid concentation in solution (mg/L)	**Ion exchange capacity (mmol/g dry membrane)**	**Swelling degree (%)**
0	3.34±0.47	109.61±10.46
25	3.25±0.19	91.76±2.44
50	3.10± 0.06	86.03±4.95

Table 5.3. Ion exchange capacity and swelling degree values of AEMs interacted with HA solutions prepared in 0.5 M NaCl

Humic acid concentation in solution (mg/L)	**Ion exchange capacity (mmol/g dry membrane)**	**Swelling degree (%)**
0	3.12±0.09	126±3.94
25	3.03±0.74	121±9.64
50	2.93± 0.43	101±10.18

Table 5.4. Ion exchange capacity and swelling degree values of AgNPs immobilized AEMs interacted with HA solutions prepared in 0.017 M NaCl

Humic acid concentation in solution (mg/L)	**Ion exchange capacity (mmol/g dry membrane)**	**Swelling degree (%)**
0	3.22±0.04	94.7±6.65
25	3.16±0.10	84.9±9.05
50	3.05±0.22	82.9±9.70

Table 5.5. Ion exchange capacity and swelling degree values of AgNPs immobilized AEMs interacted with HA solutions prepared in 0.5 M NaCl

Humic acid concentation in solution (mg/L)	**Ion exchange capacity (mmol/g dry membrane)**	**Swelling degree (%)**
0	3.07±0.214	104.6±8.65
25	2.90±0.57	96.4±5.34
50	2.76± 0.41	80.2±8.56

5.4. Conclusion

In this study, HA adsorption tests were done. The HA solutions were prepared in 0.017 M NaCl and 0.5M NaCl solutions. Ion exchange capacity and swelling degree values of bare and AgNPs immobilized AEMs were compared. Ion exchange capacity and swelling degree values decreased as the HA concentration increased. Values were lower in the case of AgNPs immobilized AEMs.

CHAPTER 6

CONCLUSIONS

- In this PhD thesis, an environmentally friendly anion exchange membranAEMe was synthesized using an elastomer, poly (epidochlorohydrin) (PECH) with natural chloromethyl groups as the polymer matrix structure.
- In this study, the swelling degree, ion exchange capacity and fixed charge density of the AEMs synthesized were investigated with the blend ratios of 1.07, 1.23 and excess diamine ratios of 1.62, 2 and 4. The FTIR and SEM analyses of the AEMs synthesized were performed. In general, the FTIR analysis resultsshowed that the quaternized ammonium groups were introduced successfully to the membrane. According to SEM results, a clear, dense and non-porous structure was observed in membranes.
- In order to examine the effect of blend ratio, membranes were prepared with blend ratios of 1.07 and 1.23 at a constant excess diamine ratio of 1.62. As the blend ratio of the membranes increased, the ion exchange capacity, swellingdegree and fixed charge density values increased. To investigate the effect of the diamine ratio, on the other hand, membranes were manufactured with an excess diamine ratio of 1.62, 2, and 4 while maintaining a blend ratio of 1.07. The values for ion exchange capacity and fixed charge density increased as the excess diamine ratio in the membranes that were produced increased. On the other hand, the values for swelling degree dropped.
- Optimum conditions were observed in EDR4-BR1.07 membrane which has the highest ion exchange capacity (3.47 mmol/g dry membrane), highest fixed charge density (5.26 mmol/ g H_2O) and the lowest swelling degree (66 %) at the same blend ratio.
- During the characterization of large-scale membranes, a high degree of swelling was initially observed, which gradually decreased in pore-filled membranes until reaching the desired value. Furthermore, it was found that the area resistance of the membranes decreased as the diamine ratio and blend ratio in the synthesized membrane increased. In addition, the field resistance was observed to decrease when the AgNPs immobilized membranes were in contact with salt solutions containing higher concentrations of NaCl.

- AgNPs were synthesized in both pH 6.0 and pH 9.0 environments, and their grain sizes were measured using a Malvern Zeta Sizer device. The average grain size of the nanoparticles obtained from the synthesis carried out at pH 6.0 was determined to be 107.4 nm, whereas the average grain size of the nanoparticles synthesized at pH 9.0 was 96.92 nm. Notably, these detected nanoparticle sizes were found to be consistent with the targeted grain size specified in the project.
- To observe the membrane structures, determine the extent of particle loading, and assess the homogeneity of the nanoparticle distribution on the membrane surface, various analytical techniques such as SEM, EDX mapping,and XPS were utilized. Notably, a color change was observed after immobilizing silver nanoparticles produced at pH 6.0 to the membrane without being subjected to an acidic environment. However, EDX mapping images revealed that agglomerations were formed when the membranes were exposed to nanoparticles produced at pH 9.0. The best and most homogeneous nanoparticle distributionwas observed in membranes immobilized with nanoparticles produced at pH 6.0.
- Upon examining the XPS Spectrum results, it was observed that the Ag3d band appeared at 368 eV and 375 eV, providing evidence of the coordination of silver nanoparticles with amine groups. Additionally, the presence of amine groups within the membrane structure was confirmed by the appearance of the N1s band at 400 eV.
- Stability tests were conducted on the membranes, which revealed that deionized water failed to stabilize the silver nanoparticles, resulting in agglomeration even at low rates. Moreover, it was found that the nanoparticle in a 0.5 M NaCl solution showed an absorbance value close to zero at a wavelength of 405 nm, indicating that the silver nanoparticles were aggregating.
- The absorbance value of the nanoparticle solution in deionized water is lower than the absorbance value of the nanoparticle in NaCl solutions at different concentrations. A low value indicates that deionized water cannot stabilize silver nanoparticles and there is agglomeration even at a low rate. As the concentration of the NaCl solution in which the silver nanoparticles were dispersed increased, the agglomeration increased with the increasing ion intensity, while the less agglomerated particles in the supernatant decreased gradually and therefore the absorbance values increased.

- In membrane stability studies with silver nanoparticles, very close to zero values were obtained at 423 nm in the spectra taken against time in 0.001 M NaCl solution, and no nanoparticle leakage was observed in the 180th minute. The absence of nanoparticle leakage from the membrane is of great importance for the RED tests in the next stages. In this context, results compatible with the target of the project were obtained.
- The ICP-MS results indicated an increase in silver release from the membrane with increasing salt concentration, while the field strength decreased. SEM images, XPS, and ICP-MS analyses further revealed a decrease in theamount of silver nanoparticles on the membrane surface with increasing NaCl concentration in the stability tests. XPS analysis showed higher Ag percentagesfor the membranes compared to the values obtained from ICP-MS analysis. This difference is likely due to the fact that XPS analysis was performed on a specific region of the membrane surface (only to a depth of 5 nm), while ICP-MS analysis involved solubilizing silver from the entire membrane in acid and analyzing the silver in solution.
- Due to the strong antibacterial activity of silver ions, it has been observed that membranes containing silver nanoparticles have a very strong antibacterial effect against E.coli.
- Both commercial (NEOSEPTA CMX) and non-commercial (CMKESD) CEMs, along with AEMs, were employed in the RED system. The impact of flow rate on the RED system was investigated, revealing that an increase in flow rate corresponded to an increase in power density. The highest power density achieved was 0.384 W/m^2 using ER4-BR1.07 and CMKESD membranes. Additionally, it was observed that the ion exchange capacity of the PFAEMs, which were modified with AgNPs, decreased, leading to a reduction in maximum powerdensity due to increased membrane resistance. The highest power density value was obtained as 0.5 W/m^2 in the short-term study with PECH-C and CMKESD membrane, since the ion exchange capacity of the CMKESD membrane is high. The maximum power density values increased due to the increase in conductivity in the silver nanoparticle immobilized membranes.

- Silver nanoparticles with an average size of 53±3 nm were synthesized using a wavelength of 400 nm and a flow rate ranging from 1.5 to 3 mL/min.

- When the content of humic acid was increased, it was found that the ion exchange capacity of the AEMs and the degree to which they swelled when they interacted with the humic acid solution both saw a considerable drop. A lower ion exchange capacity and swelling degree values are the result of pollution in the membranes caused by humic acid.

7. REFERENCES

Abidin, M.N.Z., Nasef, M.M.,Veerman, J., Towards the development of new generation of ion exchange membranes for reverse electrodialysis: A review,2022, Desalination, 537, 115854.

Agnihotri, S., Mukherji, S., Mukherji, S., 2014, Size-controlled silver nanoparticles synthesized over the range 5–100 nm using the same protocol and their antibacterial efficacy, RSC Adv., 4, 3974-3983.

Alabi, A., AlHajaj, A., Cseri, L., Szekely, G., Budd, P., Zou, L., 2018, Review of nanomaterials-assisted ion exchange membranes for electromembrane desalination, Nature Partner Journals Clean Water, 1:10 ; doi:10.1038/s41545- 018-0009-7.

Bolto, B.A., Jackson, M.B., 1984, Polyamine ion-exchange resins from polyepichlorohydrin: Resins with improved resistance to oxidation, Reactive Polymers, Ion Exchangers, Sorbents, 2 209-222.

Cho, D.H., Lee, K.H., Kim,Y.M., Park, S.H., Lee, W.H., Lee, S.M., Lee, Y.M., 2017, Effect of cationic groups in poly(arylene ether sulfone) membranes onreverse electrodialysis performance, Chem Commun (Camb), 53:2323.

Choi, J., Kim, W.S., Kim, H.K., Yang, S.C., Jeong, N.J., 2020, Ultra-thin pore-filling membranes with mirror-image wave patterns for improved power density and reduced pressure drops in stacks of reverse electrodialysis, J. Membr. Sci, MEMSCI 118885.

Choi, J.,. Kim, W.S., Kim, H.K., Yang, S.C., Jeong, S.C. (2021) Ultra-thin pore-filling membranes with mirror-image wave patterns for improved power density and reduced pressure drops in stacks of reverse electrodialysis, J. Membr. Sci., 620, 118885.

Choi, J., Yang, S.C., Jeong, N.J., Kim, H., Kim, W.S., 2018, Fabrication of an Anion-Exchange Membrane by Pore-Filling Using Catechol−1,4-Diazabicyclo-[2,2,2]octane Coating and Its Application to Reverse Electrodialysis, Langmuir, 34,10837−10846.

Cihanoğlu, A.,. Altınkaya, S.A, 2020, A facile route to the preparation of antibacterial polysulfone-sulfonated polyethersulfone ultrafiltration membranes using a cationic surfactant cetyltrimethylammonium bromide, J. Mem. Sci. 594, 117438.

Ciofalo, M., La Cerva, M., Di Liberto, M., Gurreri, L., Cipollina, A., Micale, G., 2019, Optimization of net power density in Reverse Electrodialysis, Energy, 181, 576-588.

Damodar, R.A., You, S.-J., Chou, H.-H., 2009, Study the self cleaning, antibacterial and photocatalytic properties of TiO_2 entrapped PVDF membranes,J. Hazard. Mater. 172, 1321–1328.

Daniilidis, A., Vermaas, D.A., Herber, R., Nijmeijer, K., 2014, Experimentally obtainable energy from mixing river water, seawater or brines with reverse electrodialysis, Renew. Energy, 64, 123–131.

Díaz, J.C., Kamcev J., 2021, Ionic conductivity of ion-exchange membranes: Measurement techniques and salt concentration dependence, J. Memb. Sci., 618, 118718.

Di Salvo, J.L., Cosenza, A., Tamburini, A., Micale, G., Cipollina, A., 2018, Long-run operation of a reverse electrodialysis system fed with wastewaters,Journal of Environmental Management 217 871-887.

Długołecki, P., Ogonowski, P., Metz, S.J., Saakes, M., Nijmeijer, K., Wessling, M., 2010, On the resistances of membrane, diffusion boundary layer and double layer in ion exchange membrane transport, J. Membr. Sci., 349 (2010) 369–379.

Fan, H., Yip, N.Y., 2019, Elucidating conductivity-permselectivity tradeoffs in electrodialysis and reverse electrodialysis by structure-property analysis of ion-exchange membranes, Journal of Membrane Science, 573, 668–681.

Gao, H., Zhang, B., Tong, X., Chen, Y., 2018, Monovalent-anion selective and antifouling polyelectrolytes multilayer anion exchange membrane for reverse electrodialysis, Journal of Membrane Science 567, 68–75.

Germer, W., Harms, C., Tullius, V., Leppin, J., Dyck., A., 2015, Comparison of conductivity measurement systems using the example of nafion and anion exchange membrane, Solid State Ionics. 275, 71–74.

Guo, W., Ngo, H.H., Li, J., 2012, A mini-review on membrane fouling, Bioresource Technology, 122, 27-34.

Güler E., 2014, Anion exchange membrane design for reverse electrodialysis. PhD Thesis, University of Twente, 173p.

Güler, E., Baak, W. van, Saakes, M., Nijmeijer, K., 2014, Monovalent-ion-selective membranes for reverse electrodialysis, J. Membr. Sci., 455, 254–270.

Güler, E., Elizen, R., Vermaas, D.A., Saakes, M., Nijmeijer, K., 2013, Performance-determining membrane properties in reverse electrodialysis, J. Membr. Sci. 446, 266-276.

Güler, E., Nijmeijer, K., 2018, Reverse Electrodialysis for Salinity Gradient Power Generation: Challenges and Future Perspectives, Journal of Membrane Science and Research 4, 108-110.

Güler, E., Zhang, Y., Saakes, M., Nijmeijer, K., 2012, Tailor-made anion- exchange membranes for salinity gradient power generation using reverse electrodialysis, ChemSusChem, 5 2262-2270.

Habib, Z., Khan, S.J., Ahmad, N.M., Shahzad, H.M.A., Jamal, Y., Hashmi, I., 2020, Antibacterial behaviour of surface modified composite polyamide nanofiltration (NF) membrane by immobilizing Ag-doped TiO_2 nanoparticles, Environ. Technol. (United Kingdom), 41, pp. 3657–3669.

He, Z., Gao, X., Zhang, Y., Wang, Y., Wang, J., 2016, Revised spacer design to improve hydrodynamics and anti-fouling behavior in reverse electrodialysis processes, Desalin. Water Treat., 57, 28176–28186.

Hong, J.G., Chen, Y., 2014, Nanocomposite reverse electrodialysis (RED) ion-exchange membranes for salinity gradient power generation, Journal of Membrane Science 460, 139–147 p.

Hong, J.G., Gao, H., Gan, L., Tong, X., Xiao, C., Liu, S., Zhang, B., Chen, Y., 2019, Nanocomposite and nanostructured ionexchange membrane in salinity gradient power generation using reverse electrodialysis, Advanced Nanomaterials for Membrane Synthesis and its Applications Micro and Nano Technologies, 295- 316 p.

Imedio, R.O., Coma, R.G., Fallanza, M., Ortiz, A., Ibañez, R., Ortiz, I., 2019, Comparative performance of Salinity Gradient Power-Reverse Electrodialysis under different operating conditions, Desalination, 457, 8-21.

Jang, J., Kanga, Y., Hanb, J.H., Janga, K., Kima, C.M., Kima, I.S., 2020, Developments and future prospects of reverse electrodialysis for salinity gradient

power generation: Influence of ion exchange membranes and electrodes, Desalination, 491, 114540.

Jhaveri, J.H., Murthy, Z.V.P., 2016, A comprehensive review on anti-fouling nanocomposite membranes for pressure driven membrane separation processes, Desalination, 379, 137–154.

Kamali, M., Ghorashi, S.A.A., Asadollahi, M.A., 2012, Controllable Synthesis of Silver Nanoparticles Using Citrate as Complexing Agent: Characterization of Nanopartciles and Effect of pH on Size and Crystallinity, Iran. J. Chem. Chem. Eng., 31,4.

Kim, H., Choi, J., Jeong, N., Jung, Y.G., Kim, H., Kim, D.,Yang, S.C., 2021, Correlations between Properties of Pore-Filling Ion Exchange Membranes and Performance of a Reverse Electrodialysis Stack for High Power Density, Membranes, 11, 609.

Kim, H., Jeong, N., Yang, S.C., Choi, J., Lee, M.S, Nam, J.Y., Jwa, E., Kim, B., Ryu, K., Choi, Y.W., 2019, Nernst- Planck analysis of reverse-electrodialysis with the thincomposite pore-filling membranes and its upscaling potential, Water Res., 165, 114970.

Kim D. H., Kang MS., 2016, Preparation and characterizations of ionomer-coated pore-filled ion exchange membranes for reverse electrodialysis, Membrane Journal, 26, 43-54.

Kim H. K., Lee M. S., Lee S. Y., Choi Y. W., Jeong N. J., Kim C. S., 2015, High power density of reverse electrodialysis with pore-filling ion exchange membranes and a high open area spacer, J. Mater. Chem. A. 3, 16302-16306.

Kotoka, F., Merino-Garcia, I., Velizarov, S., 2020, Surface Modifications of Anion Exchange Membranes for an Improved Reverse Electrodialysis Process Performance: A Review, Membranes, 10, 160.

Le, L. N., Nunes, S. P., 2016, Materials and membrane technologies for water and energy sustainability, Sustainable Materials and Technologies 7, 1–28.

Lee, H.J., Hong, M.K., Han, S.D., Cho, S.H., Moon, S.H., 2009, Fouling of an Anion Exchange Membrane in the Electrodialysis, 238, 60-69.

Lee, S.Y., Kim, H.J., Patel, R., Im, S.J., Kim, J.H., Min, B.R., 2007, Silver nanoparticles immobilized on thin film composite polyamide membrane:

characterization, nanofiltration, antifouling properties, Polym. Adv. Technol., 18: 562–568 p.

Lee, M.S., Kim, H.K., Kim, C.S., Suh, H.Y., Nahm, K.S., Choi, Y.W., 2017, Thin Pore-Filled Ion Exchange Membranes for High Power Density in Reverse Electrodialysis: Effects of Structure on Resistance, Stability, and Ion Selectivity, Chemistry Select, 2, 1974 – 1978.

Lee, S., Shin, M.S., Park, J.S., 2014, Anion-conducting Pore-filling Membranes with Optimization of Transport Number and Resistance for Reverse Electrodialysis, Chem. Soc. Japan, 43, 621–623.

Li, J.-H., Shao, X.-S., Zhou, Q., Li, M.-Z., Zhang, Q.-Q., 2013, The double effects of silver nanoparticles on the PVDF membrane: surface hydrophilicity and antifouling performance, Appl. Surf. Sci. 26, 663–670 p.

Li, Mei, Guo, J., Wang, Y., Wu, Y., Guo, P., Li, X., Reverse electrodialysis for power production with ion-permselective spacers and its optimization, 2022, Journal of Applied Electrochemistry, 52:871–88.

Li, W., Xie, X., Shi, Q., Zeng, H., OU-Yan, Y., 2010, Chen, Y., Antibacterial activity and mechanism of silver nanoparticles on Escherichia coli, Appl Microbiol Biotechnol, 85:1115–1122.

Liu, F., 2015, Advancing CapMix for electricity generation: System operation cell design and material selection, PhD thesis, Wageningen University, 172p.

Madaeni, S., Ghaemi, N., 2007, Characterization of self-cleaning RO membranes coated with TiO_2 particles under UV irradiation, J. Membr. Sci. 303, 221–233.

Mei, Y., Tang, C.Y., 2018, Recent developments and future perspectives of reverse electrodialysis technology: a review, Desalination, 425, 156–174.

Mehdizadeh, S., Yasukawa, M., Abo, T., Kakihana, Y., Higa, M., Effect of spacer geometry on membrane and solution compartment resistances in reverse electrodialysis, 2019, Journal of Membrane Science, 572, 271-280.

Mehdizadeh, S., Yasukawa, M., Abo, T., Kuno, M., Noguchi, Y., Higa, M., The Effect of Feed Solution Temperature on the Power Output Performance of a Pilot-Scale Reverse Electrodialysis (RED) System with Different Intermediate Distance, Membranes, 9(6), 73.

Mikac, L., Ivanda, M., Gotic, M., Mihelj, T., Horvat, L., 2014, Synthesis and characterization of silver colloidal nanoparticles with different coatings for SERS application, J Nanopart Res, 16:2748.

Mikhaylin, S., Bazinet, L., 2016, Fouling on ion-exchange membranes: classification, characterization and strategies of prevention and control. Adv. Colloid Interface Sci. 229, 34-56.

Nagarale, R.K., GohilVinod, G.S., Shahi, K., Recent developments on ion-exchange membranes and electro-membrane processes, 2006, Advances in Colloid and Interface Science, 119, 97 – 130.

Ortiz-Martínez, V.M., Gómez-Coma, L., Tristán, C., Pérez, G., Fallanza, M., Ortiz, A., Ibañez, R., Ortiz, I., A comprehensive study on the effects of operation variables on reverse electrodialysis performance, 2022, Desalination, 482, 114389.

Othman, NH, Kabay, N., Güler E., Principles of reverse electrodialysis and development of integrated-based system for power generation and watertreatment: a review, 2022, Rev Chem Eng, 38(8), 921–958.

Pandey, T.P., Maes, A.M., Sarode, H.N., Peters, B.D., Lavina, S., Vezzù, K., Yang, Y. Poynton, S.D., Varcoe, J.R., Seifert, S., Liberatore, M.W., Noto, V. Di, Herring, A.M., 2015, Interplay between water uptake, ion interactions, and conductivity in an e-beam grafted poly(ethylene-co-tetrafluoroethylene) anion exchange membrane", Phys. Chem. Chem. Phys.,17, 4367.

Pattle, R.E., 1954, Production of electric power by mixing fresh and salt water in the hydroelectric pile, Nat Biotechnol, 174:660.

Pawlowski, S., Galinha, C.F., Crespo, J.G., Velizarov, S., 2016, 2D fluorescence spectroscopy for monitoring ion-exchange membrane based technologies e Reverse electrodialysis (RED), Water Research 88, 184-198.

Pawlowski S., 2015, Experimental and Modeling Studies on Reverse Electrodialysis for Sustainable Power Generation, PhD Thesis, Universidade Nova de Lisboa, 197p.

Post, J.W., Veerman, J., Hamelers, H.V.M., Euverink, G.J.W., Metz, S.J., Nijmeijer, K., Buisman, C.J.N., 2007, Salinity gradient power: evaluation of

pressure-retarded osmosis and reverse electrodialysis, Journal of Membrane Science 288 (1-2), 218-230.

Post, J.W., 2009, Blue Energy: electricity production from salinity gradients by reverse electrodialysis, Wageningen University, PhD Thesis, 219 p.

Pourjafar S., Rahimpour A., Jahanshahi M., Synthesis and characterization of PVA/PES thin film composite nanofiltration membrane modified with TiO2 nanoparticles for better performance and surface properties, 2012, Journal of Industrial and Engineering Chemistry 18, 1398–1405.

Qin, Y., Ji, X., Jing, J., Liu, H., Wu, H., Yang, W., 2010, Size control over spherical silver nanoparticles by ascorbic acid reduction , Colloids and Surfaces A: Physicochem. Eng. Aspects 372, 172–176.

Radzig, M.A., Nadtochenko, V.A., Koksharova, O.A., Kiwi, J., Lipasova, V.A., Khmela, I.A., 2013, Antibacterial effects of silver nanoparticles on gram-negative bacteria: Influence on the growth and biofilms formation, mechanisms of action, Colloids and Surfaces B: Biointerfaces, 102, 300– 306.

Raka, Y.D., Bock, R., Karoliussen, H., Wilhelmsen, O., Burheim, O.S., 2021, The Influence of Concentration and Temperature on the Membrane Resistance of Ion Exchange Membranes and the Levelised Cost of Hydrogen from Reverse Electrodialysis with Ammonium Bicarbonate, Membranes, 11, 135.

Rana, D., Matsuura, T., 2010, Surface modifications for antifouling membranes, Chem. Rev., 110, 2448–2471.

Rashid, M.U., Bhuiyan, K.H., Quayum, M.E., 2013, Synthesis of Silver Nano Particles (Ag-NPs) and their uses for Quantitative Analysis of Vitamin C Tablets, Dhaka Univ. J. Pharm,. Sci., 12(1): 29-33.

Ratjke, S.K., Holt, T., Fiksdal, L., 1986, Effect of Biofilm Formation on Salinity Power Plant Output on Laboratory Scale, University of Trondheim, Trondheim, 14 p.

Rijnaarts, T., Moreno, J., Saakes, W., Vosb, V.M., Nijmeijer, K., 2019, Role of anion exchange membrane fouling in reverse electrodialysis using natural feed waters, Colloids and Surfaces A 560, 198–204.

Santoro, S., Tufa, R.A., Avci, A.H., Fontananova, E., Profio, G., Curcio, E., 2021, Fouling propensity in reverse electrodialysis operated with hypersaline brine, Energy, 228, 120563.

Sarode, H.N., 2015, Understanding Ion And Solvent Transport In Anion Exchange Membranes Under Humidified Conditions, Colorado School of Mines, 140p.

Silva, O.A., Osorio, A.F., Winter, C., 2016, Practical global salinity gradient energy potential, Renewable and Sustainable Energy Reviews, 60, 1387–1395.

Simões, C.,Pintossi, D., Saakes, M., Bornemanc, Z., Brilman, W., Nijmeijer, K., 2020, Electrode segmentation in reverse electrodialysis: Improved power and energy efficiency, Desalination 492, 114604.

Sprick, C.G., 2017, Functionalization of Silver Nanoparticles on Membranes And Its Influence On Biofouling, MSc. Thesis, University of Kentucky, 73p.

Steinigeweg, D., Schlücker, S., 2012, Monodispersity and size control in the synthesis of 20–100 nm quasi-spherical silver nanoparticles by citrate and ascorbic acid reduction in glycerol–water mixtures, Chem. Commun., 48, 8682– 8684.

Strathmann H., Giorno L., Drioli E., 2006, An introduction to membrane science and Technology, CNR-Servizio Pubblicazioni.

Susanto, H., Fitrianingtyas, M., Samsudin, A.M., Syakur, A., 2017, Experimental study of the natural organic matters effect on the power generation of reverse electrodialysis, Int. J. Energy Res., 41:1474–1486.

Tedesco, M., Brauns, E., Cipollina, A., Micale, G., Modica, P., Russo, G., Helsen, J., 2015, Reverse electrodialysis with saline waters and concentrated brines: a laboratory investigation towards technology scale-up, J. Membr. Sci., 492, 9–20.

Tedesco, M., Hamelers, H. V. M., Biesheuvel, P. M., 2016, Nernst-Planck transport theory for (reverse) electrodialysis: I. Effect of co-ion transport through the membranes, Journal of Membrane Science 510, 370–381.

Tian, H., Wanga, Y., Peia, Y., Crittenden, J.C., 2020, Unique applications and improvements of reverse electrodialysis: A review and outlook, Applied Energy, 262, 114482-114506.

Tong, X., Zhang, B., Fan, Y., Chen, Y., 2017, Mechanism exploration of ion transport in nanocomposite cation exchange membranes. ACS Appl. Mater. Interfaces 9, 13491–13499 p.

Tongwen, X., Weihua, Y., 2001, Fundamental studies of a new series of anion exchange membranes: membrane preparation and characterization, Journal of Membrane Science, 190, 159-166.

Tristán, C., Fallanza, M., Ibáñez, R., Ortiz, I., 2020, Recovery of salinity gradient energy in desalination plants by reverse electrodialysis, Desalination, 496, 114699-114710.

Tuan, C.M., Tinh, V.D.C, Kim, D., 2020, Anion exchange membranes prepared from quaternized polyepichlorohydrin cross-linked with 1-(3-aminopropyl)imidazole grafted poly(arylene ether ketone) for enhancement of toughness and conductivity, Membranes, 10, 138.

Tufa, R.A., Pawlowski, S., Veerman, J., Bouzeka, K., Fontananovad, E., Profiod, G., Velizarov, S., Crespo, J.G., Nijmeijer, K., Curciod, E., 2018, Progress and prospects in reverse electrodialysis for salinity gradient energy conversion and storage, Applied Energy, 225, 290–331.

Uz, M., Mahlicli, F.Y., Seker, E., Altinkaya, S.A., 2020, Development of AgCl-TiO_2 xerogels entrapped antibacterial polyacrylonitrile membranes: The effect of high salinity water on silver release, antibiofouling and antibacterial efficacies, Desalination 492, 114496.

Vandiver, M.A., 2015, Effect of hydration on the mechanical properties of anion exchange membranes, PhD Thesis, Colorado School of Mines, 183p.

Vaselbehagh, M., Karkhanechi H., Mulyati, S., Takagi, R., Matsuyama, H., 2014, Improved antifouling of anion-exchange membrane by polydopamine coating in electrodialysis process, Desalination 332, 126–133.

Vaselbehagh, M., Karkhanechi, H., Takagi, R., Matsuyama, H., 2017, Biofouling phenomena on anion exchange membranes under the reverse electrodialysis process, J. Membr. Sci., 530, 232–239.

Vatanpour, V., Madaeni, S.S., Khataee, A.R., Salehi, E., Zinadini, S., Monfared, H.A., 2012, TiO2 embedded mixed matrix PES nanocomposite membranes: influence of different sizes and types of nanoparticles on antifouling and performance, Desalination, 292, 19–29 p.

Veerman J., Saakes, M. Metz, S.J., Harmsen, G.J., 2009, Reverse electrodialysis: performance of a stack with 50 cells on the mixing of sea and river water, Journal of Membrane Science, 327,136-144.

Veerman, J., Saakes, M., Metz, S.J., Harmsen, G.J., 2011, Reverse electrodialysis: A validated process model for design and optimization, Chemical Engineering Journal, 166, 256–268.

Vermaas, D.A., Bajracharya, S., Sales, B.B., Saakes, M., Hamelersa, B., Nijmeijer, K., 2013, Clean energy generation using capacitive electrodes in reverse electrodialysis, Energy Environ. Sci., 6, 643-651.

Vermaas, D.A., Kunteng, D., Saakes, M., Nijmeijer, K., 2013, Fouling in reverse electrodialysis under natural conditions, Water Res., 47, 1289–1298.

Vermaas, D.A., Kunteng, D., Veerman, J. Saakes, M., Nijmeijer, K., 2014,Periodic feedwater reversal and air sparging as antifouling strategies in reverse electrodialysis, Environ. Sci. Technol., 48, 3065–3073.

Vital, B., V. Torres, E., Sleutels, T., Cristina Gagliano, M., Saakes, M., V.M. Hamelers, H., Fouling fractionation in reverse electrodialysis with natural feed waters demonstrates dual media rapid filtration as an effective pre-treatment for fresh water, 2021, Desalination, 518, 115277.

Yang S.C., Choi Y.W., Choi J., Jeong N., Kim H., Nam JY., Jeong H., 2019, R2R fabrication of pore-filling cation-exchange membranes via one-time impregnation and their application in reverse electrodialysis, ACS Sustainable Chem. Eng. 7 14, 12200-12213.

Yip, N.Y., Elimelech, M., 2014, Comparison of energy efficiency and power density in pressure retarded osmosis and reverse electrodialysis, Environmental Science and Technology, 48, 11002−11012.

Yuksel, M., Tas, B., Imer D.Y., Koyuncu, I., 2014, Effect of silver nanoparticle (AgNP) location in nanocomposite membrane matrix fabricated with different polymer type on antibacterial mechanism, Desalination, 347, 120-130.

Zhang, J., Wang, G., Zhang, J., Xu, Z., Zhao, Y., Wang, Y., She, F., Gray, S., Kong, L., 2021, Substrate-Independent, Regenerable Anti-Biofouling Coating for Polymeric Membranes, Membranes, 11(3), 205.

Zhu, X., Bai, R., Wee, K.H., Liu, C., Tang, S.L., 2010, Membrane surfaces immobilized with ionic or reduced silver and their anti-biofouling performances, Journal of Membrane Science 363, 278–286.

8. ACKNOWLEDGEMENT

This study was supported by Concert-Japan (Project number: TÜBİTAK 118M804). I am especially grateful for the scholarships given by TÜBİTAK.

I would like to express my deepest and sincere gratitude to my advisor Prof. Dr. Nalan KABAY, and co-advisor Assoc. Prof. Dr. Enver Güler for their support, encouragement, guidance, and patience throughout the thesis.

I would like to thank my PhD thesis committee and jury members, Prof. Dr. Levent BALLİCE, Prof Dr. Sacide ALSOY ALTINKAYA, Prof. Dr. Müşerref ARDA, Prof. Dr. Serap BOZKURT for sharing their valuable knowledge to improve the quality of my thesis.

I acknowledge Erasmus Training programme for visiting Cantabria University, Spain, for 2 months. I would like to thank Prof. Dr. Inmaculada ORTIZ, Assoc. Prof. Dr. Nazely DIBAN for accepting me to her laboratory as an Erasmus trainee and Lucia GOMEZ COMA for helping me do the tests.

I acknowledge Mitsubishi Chemical, Japan, especially Mr Ando Kiyoto to send us PAN sample and Osaka Soda Co., Japan for PECH polymer.

I also thank Prof. Dr. Ali TUNCEL, Assoc. Prof. Dr. Kadriye Özlem HAMALOĞLU and Burcu GÖKÇAL, Hacettepe University, for the help in the synthesis of silver nanoparticles. I would like to thank Dr. Aydın CİHANOĞLUfor the help in preparation of large-scale membranes, also Dr. Esra ALTIOK and Tuğçe Zeynep KAYA for the help in the RED tests.

I would like to thank Nazlı Deniz SARIYILDIZ for encouraging, giving hope and strength and always being my side and supporting me throughout my doctorate education.

Lastly, I would like to thank my dear family and Prof. Dr. Ayşe LAHUR KIRTUNÇ for their endless support, understanding, and love.

CV

EDUCATION INFORMATION

- **14.01.22/17.03.2022-**Erasmus Traineeship- University of Cantabria
- **02.2019/06.2023-** PhD- Ege University- Graduate School of Natural and Applied Sciences- Chemical Engineering Department
- **01.2015/02.2017-**Msc. -Ege University- Graduate School of Natural and Applied Sciences- Materials Science and Engineering Department
- **09.2009/07.2014-** Ege University- Faculty of Engineering –Chemical Engineering Department
- **09.2005/06.2009-** Bornova Suphi Koyuncuoglu High School, Physical Sciences, Highest Ranked Student

LANGUAGE SKILLS

- English

Reading: Fluent **Speaking:** Very Well **Writing:**Fluent

WORK EXPERIENCE

- Ege University Chemical Engineering Department-TÜBİTAK Project Assistant- 15.04.2019/08.2022

Job description: Following the current literature, making experiments in the laboratory about the project and preparing main and interim reports, preparing papers or presentations.

- A Fire Security A.S.-Quality Engineer- 12.02.2018/26.10.2018

Job description:

Integrated quality management system preparations, preparation of quality system documents, follow-up and updating, product certification studies, organization and follow-up of calibration activities of devices in the factory, being responsible for laboratories, performing analyzes and

interpreting results, conducting final quality control activities, evaluating customer complaints, initiating and following corrective and preventive actions, coordinating input quality control activities for materials provided from suppliers.

- Egemet Calibration Measurement Ltd. Sti – Quality Engineer- 26.04.2017/30.09.2017

Job description: Preparation of annual calibration and verification programs, preparation of personnel training and authorization matrix, making necessary revisions in quality documents and processing them into CANIAS ERP system, calculating measurement uncertainties and processing them into the Excel system, following up and revising current standards.

Additional job description: Translation of MSDS and device functions

- Ege University Mechanical Engineering Department-TÜBİTAK Project Assistant- 01.06.2015/10.02.2017

Job description: Following the current literature, making trials in the laboratory about the project and preparing main and interim reports, preparing papers or presentations

Additional job description: Assisting the work of the TÜBİTAK 1003 project on the project studies for the Development of High Performance Reflective and Receiving Surfaces

INTERNSHIP INFORMATION

- BTM Insulation 08.2012-09.2012
- MOPAK A.Ş. 06.2013- 07.2013

AFFILIATED ORGANIZATIONS

- TMMOB Chamber of Chemical Engineers
- Ege University Turkish Folk Dance Ensemble
- Ege University Photography Ensemble
- Ege University Engineering Ensemble
- BORDER Youth and Sports Club
- Ege University Graduate Association Folk Dance Ensemble

- LÖSEV- Health and Education Foundation for Children with Leukemia-Stand and Training Volunteer
- Aegean Forest Foundation
- PARILTI- Support association for children who cannot see

HONORS AND AWARDS

- Suphi Koyuncuoglu High School Highest Ranked Place
- Ege University Chemical Engineering Department Student Representation
- LÖSEV-Volunteer of the year

CERTIFICATES

- 11.2019- 6th MEMTEK International Symposium on Membrane Technologies and Applications
- 07.2018- Time management- Elginkan Foundation
- 06.2018- Change and Continuation Improvement (KAI-ZEN)- Elginkan Foundation
- 06.2018- Internal auditor- Hakan SEMERCİ
- 05.2018- Statistical Process Control (SPC)- Hakan SEMERCİ
- 05.2018- Measurement System Analysis (MSA)- Hakan SEMERCİ
- 04.2018- Process management for QMS in the automotive industry- Hakan SEMERCİ
- 04.2018- IATF 16949:2016 Production Part Approval Process for QMS (ver-4) -Hakan SEMERCİ
- 05.2018- Advanced Product Quality Planning Training -Hakan SEMERCİ
- 05.2018- Measurement System Analysis- Hakan SEMERCİ
- 03.2018- IATF 16949:2016 Basic Information Training- Hakan SEMERCİ
- 01.2016- POLIKOM-International Workshop on Special Topics on Polymeric Composites- Organizing Committee
- 02.2015- LOOPEGE Graduate Students Orientation Programme
- 08.2014- ISO 9001:2008 Basic Quality Management Training- RODOS GROUP

- 08.2014- ISO 1400:2014 Environmental Management System Training-RODOS GROUP
- 08.2014- Risk Analysis Training- RODOS GRUP
- 08.2014- OHSAS 18001 Occupational Health and Safety Management Training- RODOS GROUP
- 08.2014- ISO 19011 Internal Auditor Training- RODOS GROUP
- 08.2014- ISO 22000:2005 HACCP Food Safety Education- RODOS GRUP

PROJECTS

- TÜBİTAK- Superior functionality: Composite / mixed matrix porous methods in membrane processing processes
- TÜBİTAK 1001- Enhancement of the Electrical, Thermal and Mechanical Properties of Aeronautical Composites via Graphene Incorporation
- Undergraduate Diploma Project: Degradation of Atrazine Using Floating Photocatalytic Composite Particles Formed by Pickering Emulsion and Membrane Emulsification
- Msc. Diploma Project: Influences of the Graphene Obtained Through the Grinding of Graphite to the Properties of Epoxy Nanocomposites

INTERNATIONAL PUBLICATIONS

Papers:

- Eti, M., Othman, N.O., Güler, E., Kabay, N., Ion Exchange Membranes for Reverse Electrodialysis (RED) Applications-Recent Developments, 2021, Journal of Membrane Science and Research 7, 260-267 (Review article).
- Eti, M., Cihanoğlu, A., Güler, E., Gomez-Coma, L., Altıok, E., Arda, M., Ortiz I., Kabay, N., Further Development of Polyepichlorohydrin Based Anion Exchange Membranes for Reverse Electrodialysis by Tuning Cast Solution Properties, 2022, Membranes, 12,1192.
- Eti, M., Cihanoğlu, A., Altıok, E., Hamaloğlu K.Ö., Güler,E., Tuncel, A., Kabay, N., Preparation and Characterization of AgNps and AgNps Immobilized AEMs (manuscript to be submitted).

Book chapters:

Güler, E., Cihanoğlu, A., Altıok, E., Kaya, T.Z., Eti, M. Kabay, N. (2023) Chapter 16: Green Energy Generation Using Membrane Technologies Based on Salinity Gradient, Green Membrane Technology Towards Environmental Sustainability, Dumee L., Sadrzadeh, M., A.Shirazi, M.M, Elsevier, in press.

Presentations:

- Eti, M., Cihanoğlu, A., Altıok, E., Hamaloğlu, K.Ö., Güler, E., Tuncel, A., Kabay, N., Preparation of Pore Filling Anion Exchange Membranes for Salinity Gradient Energy Production by Reverse Electrodialysis Method, International Student Conference on Advance Science and Technology, The 17th ICAST 2022, December 1-2, 2022, Kumamoto University, Japan.
- Eti, M., Cihanoğlu, A., Hamaloğlu, K.Ö., Gökçal, B., Güler, E., Tuncel, A., Kabay, N., Synthesis and Characterization of Composite Antibacterial Anion Exchange Membranes for Reverse Electrodialysis Applications, 6t h International Symposium on "Green and Smart Technologies for a Sustainable Society", 9-10 December 2021. (Video-Oral)
- Eti, M., Cihanoğlu, A., Hamaloğlu, K.Ö., Gökçal, B., Güler, E., Tuncel, A., Kabay, N., Antibacterial Behavior of Novel Anion Exchange Membranes Synthesized for Reverse Electrodialysis, The 16th ICAST 2021, 2-3 December 2021. (Oral)
- Eti, M., Gökçal, B., Hamaloğlu, K.Ö., Cihanoğlu, A., Güler, E., Tuncel, A., Kabay, N., Synthesis and characterization of Composite Antibiofouling Anion Exchange Membranes for reverse electrodialysis applications, The 5th KOMPEGE 2021, 4-6 November 2021. (Oral)
- Eti, M., Karakoç, E., Altıok, E., Kaya, T.Z., Cihanoğlu, A., Güler, E., Kabay, N., Synthesis and Application of Novel Anion Exchange for Salinity Gradient Energy Production by Reverse Electrodialysis, International workshop on "Woman Scientists Working on Membranes" organized by Izumi Kumakiri, Yamaguchi University, 05.10.2021. (Oral)
- Karakoç, E., Eti, M., Kabay, N., Güler, E., Ters Elektrodiyaliz Sistemi için Sentezlenen Anyon Değiştirici Membranlarda Poliepiklorhidrin

Türevi Polimerlerin Etkisi, UKMK2020, 14. Ulusal Kimya Mühendisliği Kongresi, 10-12 Haziran 2021, Konya Teknik Üniversitesi.

- Gökçal, B., Eti M., Karakoç, E., Hamaloğlu, K.Ö., Güler, E., Kabay, N., Tuncel, A., Kirlenmeye Dirençli Membranlar: Gümüş Nanopartikül İmmobilize Edilmiş Poliepiklorhidrin Esaslı Anyon Değiştirici Membranların Sentezi, UKMK2020, 14. Ulusal Kimya Mühendisliği Kongresi, 10-12 Haziran 2021, Konya Teknik Üniversitesi.
- Eti, M., Karakoç, E., Güler, E., Kabay, N., Ters Elektrodiyaliz Yöntemi ile Tuzluluk Gradyan Enerjisi Üretimi için Özgün Anyon Değiştirici Membranların Sentezi ve Karakterizasyonu, UKMK2020, 14. Ulusal Kimya Mühendisliği Kongresi, 10-12 Haziran 2021, Konya Teknik Üniversitesi
- Eti M., Karakoç, E., Güler, E., Kabay, N. Synthesis of Novel Anion Exchange Membranes for Salinity Gradient Energy Production by Reverse Electrodialysis (RED) Method, 15th International Student Conference on Advance Science and Technology, December, 2020, Kumamoto, Japan (Online), (oral presentation, extended abstract).
- ETİ M, Ersü G, Seviğ G, İkizler B, Altay L, Erden S. Large Scale Graphene Sythesis By Ball Milling. International Workshop on Special Topics on PolymericComposites (POLIKOM), Bornova, February 2016 (oral, abstract).
- Ersü G, Seviğ G, ETİ M, Altay L, İkizler B, Erden S. Continuous CVD Graphene Growth. International Workshop on Special Topics on Polymeric Composites (POLIKOM), Bornova, February 2016, (oral, abstract).
- Seviğ G, Ersü G, ETİ M, İkizler B, Altay L, Erden S. Preparation of CVD Graphene Substrates Via Electroless Copper Plating. International Workshop on Special Topics on PolymericComposites (POLIKOM), Bornova, February 2016, (oral, abstract).

REFERENCES

- Assoc. Prof. Dr. Seçkin Erden, Ege University Mechanical Engineering Department

Tel: +90545 281 58 27 e-mail: seckin.erden@gmail.com

- Prof. Dr. Rasim İPEK, Ege University Mechanical Engineering Department

Tel: +90532 681 00 33 e-mail: ipek.rasim@gmail.com

INTERESTS

Folk dances, photography, environmental protection activities